



The
University
Of
Sheffield.

Defining the Role of Complement Factor B of the Alternative Complement Pathway in Diabetic Retinopathy

By:

Hannah Louise Murray

A thesis submitted in partial fulfilment of the requirements for the degree of
Doctor of Philosophy

The University of Sheffield
Faculty of Engineering.
School (or Department) of Materials Science and Engineering

March 2019

Defining the Role of Complement Factor B of the Alternative Complement Pathway in Diabetic Retinopathy by Hannah Murray is licensed under CC BY-NC-ND 4.0. To view a copy of this license, visit <https://creativecommons.org/licenses/by-nc-nd/4.0>

Contents

Abstract	vi
Acknowledgements	viii
List of Abbreviations	xi
List of Figures	xiv
List of Tables.....	xvi
1. Introduction.....	1
1.1 Our Vascular System.....	2
1.2 Anatomy of Blood Vessels	2
1.3 Blood Vessel Formation.....	4
1.4 Angiogenesis	6
1.4.1 Intussusceptive Angiogenesis.....	7
1.4.2 Sprouting Angiogenesis.....	7
1.4.3 Regulating Angiogenesis	9
1.4.4 Vascular Endothelial Growth Factor	10
1.5 The Retina	11
1.5.1 Basic Anatomy	11
1.5.2 Retinal Vascularisation.....	14
1.5.3 Immune Privilege	15
1.6 Diabetic Retinopathy.....	16
1.6.1 The Development and Progression of Diabetic Retinopathy ..	17
1.6.2 Retinal Damage Without Visible Abnormalities.....	18
1.6.3 Non-Proliferative Diabetic Retinopathy.....	18
1.6.4 Proliferative Diabetic Retinopathy.....	20
1.7 Prevention of Diabetic Retinopathy	22
1.7.1 Prevention by Glycaemic Control.....	22

1.7.2	Prevention by Blood Pressure Control	23
1.8	Management of Proliferative Diabetic Retinopathy	24
1.8.1	Laser Photocoagulation	24
1.8.2	Management: Vitrectomy.....	25
1.8.3	Anti VEGF-Agents	26
1.9	The Complement System.....	27
1.9.1	Complement Activation	27
1.9.2	Effectors of the Complement System	32
1.9.3	Regulation of the Complement System	33
1.9.4	Complement and Retinal Diseases.....	34
1.9.4.1	Complement and Age-Related Macular Degeneration.....	35
1.9.4.2	Complement and Diabetic Retinopathy	38
1.10	Summary	42
1.11	Aims and Objectives	43
2	Materials and Methods	45
2.1	Human Patient Samples.....	45
2.2	Animal Husbandry	45
2.3	STZ Diabetic Mouse Model	45
2.4	Oxygen-Induced Retinopathy (OIR) Mouse Model.....	46
2.5	Protein Isolation from Retinal Tissue	47
2.6	Sodium Dodecyl Sulphate Polyacrylamide Gel Electrophoresis (SDS-PAGE)	48
2.7	Western Blotting: Wet Transfer	48
2.8	Target Detection	49
2.9	Western Blot Stripping.....	50
2.10	RNA Isolation from Retinal Tissue.....	50
2.11	Quantification of DNA and RNA by Spectroscopy	51
2.12	First Strand cDNA Synthesis.....	51

2.13	SYBR® Green Real-Time PCR.....	51
2.14	Cell Culture Basics.....	52
2.15	Thawing Cells	52
2.16	Counting Cells.....	53
2.17	Primary Cells: Culture and Sub-Cultivation	54
2.18	Primary Cells: Cryopreservation.....	55
2.19	Freestyle 293-F Cells: Culture and Sub Cultivation.....	55
2.20	Freestyle 293-F Cells: Cryopreservation	56
2.21	Molecular Cloning of CFB Sequence.....	56
2.22	Polymerase Chain Reaction (PCR)	57
2.23	Agarose Gel Electrophoresis	57
2.24	PCR Product Purification.....	58
2.25	Restriction Digestion	58
2.26	Agarose Gel Purification.....	59
2.27	Ligation	59
2.28	Transformation	59
2.29	Mini-Prep.....	60
2.30	Freestyle 293-F Transfection.....	60
2.31	Protein Purification	62
2.31.1	Buffer Preparation	62
2.31.2	Protein Concentration	62
2.31.3	Buffer Exchange	63
2.31.4	Protein Binding	63
2.31.5	Elution.....	63
2.31.6	Dialysis	64
2.31.7	Protein Purity	65

2.32	Primary Cell Transfection: Small Interfering RNA (siRNA) Silencing	65
2.33	Primary Cell Transfection: CFB Over-expression	66
2.34	Growth factors and Inhibitor Treatments	66
2.35	Cell Viability Assay.....	67
2.36	Cell Proliferation Assay	68
2.37	Matrigel® Network Formation	69
2.38	Transwell Migration Assay	70
2.39	Aortic Ring Sprouting Assay.....	71
2.40	Fetal Metatarsal Sprouting Assay	73
2.41	RNA Isolation from Cell Lines	74
2.42	Biochemical Methods.....	75
2.42.1	Protein Isolation from Cell Lysates	75
2.43	Statistical Analysis.....	76
3	Results.....	77
3.1	Characterising the Expression of Complement Factor B Using Rodent Models and Human Patient Samples	77
3.2	The Role of CFB in Regulating Retinal Angiogenesis.....	81
3.3	Investigating the relationship between Complement Factor B and VEGF-A and VEGFR2.....	98
4	Discussion	106
4.1	Characterising the Expression of Complement Factor B Using Rodent Models and Human Patient Samples	107
4.2	The Role of CFB in Regulating Retinal Angiogenesis.....	111
4.3.	Investigating the relationship between Complement Factor B and VEGF-A and VEGFR2.....	114
5	Conclusion and Future Work.....	117
6	References	122

7	Supplementary Figures	142
8	Appendix	146
8.1	General Laboratory Equipment and Consumables	146
8.2	Buffers	149
8.2.1	General Laboratory Buffers	149
8.2.2	Recombinant CFB Protein Purification Buffers	150
8.2.3	Commercially Available Enzymes and Buffers	150
8.3	Primary and Secondary Antibodies	151
8.4	Culture Media	151
8.5	Molecular Biology Techniques	152
8.5.1	Ligation	152
8.5.2	Polymerase Chain Reaction	152
8.5.3	First Strand cDNA Synthesis	153
8.5.4	SYBR® Green Real-Time PCR	153
8.5.5	Sodium Dodecyl Sulphate Polyacrylamide Gel Electrophoresis (SDS-PAGE)	154

Abstract

The most advanced stage of diabetic retinopathy, proliferative diabetic retinopathy, is characterised by retinal neovascularization due to wide spread retinal ischemia. While laser photocoagulation has remained the gold standard treatment for decades, anti-vascular endothelial growth factor agents are now increasingly used to treat proliferative diabetic retinopathy. Although evidence supports the use of anti-vascular endothelial growth factor agents, there are several limitations to this treatment that suggest alternative therapies should be explored.

Poorly controlled complement activation is now associated with many pathologies, and recent evidence implicates complement dysregulation in the pathogenesis of several neovascular ocular diseases, including diabetic retinopathy. Although evidence that complement activation may contribute to vascular pathology is promising, crosstalk between the complement system and neovascularisation remains largely unclear. Taking a step back to understand the role of complement components in diabetic retinopathy would not only provide a more in-depth knowledge of the cellular and molecular mechanisms involved in disease pathogenesis, but it could also highlight novel therapeutic targets for DR and other vasoproliferative diseases in the eye.

Therefore, the objectives of the studies presented in this thesis were to test to test the hypothesis that complement has a novel function in angiogenesis which is separate from its characterised role as an immune surveillance system within the ocular environment. This work is specifically focused on exploring the role of the central component of the alternative complement pathway, complement factor B in regulating retinal angiogenesis.

Initially, CFB expression was characterised using rodent models and human patient samples. In the retina of STZ-induced diabetic mice there was no difference in CFB expression between buffer-injected controls and STZ-induced diabetic mice. Similarly, characterisation of systemic CFB levels in human

patient serum samples revealed no differences between control and diabetic patients at different stages of retinopathy. However, analysis of ocular CFB levels in human aqueous samples, revealed a higher expression in diabetic patients with retinopathy compared to diabetic patients without. The well-established mouse model of oxygen induced retinopathy was carried out to study CFB expression in pathologic vessel formation. RT-qPCR analysis demonstrated that CFB was significantly upregulated in mice retina subject to oxygen-induced retinopathy.

To establish the impact of CFB on retinal vascular cell function and angiogenesis, *in vitro* and *ex vivo* angiogenesis assays were carried out. Results demonstrate that CFB was able to promote human retinal endothelial cell viability, proliferation, tube formation, Transwell migration, and aortic ring sprouting, thus indicating a pro-angiogenic role of CFB.

Finally, to elucidate the mechanism through which CFB exerts its pro-angiogenic function the relationship between CFB and the VEGF signalling system was investigated using *in vitro* cultures of human retinal endothelial cells. Observations from these preliminary mechanistic studies revealed that CFB mediates VEGF gene expression, and VEGFR2 gene and protein expression. And that the pro-angiogenic function of CFB is upstream of, and acts through the VEGF signalling pathway.

Several reports have implicated complement and complement related proteins in the development of DR. However, few studies have investigated the more precise role played by CFB and the mechanism(s) by which complement mediates its tissue damaging effects. Collectively, results from this study clearly indicate a pro-angiogenic role of CFB in DR associated neovascularisation.

Acknowledgements

More than just research and writing has gone into this project. So many family, friends and colleagues have been part of the process, guiding me along the path that has gotten me here. Without each and every one of you I would not be where I am today. I love you all dearly.

I would like to start by thanking my Singapore supervisor, Dr Wang Xiaomeng, for your support and guidance during my time spent overseas. From my first day joining a new lab group in a new country you made me feel instantly welcome and continue to do so even now. This PhD would not have been possible without your knowledge, motivation, and vision. The experience I have had working as part of your group has been invaluable in helping me learn how to 'do research', and I will be forever grateful for the faith you have had in me. I would also like to express a huge thank you to my Sheffield supervisor, Dr Gwendolen Reilly. Thank you for taking a chance on me and taking me on board as a 'waif and stray' PhD student when it felt like I had nowhere else to go. Your overwhelming wisdom, enthusiasm, and encouragement has driven me to keep going, even through the toughest times.

It wasn't easy moving to a new country far away from home, so to the members of the XW lab group I want to say a huge thank you for the immense kindness and support you have shown me, and for all the knowledge you have shared. A special thank you goes to my mentor and friend, Beiying, for teaching me everything I need to know in the lab, and for guiding me through my first international conference. I am incredibly grateful for your patience and compassion. You are someone who I will continue to look up to and aspire to be like as a scientist.

To all my amazing friends, both back in the U.K and in Singapore (I wish I could name you all), your support and encouragement is worth so much more than I can express on paper. Thank you for always making me laugh, for always checking in to make sure I'm ok, for picking me up and dusting me down when

things have gotten hard, for loving me during both the good and the bad times, for being my voice of reason and instilling confidence, for celebrating every accomplishment no matter how small, for taking me into your homes and making sure I am well fed, and most importantly for always being around for a drink.

I owe a huge thanks to my family whose love and unwavering support has not only helped me through this PhD, but also through life in general.

A very special thank you goes to my incredible parents, Tina and Paul. I cannot thank you enough for providing me with the opportunity to be where I am today. You have forever encouraged me to pursue whatever makes me happy and your belief in me has given me the confidence that I can achieve whatever I put my mind to. I love you so much.

To my amazing sister, Bethan, thank you for being top cheerleader, constantly saying 'you've got this'. Thank you for the daily text messages that never fail to put a smile on my face. You are my best friend and number one partner in crime.

Lastly, these acknowledgments would be incomplete without thanking the biggest source of my strength, my boyfriend, Dr Jonathan Cox. Despite living in different countries, you have always been there for me. You have always had faith in me even when I didn't have faith in myself. I can confidently say the best outcome from these past four years has been meeting you.

I would like to dedicate this thesis to my wonderful Grandad who sadly passed away during the final months of my PhD. He was my biggest supporter and forever encouraged me in all my pursuits. I miss him incredibly. I hope this makes you proud.

List of Abbreviations

ACE	Angiotensin-Converting Enzyme
ADA	American Diabetes Association
AGE	Advanced Glycation End-Product
AMD	Age Related Macular Degeneration
ANOVA	One-Way Analysis of Variance
AP	Alternative Pathway
APC	Tolerance-Promoting Antigen-Presenting Cells
AR	Aldose Reductase
AR	Aldose Reductase
ARM	Aortic Ring Media
BM	Basement Membrane
BM	Basement Membrane
BRB	Blood Retinal Barrier
BRB	Blood-Retina Barrier
BSA	Bovine Serum Albumin
CGRP	Calcitonin Gene-Related Peptide
CNS	Central Nervous System
CNV	Choroidal Neovascularisation
CP	Classical Pathway
DAG	Diaglycerol
DAG	Diaglycerol
DCCT	Diabetes Control and Complications Trial
DM	Diabetes Mellitus
DMA	Macular Oedema
DR	Diabetic Retinopathy
DRS	Diabetic Retinopathy Study
EBM-2™	Endothelial Basal Media
EC	Endothelial Cell
ECM	Extracellular Matrix
EDIC	Epidemiology of Diabetes Intervention and Complications Study
EGM-2™	Endothelial Growth Medium
eNOS	Endothelial Nitric Oxide Synthetase
ETDRS	Early Treatment Diabetic Retinopathy Study
FA	Fluorescein Angiography
Fab	Recombinant Antibody Fragment
FAZ	Foveal Avascular Zone
FBG	Fasting Blood Glucose
FBS	Foetal Bovine Serum
FDA	Food and Drug Administration
FEM	Freestyle Expression Medium
GCL	Ganglion Cell Layer
GFAT	Glutamine: Fructose-6-Phosphate Amidotransferase
HbA1c	Haemoglobin A1c
HGF	Hepatocyte Growth Factor

HREC	Human Retinal Microvascular Endothelial Cell
IACUC	Institutional Animal Care and Use Committees
iBRB	Inner Blood-Retina Barrier
ILM	Inner Limiting Membrane
IMAC	Immobilised Metal Ion Affinity Chromatography
IMS	Industrial Methylated Spirit
INL	Inner nuclear Layer
IP	Intraperitoneal
IRMA	Intraretinal Microvascular Abnormalities
LB	Luria-Bertani
LP	Lectin Pathway
MAC	Membrane Attack complex
MBL	Mannose Binding lectin
MMP	Matrix Metaloproteinases
MnSOD	Manganese Superoxide Dismutase
NPDR	Non-Proliferative Diabetic Retinopathy
oBRB	Outer Blood-Retina Barrier
OIR	Oxygen Induced Retinopathy
ONL	Outer Nuclear Layer
PAI-1	Plasminogen Activator Inhibitor-1
PBS	Phosphate Buffered Saline
PCR	Polymerase Chain Reaction
PDR	Proliferative Diabetic Retinopathy
PFA	Paraformaldehyde
PKC	Protein Kinase C
PRP	Pan-Retinal Laser Photocoagulation
PVDF	Polyvinylidene Fluoride
qRT-PCR	Quantitative Real Time Polymerase Chain Reaction
RAGE	Advanced Glycation End-Product Receptor
RCULA	Responsible Care and Use of Laboratory Animals
RGC	Retinal Ganglion Cell
rhCFB	Recombinant Human Complement Factor B
ROS	Reactive Oxygen Species
RPE	Retinal Pigment Epithelium
SDS-PAGE	Sodium Dodecyl Sulphate Polyacrylamide Gel Electrophoresis
SEM	Standard Error of Mean
shRNA	Short Hairpin RNA
siRNA	Small Interfering RNA
SMC	Smooth Muscle Cell
SMC	Smooth Muscle Cell
STZ	Streptozotocin
TBST	Tris Buffered Saline 0.01% Tween
TCA	Tricarboxylic Acid Cycle
TGFβ	Transforming Growth Factor- β
tSNP	Tagging Single Nucleotide Polymorphism
UCP-1	Uncoupling Protein 1
UDP-GlcNAc	(Uridine Diphosphate)-N-Acetylglucosamine
UKPDS	United Kingdom Prospective Diabetes Trial
VEGF	Vascular Endothelial Growth Factor

VEGFR2
 α -MSH

Vascular Endothelial Growth Factor Receptor 2
 α -Melanocyte-Stimulating Hormone

List of Figures

Figure 1: Schematic representation of the basic structure of blood vessels.....	4
Figure 2: Schematic representation of Vasculogenesis.....	5
Figure 3: Schematic representation of angiogenesis and stabilisation.....	6
Figure 4: Schematic representation of sprouting angiogenesis	8
Figure 5: Schematic representation outlining the cellular circuitry of the retina and the retinal blood vessels.....	11
Figure 6: Retinal vasculature in normal and diabetic eyes.....	21
Figure 7: Clinical signs of DR in a fundoscopic examination	22
Figure 8: Schematic representation of the three pathways of complement activation	29
Figure 9: Schematic representation of the alternative pathway of complement activation	31
Figure 10: Schematic of the mouse model of OIR	46
Figure 11: Schematic outline of the rhCFB cloning strategy	57
Figure 12: CFB expression in the retina of STZ-induced diabetic mice.....	78
Figure 13: CFB expression in human patient serum samples	79
Figure 14: CFB expression in human patient aqueous samples.....	80
Figure 15: CFB gene expression in the retina of OIR mice	81
Figure 16: rhCFB treatment promotes HREC viability.....	83
Figure 17: CFB overexpression increases HREC viability	83
Figure 18: 1 CFB silencing reduces HREC viability.....	84
Figure 19: Recombinant CFB treatment promotes HREC proliferation	85
Figure 20: CFB overexpression promotes HREC proliferation.....	86
Figure 21: CFB knockdown reduces HREC proliferation.....	87
Figure 22: Recombinant CFB treatment promotes HREC transwell migration.	89
Figure 23: CFB silencing reduces HREC transwell migration	90
Figure 24: Recombinant CFB treatment promotes HREC network formation.	92
Figure 25: CFB overexpression promotes HREC network formation.	93

Figure 26: CFB silencing reduces HREC network formation.....	94
Figure 27: Recombinant CFB treatment promotes vessel outgrowth in the aortic ring explant assay.....	96
Figure 28: Recombinant CFB treatment promotes vessel outgrowth in the aortic ring explant assay.....	97
Figure 29: Recombinant CFB treatment induces VEGF-A and VEGFR2 mRNA expression.....	100
Figure 30: CFB silencing reduces VEGF-A and VEGFR2 mRNA expression.....	100
Figure 31: CFB silencing reduces VEGFR2 but not VEGF-A protein expression.....	102
Figure 32: Linifanib attenuates CFB induced HREC network formation..	105
Figure 33: A schematic representation of the proposed mechanism of action of CFB in retinal neovascularisation in DR.....	121
Figure 34: Transient transfection of HRECs using siRNA results in a downregulation of CFB mRNA expression.....	142
Figure 35: Transient transfection of HRECs results in an up-regulation of CFB mRNA expression.....	143
Figure 36: Linifanib treatment reduces HREC network formation in a dose dependent manner.....	145

List of Tables

Table 1: A table outlining the of the Key Regulators of Angiogenesis	9
Table 2: A table outlining the key membrane bound and soluble complement regulatory proteins	33
Table 3: List of general laboratory equipment used	146
Table 4: List of general laboratory consumables used	147
Table 5: List of general laboratory chemicals used.....	147
Table 6: List of general buffers and solutions used	149
Table 7: Sodium phosphate buffer components.....	150
Table 8: Stock buffers for binding and elution buffers.....	150
Table 9: List of enzymes and commercially available buffers/kits used..	150
Table 10: List of primary antibodies. IF - immunofluorescence WB- Western Blot.....	151
Table 11: List of secondary antibodies. IF - immunofluorescence; WB - Western Blot.....	151
Table 12: Summary of the composition of HREC EGM-2 media.....	151
Table 13: Summary of the composition of ex vivo assay media	152
Table 14: Summary of the Quick Ligation reaction components	152
Table 15: Summary of the PCR mastermix components.....	152
Table 16: Thermocycling conditions for PCR amplification	152
Table 17: Components of qScript® cDNA Supermix reaction	153
Table 18: Mouse primer sequences for RT-qPCR.....	153
Table 19: Human primer sequences for RT-qPCR.....	153
Table 20: SYBR® Green reaction volume composition.....	153
Table 21: RT-qPCR Cycling conditions.....	154
Table 22: Composition of SDS-PAGE gels	154

1. Introduction

Diabetes mellitus (DM) is a metabolic disease that has seen a dramatic increase over the past century, and with approximately 350 million people affected worldwide it is now considered to be a global epidemic^{1,2}: by 2035 this number is projected to increase to 600 million³. It can be defined as “a state in which homeostasis of carbohydrate and lipid metabolism is improperly regulated by insulin”⁴ and when sustained for a prolonged period this homeostatic imbalance ultimately leads to chronic hyperglycaemia⁵. Exacerbated by risk factors including genetics, hypertension and diet, chronic hyperglycaemia then acts through several downstream metabolic pathways to initiate vascular dysfunction⁶.

Vascular complications arising from diabetes the major causes of morbidity and mortality seen in diabetic patients^{7,8}, and they can be broadly categorised into macro- or microvascular diseases. Diabetes associated dysfunction affecting large arteries supplying the heart, the brain and lower extremities are major causes of myocardial infarction, stroke and lower limb amputation⁹. On the other hand, microvascular abnormalities can affect the retina (retinopathy), kidneys (nephropathy) and peripheral nerves (neuropathy)^{9,10}.

Of the three major manifestations of microvascular diseases, diabetic retinopathy (DR) is the most common, with an overall prevalence of over 40% in diabetic patients¹¹. It is a major cause of visual impairment and blindness in working age adults worldwide, representing a substantial burden to patients, their families, health-care systems, and national economies².

1.1 Our Vascular System

Blood vessels line the entire circulatory system and play a central role in mediating physiology and pathogenesis. The vascular network is an elaborate transport system to supply oxygen and essential nutrients to tissues, and to facilitate the removal of metabolic waste products¹². This process begins at the heart that pumps blood into hierarchical, organised vascular branches that span across multiple orders of magnitude (μM to cm)^{13,14}. The macrovasculature (including the arterial, venous, and lymphatic systems) regulates bulk oxygen delivery to accommodate systemic metabolic demands^{15,16}. On the other hand, the microvasculature network (including capillaries, pre-capillary arterioles, post-capillary venules and collecting venules) regulates local perfusion and conducts blood-tissue exchange of macromolecules^{15,17} (*please refer to **Figure 1***).

1.2 Anatomy of Blood Vessels

Studies of vessel architecture have reported similarities in the basic wall structure of most blood vessels^{18,19}. The innermost luminal wall, also known as the tunica intima, is comprised of a single layer of endothelial cells (EC)s, that align themselves in parallel to the blood flow. This layer, also known as the endothelium, is highly metabolically active and critically regulates vessel homeostasis by governing the expression of a multitude of signalling molecules that regulate vessel permeability, vascular tone, extramural cell growth and migration, inflammatory responses and haemostatic function^{18,20,21}. Endothelial phenotypes vary between species, organs, vascular bed, and spatial and temporal distribution¹⁷. ECs demonstrate remarkable heterogeneity in cell morphology, function, gene expression, and antigen composition to serve specialised functions based on the physiological needs in the local microenvironment^{22,23}. For example, the ECs found in the retinal microcirculation are non-fenestrated and tightly associated to form the blood-

retinal barrier that restricts paracellular and transcellular movement of solutes to maintain retinal homeostasis and proper retinal function. On the contrary, the glomerular endothelium is highly fenestrated to regulate high flux filtration of fluid and small solutes^{15,24}. The endothelial layer is the only common cellular component of capillaries, the simplest vascular structures with the smallest diameter²⁵. Ensheathing the endothelium is the tunica media layer which contains mural cells (smooth muscle cells, pericytes, and fibroblasts) sharing a common basement membrane with the ECs^{26,27}. In the macrovascular circulation layers of vascular smooth muscle cells (vSMC)s wrap around macrovascular ECs to provide mechanical support and to regulate vascular tone and blood flow²⁸. Instead of vSMCs, a discontinuous coat of pericytes (PC)s surround the microvascular ECs²⁹. The PC:EC ratios, ranging from 1:1 and 1:10, differs across different tissue beds, often found to be enriched at the EC-EC junctions and branch points. Just like ECs, the perivascular cells also feature distinct morphology, protein expression profile and functional plasticity³⁰. For instance, mesangial cells are specialised renal pericytes that participate in ultrafiltration at the glomerulus, whereas hepatic stellate cells are specialised hepatic pericytes with additional fat-storing capacities³¹.

Lastly, large calibre arteries and veins are wrapped in an additional layer known as the outer tunica adventitia which contains a collagen-rich ECM and interacting cell types including quiescent fibroblasts, nerve cells, resident macrophages, T-lymphocytes, B-lymphocytes, mast cells, and dendritic cells^{31,32}. Besides providing mechanical support to the blood vessel, it serves as a biological compartment facilitating the retrieval, integration, storage and release of key regulators that are critical for blood vessel activation and homeostasis³³. Moreover, recent studies also suggested that this outermost layer of the blood vessel also functions as a niche for resident vascular progenitor cells³².

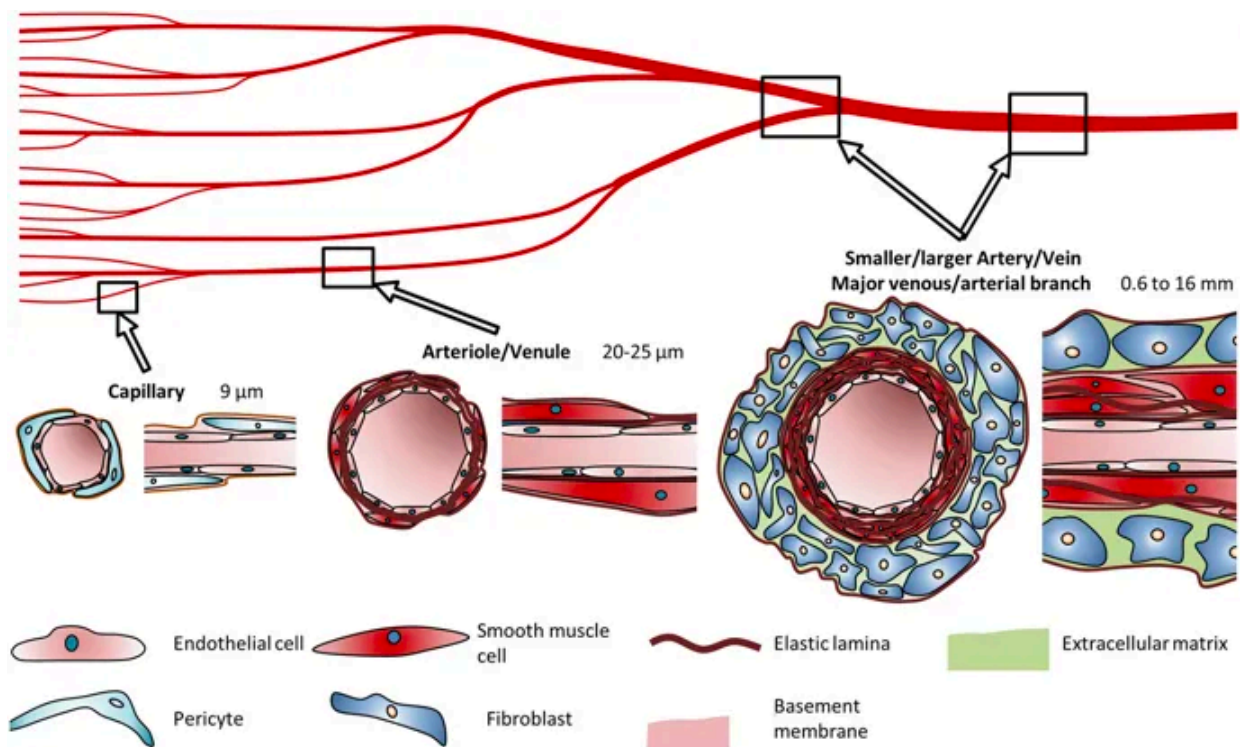


Figure 1: Schematic representation of the basic structure of blood vessels. Blood vessels are organised as capillaries, arterioles and venules, or arteries and veins. Capillaries are the most abundant blood vessels in our body. They consist of ECs surrounded by pericytes embedded within the EC basement membrane. Arterioles and venules SMCs that are able to contract and regulate blood flow. Besides the endothelium and mural cell layers, arteries and veins contain an additional layer of connective tissue with a mixture of different cell types. (Adapted from Nature: Scientific Reports, volume 8, pages 1-13 (11th July 2018)³⁴ <https://creativecommons.org/licenses/by/4.0/>)

1.3 Blood Vessel Formation

Blood vessel formation is a highly complex and tightly regulated process that results in the establishment of a vasculature that supports vital systems of the body. The cardiovascular system is the first organ system to form during embryonic development³⁵ however at the earliest stage of vertebrate embryogenesis the embryos develop in the absence of a functional vascular

network with nutrients and waste products being exchanged by passive diffusion³⁶. From the third week of gestation a functional vascular network begins to form to ensure an adequate supply of oxygen, nutrients and growth factors, and enable efficient removal of waste products from growing embryos³⁷. During this time *de novo* blood vessel formation occurs through the differentiation of mesenchymal cells into ECs in a process termed vasculogenesis³⁸ (please refer to **Figure 2** for a schematic representation of *vasculogenesis*). Mesodermal progenitor cells in the mesodermal compartment of the developing embryo give rise to groups of homogenous cells termed hemangioblasts or blood islands. During proliferation and differentiation, cells in the centre of these blood islands give rise to hemopoietic stem cells (HSCs) and cells on the periphery give rise to endothelial progenitor cells (EPCs)³⁹. As blood islands merge, the HSCs develop into blood cells and the EPCs form a primitive vascular plexus of small capillaries. Once a primitive vascular network is formed it then expands by angiogenesis and subsequently matures into a system of stable vessels⁴⁰.

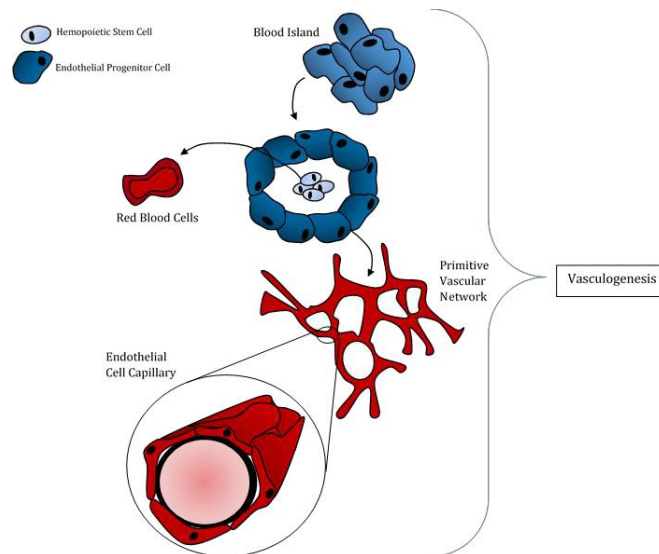


Figure 2: Schematic representation of Vasculogenesis. Vasculogenesis is the *de novo* formation of the first capillaries. Aggregations of cells called blood islands form in the embryonic yolk sac. They contain a homogenous collection of cells called hemangioblasts that develop into hemopoietic stem cells (HSCs) and endothelial progenitor cells (EPCs). Blood islands merge: HSCs develop into blood cells and EPCs develop into a primitive capillary plexus.

1.4 Angiogenesis

Angiogenesis is the growth of blood vessels from the existing vasculature. It occurs throughout life in both health and disease. Mature vessels are quiescent in nature and only transit into an activated state during specific growth periods, or in response to tissue injury²⁸. Once a primitive vascular network is formed via vasculogenesis, it progressively expands and remodels via angiogenesis giving rise to a mature, highly organised system of stable blood vessels. This process can be split into two distinct processes; sprouting and non-sprouting (intussusceptive) angiogenesis (*please refer to **Figure 3***).

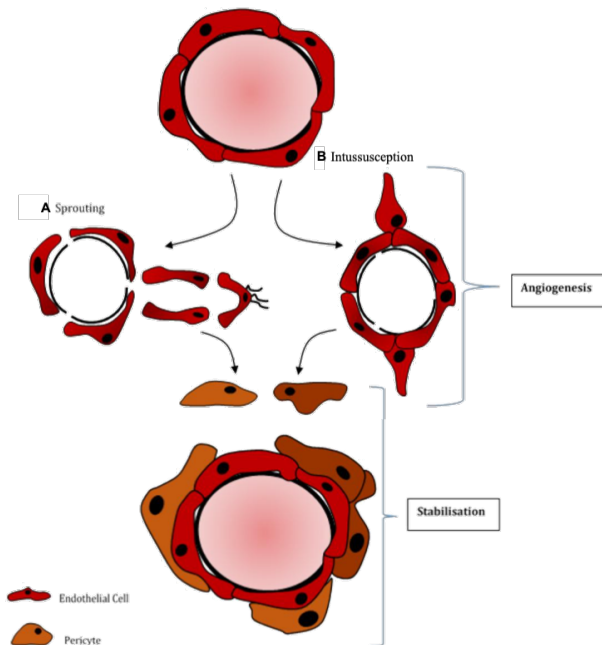


Figure 3: Schematic representation of angiogenesis and stabilisation. A, Sprouting angiogenesis. ECs sprout from the parent vessel by proliferation and migration, extending into the surrounding matrix. ECs proliferate to elongate the sprout and eventually fuse with others to form a closed loop, allowing for the initiation of blood flow. **B,** Intussusceptive angiogenesis. New blood vessels are created by splitting of an existing blood vessel. ECs on opposite sides of a capillary protrude into the lumen until they form contacts. These contacts form an EC bilayer which is then reorganised so that it becomes perforated at the centre. After angiogenesis stabilisation occurs whereby pericytes are recruited to stabilise the neo-vessel so that it becomes fully functional.

1.4.1 . Intussusceptive Angiogenesis

A variant of angiogenesis is intussusceptive angiogenesis whereby vessels are divided into two via the formation of intraluminal pillars and splitting of the lumen⁴¹. Briefly, ECs situated on opposite sides of a capillary protrude into the lumen until they form contacts, also known as intraluminal pillars. These contacts, strengthened by the formation of inter-endothelial junctions, form an EC bilayer which is then reorganised in such a way that it becomes perforated at the centre. Finally, ECs retract and the newly formed pillar is invaded by fibroblasts and pericytes which lay down collagen fibrils, causing the pillar to increase in size. Unlike sprouting angiogenesis EC proliferation is not a critical part of this process⁴¹; initially it only requires reorganisation of existing ECs. As a result, intussusception is a fast and efficient process. Since intussusception is a reorganisation of existing cells it allows for a large increase in the number of capillaries without the need for a corresponding increase in the number of ECs. This is especially important in the developing embryo as there are not enough resources to create a rich microvasculature with new cells each time a vessel develops. In addition to forming new capillary structures, intussusceptive growth plays a major role in branching geometry and vascular pruning of larger vessels^{42,43}. The first *in vivo* documentation of intussusceptive microvascular growth was demonstrated by video microscopy in a chick chorioallantoic membrane. Since then this process has been detected in other organs, tissue repair processes and also in tumour angiogenesis.

1.4.2 . Sprouting Angiogenesis

The term angiogenesis was first coined by John Hunter in 1787^{44,45}. It is commonly used to describe the process of vascular growth, but in the strictest sense it refers to the growth of new blood vessels from pre-existing vasculature⁴⁶. It results in new vessels composed of ECs that branch out from a parent vessel by proliferation and migration, extending into the surrounding matrix³⁹. In response to stimulatory signals, ECs become activated and vascular

permeability increases which allows for the invasion of plasma proteins that lay down an ECM framework. Matrix metalloproteinases (MMPs) are also induced to degrade the basement membrane by proteolytic degradation allowing pericytes to liberate themselves from the vessel wall⁴⁷. Once the path has been cleared, proliferating ECs migrate onto this provisional ECM and form an endothelial sprout⁴⁸. To build a perfused tube a single EC (tip cell) leads the sprout, whilst subsidiary ECs (stalk cells) proliferate to elongate the sprout and establish a lumen⁴⁹. To allow for the initiation of blood flow, tip cells at the leading edge of endothelial sprouts fuse with one another forming a closed loop⁵⁰. Finally, for a blood vessel to become fully functional it is stabilised by pericytes, which in the final stages of angiogenesis are recruited to the neo-vessel, laying down a basement membrane and thus reinforcing vascular structure⁵¹ (please refer to **Figure 4** for a schematic representation of sprouting angiogenesis).

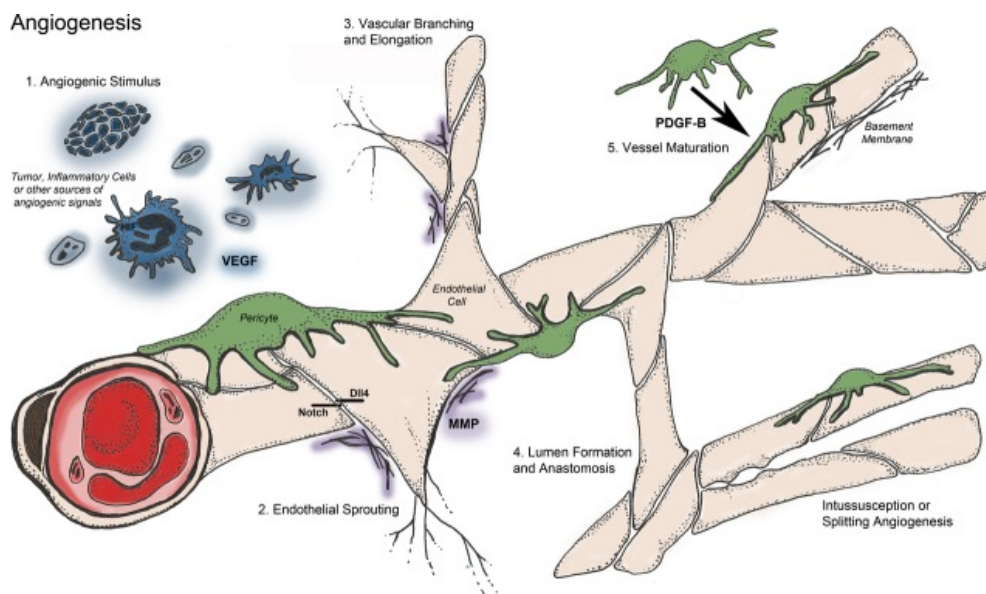


Figure 4: Schematic representation of sprouting angiogenesis. Sprouting angiogenesis begins with **1** ED activation upon exposure to an angiogenic stimulus, **2** EC sprouting initiation mediated by basement membrane degradation and ECM remodelling, followed by **3** EC proliferation and directed migration leading to vascular outgrowth and stlk extension. The nascent vessel undergoes **4** lumen formation and anastomosis before finally undergoing **5** maturation and stabilisation by mural cells. (Adapted from Journal of Cellular and Molecular Medicine, volume 18, pages 1491-1508 (2nd September 2014)⁵² <https://creativecommons.org/licenses/by/4.0/>)

1.4.3 Regulating Angiogenesis

To put simply, vascular development can be broken down into the following processes; formation, stabilisation, branching, remodelling and maturation. In order to develop without a glitch these processes are tightly regulated by a fine balance of molecular mechanisms, and perturbation of this balance can lead to excessive or insufficient angiogenesis. Abnormal blood vessel growth, whether it be too much or too little is now recognised as a common denominator underlying many disease states⁵³. The importance of angiogenesis in health and disease has prompted extensive investigations to identify the multitude of molecular regulators that are fundamentally important in this process (*please refer to **Table 1** for examples of key regulators and inhibitors of angiogenesis*). With rapid advancements in the cellular and molecular biology of angiogenesis, many of these angiogenic agents are now rigorously examined for their biological activities, clinical efficacies and safety to translation into therapeutic benefits⁵⁴.

Table 1: A table outlining the of the Key Regulators of Angiogenesis (Adapted from Postgraduate Medical Journal, volume 81, pages 236-242 (5th April 2005)⁴⁵)

Activators	Inhibitors
Angiogenin	Angiostatin (plasminogen fragment)
Angiopoietin-1	Anti-angiogenic anti-thrombin III
AC133	Canstatin
Chemokines*	
Del-1	Cartilage derived inhibitor (CDI)
β-estradiol	CD59 complement fragment
Ephrins	Endostatin (collagen XIII fragment)
FGF-αβ	Fibronectin fragment
FGF	Fragment of SPARC
Follistatin	Heparinases
HGF	HCG
Id1/Id3	IFN-αβγ
Integrins, αVβ3, αVβ5, α5β1	Interferon inducible protein (IP-10)
IL8	IL4, IL12, IL18
Leptin	2-methoxyestradiol
MCP-1	Maspin
MMPs	Kringle-5 (plasminogen fragment)
NOS	Osteopontin fragment
PLGF	Placental ribonuclease inhibitor
PDGF-BB	Plasminogen activator inhibitor
Pleiotrophin (PTN)	PEDF (pigment epithelium derived growth factor)
Platelet derived endothelial cell growth factor (PD-ECGF)	PF4
P1GF	
Proliferin	Prolactin 16 kDa fragment
TGF-αβ*	Retinoids
TNF-α	Tissue inhibitor of metalloproteinases (TIMPs)
VE cadherin	TSP-1
VEGF	Vasculostatin

1.4.4 Vascular Endothelial Growth Factor

The VEGF family of growth factors is the most well-recognised family of pro-angiogenic regulators for their pivotal role in endothelial functions. In mammals, the family consists of five members; VEGF-A – VEGF-D and placental growth factor (PlGF). VEGF-A, the prototypical ligand, was originally discovered as vascular permeability factor (VPF) in the late 1980's⁵⁵ and in 1989 it was characterised and sequenced by different groups of investigators as an endothelial growth factor and renamed as VEGF⁵⁶. In humans VEGF-A is encoded by a single gene with eight exons and seven introns, which can be alternatively spliced into at least nine major variants including VEGF₁₂₁, VEGF₁₄₅, VEGF₁₄₈, VEGF₁₆₂, VEGF₁₆₅, VEGF₁₈₃, VEGF₁₈₉, and VEGF₂₀₆⁵⁷. These variants differ in their bioavailability and interaction with VEGF receptors, leading to distinct effects in angiogenesis^{58,59}. VEGF₁₆₅ is regarded as the most predominant and biologically potent isoform of VEGF in promoting angiogenesis and EC permeability^{60,61}.

VEGF family members transduce their signal intercellularly by binding to membrane-bound tyrosine kinase receptors, VEGF receptor (VEGFR-) 1 to 3. VEGFR-1 and VEGFR-2 are mainly expressed on ECs, although other cell types can also express these receptors⁶². The biological activities of VEGF-A are controlled mainly by the receptor VEGFR-2⁶³. The binding of VEGF to VEGFR-2 induces downstream receptor dimerization and auto-phosphorylation of specific tyrosine residues within the dimeric complex^{64,65}. Subsequently, activation of specific intracellular signalling transducers eventually up-regulate target genes that facilitate EC proliferation, migration, adhesion, lumenisation, and survival^{64,66}.

1.5 The Retina

1.5.1 Basic Anatomy

The retina is an extension of the forebrain. It is consisted of a dense layer of specialised cell bodies separated by layers of neurites (*please refer to **Figure 5** for a schematic representation of the retinal structure*).

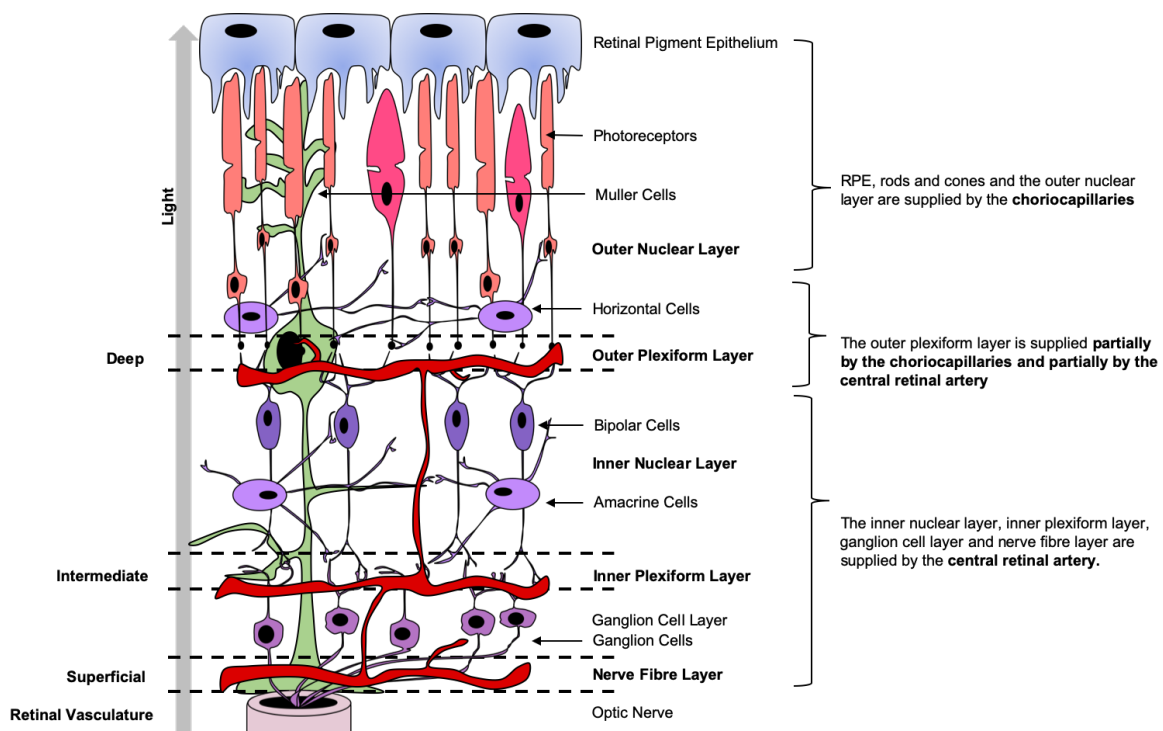


Figure 5: Schematic representation outlining the cellular circuitry of the retina and the retinal blood vessels. Light detected by the retina is absorbed by photoreceptors, converted to electrical signals, and transmitted through the retinal layers via an intricate network of neuronal cells, made up largely of bipolar and ganglion cells. The signals converge at the optic disc and are conveyed to the brain for further processing by the optic nerve. Retinal blood vessels line the inner surface of the retina. Three capillary plexuses are embedded among retinal neurons: the superficial layer lies within the nerve fibre layer (NFL) with branches extending into the ganglion cell layer (GCL), while the intermediate and deep capillary plexuses align along each sides of the inner nuclear layer (INL). (Adapted from Progress in Retinal and Eye Research, volume 5, pages 1-40 (23 June 2015)⁶⁷ and Frontiers in Physiology, volume 9, pages 1-14 (13 July 2018)⁶⁸ <https://creativecommons.org/licenses/by/4.0/>).

It functions to absorb photons of light entering the eye through the cornea and iris, translating these into biochemical and electrical signals which ultimately trigger nerve impulses that are sent to various visual centres of the brain through the fibres of the optic nerve. The vitreous side of the retina is referred to as the 'inner' layer, while the side of the retina closer to the sclera is referred to as the 'outer layer'.

The macula, defined by the area that contains the yellow pigment xanthophyll⁶⁹, is a small but important area in the centre of the retina. The fovea, found at the centre of the macula, is a highly specialised region responsible for visual acuity⁶⁹. It contains the highest density of cone receptors (reaching more than 200,000 mm²)⁷⁰ and its most obvious feature is a small depression known as the foveal pit, in which the inner retinal layers are displaced to allow direct illumination of the photoreceptors. The fovea is also comprised of an area lacking a vascular supply, this region is called the foveal avascular zone (FAZ)⁷¹. Since incoming light has to pass through the entire retina before it reaches the photoreceptors cellular elements can cause retinal light scattering, which consequently reduces visual sensitivity and acuity, and decreases the quality and brightness of the visual image⁷². The unique characteristics of the fovea help reduce the transparency of the retina which improves visual acuity by minimising retinal light scattering^{72,73}.

Retinal cells can be grouped into three general types; photoreceptor cells, neural cells, and glial cells. Moving from the outer to inner retina, the two specialised photoreceptor cells (rods and cones) lie outermost in the retina forming the outer nuclear layer (ONL). They are composed of a membranous disk containing a photoreceptive pigment which absorbs photons from incoming light leading to electrical polarisation, which initiates a sensory cascade that stimulates the succeeding neurons of the retina, allowing a neural signal to be fed to the brain via the optic nerve in a process known as visual photo-transduction⁷⁴.

Neural cells of the retina include bipolar, ganglion, horizontal and amacrine cells. Bipolar cells form synaptic contacts with the photoreceptors⁷⁵. They are arranged between photoreceptor cells and ganglion cells in the inner nuclear layer (INL), receiving their information from photoreceptors and relaying this information to the ganglion cell layer (GCL) for further processing⁷⁵. Horizontal and amacrine cells are found in the outer and inner retina respectively, and they help modulate signals along this 'vertical' pathway (from photoreceptor to bipolar cells)⁷⁶. The final output neurons of the retina are ganglion cells in the GCL, where all visual information converges. They transmit information through the optic nerve into the brain's visual centre for vision perception.

The three main types of glial cells in the mammalian retina are Müller cells, astrocytes, and resident microglia⁷⁷. They provide structural support and help maintain retinal homeostasis by providing metabolic support to retinal neurons through releasing neurotrophic factors and phagocytosing neuronal debris⁷⁸. The principal glial cells, Müller cells, are homogeneously distributed throughout the retina; they have their cell bodies within the INL and span across the entire thickness of the retina. They support neuroretinal architecture and provide nourishment to all the constituent cells⁷⁹. Müller cells also help redistribute metabolic waste of the photoreceptor activity⁷⁷. Astrocytes, named after their stellate morphology are located almost exclusively in the innermost GCL⁸⁰. The presence and distribution of retinal astrocytes is correlated with the presence and distribution of retinal blood vessels⁸¹: vascularised areas of the retina contain high numbers of astrocytes whereas avascular regions contain no astrocytes⁷⁷. As the main producers of vascular endothelial growth factor (VEGF) during normal and pathological vascularisation⁸², they are strongly implicated in the proper development and functioning of the retinal vasculature⁸³. As with Müller cells, astrocytes mediate the survival of retinal cells through the release neurotrophic factors. They also provide anti-oxidative support, aid in the formation and removal of synapses and are involved in the maintenance of the blood retinal barrier (BRB)⁸⁴. However, in the presence of pathogenic stimuli, astrocytes up-regulate their expression of various genes

encoding cytokines, chemokines and elements of the complement cascade, thereby compromising the integrity of the BRB⁸⁵. When activated, astrocytes are also able to cause activation of the third class of glial cells, the microglia⁸⁶. Microglia represent the tissue macrophage population of the central nervous system (CNS)⁶⁷. They are the only haematopoietic cells within the CNS. During development these cells enter from the bloodstream, develop from myeloid progenitors and differentiate into microglia⁸⁷. As a result, they maintain numerous cellular antigens present in macrophages and monocytes^{87,88}. In the healthy retina, microglia are described as 'resting' or 'ramified'. They have extensively branched processes and act as surveillant cells that continuously monitor the surrounding tissue. When the retina becomes diseased or damaged microglial cells become activated and their morphology is significantly different to those found in healthy tissue. Activated microglia have enlarged cell bodies, shortened processes, and increased expression of myeloid markers⁸⁷. Microglia are the resident inflammatory cells in the retina. On activation they respond by secreting cytokines, growth factors and neurotrophic factors⁸⁹. They can be stimulated into a macrophagic function and engage in phagocytosis of degenerating retinal neurons. In addition, they can also express molecules that are associated with an ability to stimulate T cells with antigen presentation^{87,90}.

1.5.2 Retinal Vasculatisation

The adult retina is a highly metabolic tissue with the highest oxygen consumption per unit weight of any human tissue⁹¹. To meet these high metabolic demands without obstructing light transmission, the retinal circulation is highly specialised⁹². It originates from two sources, the retinal and choroidal vessels, both of which arise from the ophthalmic artery⁹³. The choroidal vasculature, between the RPE and sclera, supplies oxygen and nutrients to the RPE and the photoreceptors. The inner retinal cells however, receive nutrients and oxygen from the central retinal artery (CRA) which receives 20-30% of the ocular blood flow. The CRA enters the eye at the optic nerve head⁹⁴ where it branches into two major trunks, the superior and inferior arteries. These then

divide further to form the nasal and temporal branches that supply the four quadrants of the retina. As the large arteries extend within the retina toward the periphery they continue to bifurcate, forming arteries with progressively smaller diameters that provide a blood supply to the inner retinal layers. These smaller arterioles give rise to two types of capillary systems: horizontal branches that supply the GCL and deep branches that enter the INL. Venous outflow from the retina begins with drainage from the capillary network by venules and veins, which run from the peripheral retina towards the optic nerve head. They coalesce into the central retinal vein, and exit the eye parallel and counter-current to the central retinal artery with the optic nerve⁹⁵.

1.5.3 Immune Privilege

The human body is protected from the invasion and damage of pathogens by a highly evolved and complex immune response. However, these destructive responses not only target invading pathogens but also attack host tissues, which impose devastating consequences. To maintain optical stability, the retina is protected by a sophisticated system that allows it to have immune privilege meaning the body's normal inflammatory immune response is limited. This system is made up of physical barriers, an inhibitory microenvironment composed of cell-bound and soluble factors, and tolerance-promoting antigen-presenting cells (APCs)⁹⁶.

Firstly, the retina is protected by two barriers that help to maintain a highly regulated chemical environment. The outer blood-retina barrier (oBRB) is achieved by the RPE cell layer and acts as a filter to regulate the movement of solutes and nutrients from the choroid to the sub-retinal space^{97,98}. The inner blood-retina barrier (iBRB) comprises the retinal vasculature and is formed by the endothelial cells (ECs) that line the lumen of retinal blood vessels⁹⁹. Both the oBRB and iBRB owe their functionality to the tight junctions that are located on the basolateral side between RPE cells and ECs, respectively¹⁰⁰. Tight junctions are transmembrane and cytosolic proteins that create a highly

selective barrier, allowing exchange of respiratory gases, amino acids, salts and sugars, but preventing circulating cells, macromolecules and pathogens from permeating the retinal parenchyma¹⁰¹. In a process known as immunological ignorance, the BRB segregates retinal antigens within the intraocular compartment thereby avoiding T cell activation and creating a functional absence of interactions between the immune system and retinal antigens¹⁰². Secondly, the retina lacks a lymphatic system, so endogenous insults are unlikely to be detected by circulating or choroidal/extraocular immune cells^{101,103}. Finally, the retina possesses an immune regulatory system that is carried out by cells in the local microenvironment. These cells can inhibit the activity of myeloid cells by binding to their ligands *via* the expression of various cell-bound membrane receptors. In this manner activated cells that might otherwise attack and destroy retinal tissue are neutralised, and the retina is spared injury. In addition, retinal cells also possess mechanisms to induce the death of infiltrating immune cells^{104,105}. Soluble factors secreted into the retina is another immunosuppressive mechanism that inhibits the activity of immune-competent cells. Transforming growth factor - β (TGF- β) for example, is a potent suppressor of the activation of T cells, natural killer cells and macrophages¹⁰⁶. Other factors include calcitonin gene-related peptide (CGRP) and α -melanocyte-stimulating hormone (α -MSH), which act on activated macrophages and prevent them from secreting pro-inflammatory cytokines¹⁰⁶.

1.6 Diabetic Retinopathy

Broadly speaking, diabetes mellitus (DM) is a class of metabolic diseases characterised by chronic hyperglycaemia¹⁰⁷. Epidemiologically, DM exists as a major public health problem that has reached an epidemic globally^{108,109}. It has been projected that the number of patients with DM is estimated to increase from 382 million in 2013 to 592 million by 2035¹¹⁰. In addition to the alarming magnitude of DM, around 50% of patients with diabetes are undiagnosed¹¹¹ and these patients are likely to have a faster degree of progression because of the delay in diagnosis and treatment¹¹¹.

DM has a poignant role in the development of diabetic microvascular complications including diabetic nephropathy, neuropathy and retinopathy¹¹². DR, the most common microvascular complication of DM, is a major cause of vision loss in working-age population worldwide. The overall prevalence of DR in adults with DM is greater than 40%, with approximately 7% developing advanced stage, vision threatening proliferative diabetic retinopathy (PDR)¹¹³. The prevalence of DR increases with prolonged duration of diabetes¹¹⁴ and with recent improvements in reducing diabetes-related macrovascular mortality more patients live long enough to develop DR¹¹⁵: over 50% of patients who have had DM for over 25 years will develop DR¹¹⁶. As the global prevalence of DM continues to increase, the number of DR patients is expected to increase from 37.3 million in 2010 to 56.3 million by 2030¹¹⁷, bringing with it substantial economic loss to patients, families, health-care systems and national economies.

1.6.1 The Development and Progression of Diabetic Retinopathy

DR is a progressive disease of the retina characterised by a complex pathogenesis involving multiple cell types, molecules, and growth factors¹¹⁸. The defining features of DR include thickening of the basement membrane shared between ECs and pericytes, pericyte loss, EC hyperpermeability, microaneurysm and local tissue ischemia which triggers abnormal vessel formation in the eye ultimately leading to visual impairment and blindness. The development of DR is slow and can be categorised into stages: retinal damage without any visible microvascular abnormalities; non-proliferative retinal microvascular changes referred to as non-proliferative diabetic retinopathy (NPDR); advanced proliferative DR (PDR) (*please refer to **Figure 6** and **Figure 7***).

1.6.2 Retinal Damage Without Visible Abnormalities

Traditionally DR has been viewed as a microcirculatory disease of the retina, however more recently it is now considered to be a more complex complication of diabetes in which neurodegeneration plays a role¹¹⁸. Neuroretinal damage leads to diminished retinal functions such as the loss of chromatic discrimination and contrast sensitivity, delayed dark adaptation, and abnormal visual fields^{119,120}. Rather than an early event of DR progression neurodegeneration was believed to be a late manifestation, however these alterations have been observed to occur in patients without or with only minimal DR, i.e. early in disease progression before vascular pathology is detected in ophthalmic examination¹²¹⁻¹²⁴. As a result it is now believed to predate and also participate in the development of microcirculatory abnormalities that occur in DR¹²⁵.

The two hallmark features of retinal neurodegeneration are neural apoptosis and glial activation¹²⁶. Neural apoptosis is first detected in retinal ganglion cells (RGCs) located in the inner retina, and consequently their loss results in a reduction in thickness of the GCL¹²⁷. Neural apoptosis is accompanied by glial cell dysfunction, referred to as glial activation or reactive gliosis. Glial activation is the general response to injury and inflammatory stimuli in glial cells, and causes neuronal damage *via* early phagocytosis of normal neurons, production of neurotoxins and induction of apoptotic changes¹²⁸. No consensus has been reached as to which of these elements (apoptosis or glial activation) is the first to occur. Nevertheless, these two mechanisms are critical in maintaining neuronal integrity which is essential for maintaining the normal functioning of the retina¹²⁹.

1.6.3 Non-Proliferative Diabetic Retinopathy

The earliest vascular change observed in the retina is capillary degeneration, which is characterised by BM thickening, endothelial injury leading to disruption of tight junctions, and pericyte loss. Pericytes are specialised peri-vascular

support cells that exist in close proximity to ECs, at an almost 1:1 ratio in the retina¹³⁰. They elongate and wrap around the endothelium, sharing a basement membrane¹³¹. Pericytes fulfil important functions including, regulation of vascular diameter and capillary blood flow, vessel stabilisation and maintenance of the BRB¹³². In addition, pericytes release TGF- β which acts on neighbouring ECs, inhibiting their proliferation and maintaining them in a quiescent state¹³³. Pericytes are therefore essential components of the microvessel and are crucial for normal EC function, vessel stability and blood flow regulation¹³⁴. The death of vascular retinal pericytes in DR results in the formation of 'ghost capillaries'. Without the protection of pericytes, ECs become activated and proliferative leading to the development of microaneurysm and vessel dilation. They eventually rupture to form haemorrhages deep within the retina. Because of their dot-like appearance, they are sometimes referred to as "dot-and-blot" haemorrhages. Microaneurysms and dot intraretinal haemorrhages are the first clinically detectable abnormalities seen in DR¹³⁵. Loss of pericytes also affects the integrity of the BRB, allowing the passage of intravascular fluid containing proteins, lipids, and inflammatory mediators into the interstitial space. This fluid leaves behind yellow deposits composed of extracellular lipid by-products that are referred to as hard exudates. Diabetic macular oedema (DME) is another consequence of these abnormalities and is caused by the leakage of plasma from the small blood vessels into the macula. During NPDR the retinal endothelium also becomes activated, inducing the release of pro-inflammatory cytokines leading to early and persistent inflammatory condition in the retinal microenvironment. This promotes leukocyte activation, leukocyte adhesion to the vascular endothelium¹³⁶ and further BRB breakdown, contributing to the obstruction of retinal capillaries¹³⁷. The microvascular BM is a thin sheet of ECM with an intricate architecture that serves as part of the barrier to control vascular permeability. It provides a mechanical framework on which cells reside, a substrate for adhesion and inter-cellular communication, and a selective barrier to filtration¹³⁸. In DR, the BM becomes thickened because of increased synthesis and reduced degradation of its components (type IV collagen, laminin, fibronectin, heparan sulphate proteoglycans)¹³⁷. These structural and

compositional alterations to the BM impaired oxygen and nutrient delivery to pericytes contributing to pericyte dropout¹³⁹.

As the severity of NPDR progresses, gradual non-perfusion of the retinal vascular bed increases, which ultimately results in regions of retinal ischemia. As demonstrated by fundoscopic examination, eyes with severe NPDR show 'cotton wool' spots, indicating a large area of retinal ischaemia or infarction¹³⁶. Intraretinal microvascular abnormalities (IRMA) are also observed in severe NPDR, which are characterised by dilate vessels that are tortuous and irregular in calibre¹³⁶.

1.6.4 Proliferative Diabetic Retinopathy

The most advanced stage of DR, PDR, is characterised by aberrant angiogenesis. In the eye, highly vascular structures and completely avascular structures lie in close proximity to each other¹⁴⁰ (a feature most obviously depicted in the fovea), therefore tight regulation of vascular growth and quiescence is crucial to the maintenance of healthy retinal tissue and visual acuity^{140,141}. Vascular growth occurs mainly during embryonic development and is almost non-existent in the adult eye¹⁴⁰, therefore the formation of new blood vessels in the retina represents cases where this delicate balance has been disturbed¹⁴². The main pathogenetic factor involved in PDR is chronic hypoxia, which is a potent inducer of tissue angiogenesis. The hypoxic environment results in an over-expression of growth factors, cytokines, chemokines and adhesion molecules, which together constitute a complex inflammatory response that results in aberrant, pathological angiogenesis (*please refer to section 1.4.2. for a more detailed description of the angiogenic process*). Pathological retinal angiogenesis generates chaotically orientated and physiologically deficient vessels that are fragile and leaky, and are unable to perfuse the ischemic tissue, which further exaggerates the ischemic burden of the affected retina leading to vicious cycle of tissue hypoxia and neovascularization. Furthermore, these new vessels are prone to bleeding and

tend to grow into the vitreous body. With age the vitreous begins to shrink, pulling on these fragile vessels and causing them to tear, which ultimately results in vitreous haemorrhage. Sometimes, these new vessels may become enveloped by a thick and dense fibrovascular tissue causing tractional retinal detachment. In the advanced stage of DR retinal detachment and vitreous haemorrhage represent the major causes of visual impairment and sudden vision loss.

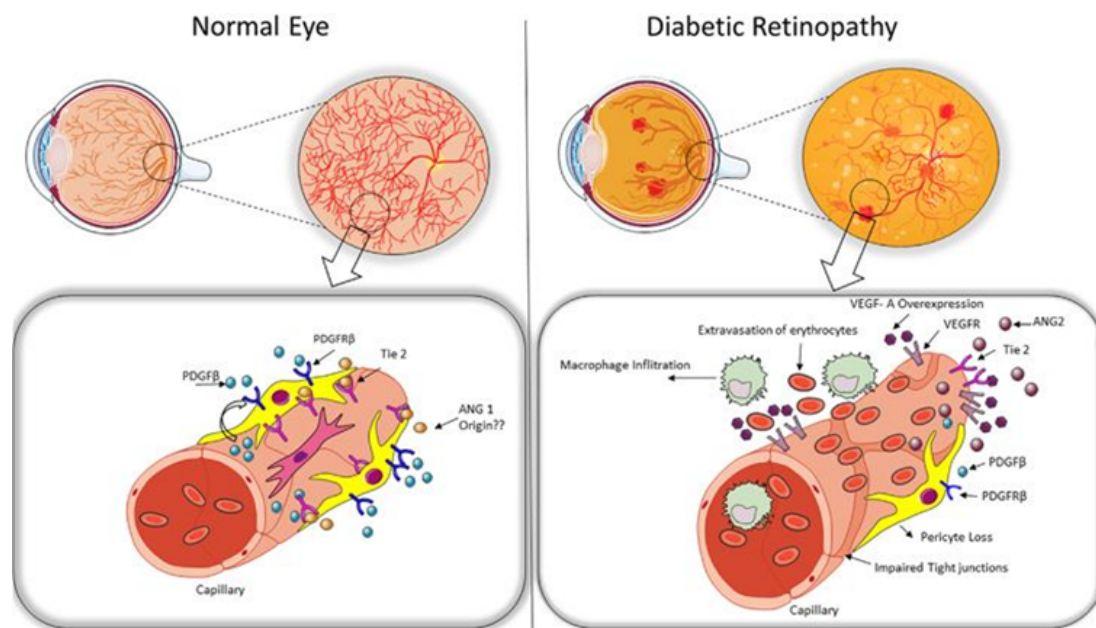


Figure 6: Retinal vasculature in normal and diabetic eyes. In normal, healthy eyes pericytes are present around blood vessels helping to maintain ECs in their quiescent state, and tight junctions maintain the integrity of the BRB. The balance of pro- and anti-angiogenic cues remains in equilibrium. Under diabetic conditions retinal blood vessels can be characterised by significant pericyte drop out, compromised BRB because of impaired tight junctions, immune cell infiltration and extravasation of red blood cells. The angiogenic equilibrium is tipped in favour of neovascular formation producing neo-vessels that are fragile and ‘leaky’ (Adapted from Eye, volume 32, pages 483-486 (March 2018)¹³².

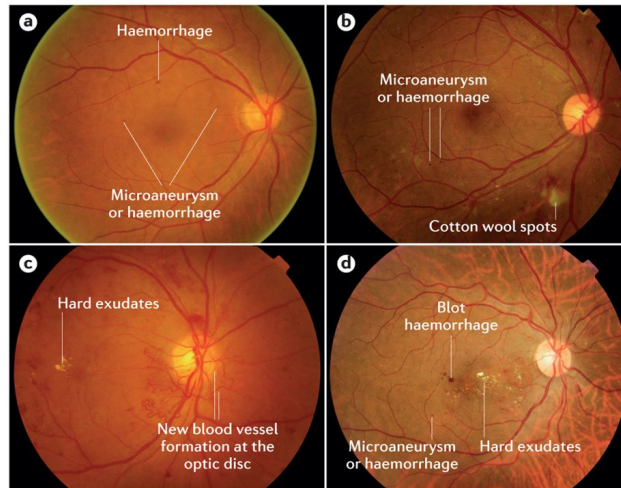


Figure 7: Clinical signs of DR in a fundoscopic examination. A, Mild NPDR; microaneurysms form in the blood vessels bursting to form haemorrhages. **B,** Moderate NPDR; changes become more severe with the addition of cotton wool spot formation. **C,** PDR; neovascularisation forms at the optic disc and hard exudates begin to form. **D,** Diabetic macular oedema; vascular leakage occurs, lipid contents accumulate in the macula and hard exudates form. (Adapted from Nature Reviews Disease Primers, Volume 2, Pages 1-16 (17 March 2016)¹³⁶)

1.7 Prevention of Diabetic Retinopathy

There are a numerous risk factors associated with DR and of these reported risk factors the duration of diabetes, hyperglycaemia and hypertension are considered the most important for DR progression¹⁴³. For patients diagnosed with diabetes, effective management of these modifiable risk factors is an important method to prevent the progression of DR¹⁴⁴.

1.7.1 Prevention by Glycaemic Control

Hyperglycaemia is one of the risk factors for DR. Results from two large scale clinical trials, The Diabetes Control and Complications Trial (DCCT) for type 1 diabetes¹⁴⁵, and The United Kingdom Prospective Diabetes Trial (UKPDS) for

type 2 diabetes¹⁴⁶, indicate that intensive glycaemic control is successful at delaying initiation and progression of DR. Over a 7-year period the DCCT investigated intensive glycaemic control vs. conventional treatment with diet control, in two type 1 diabetic patient cohorts. The primary intervention cohort recruited patients with no existing DR, whereas the secondary intervention cohort recruited patients with pre-existing mild DR. The DCCT reported that intensive therapy to maintain HbA1c at 7% (the HbA1c levels are approximately 9% in patients with type 1 diabetes) reduced the onset of new DR by 76% in comparison to patients who underwent conventional treatment. Moreover, the progression of existing DR in the secondary intervention cohort, was reduced by 50%, highlighting the importance of achieving glycaemic control early, preferably before the onset of DR. In the UKPDS study glycaemic control was investigated in patients with type 2 diabetes. Over a 12-year period the glycaemic control group (HbA1c 7%) demonstrated a 21% reduction in the risk for DR in comparison to the conventional treatment group (HbA1c 7.9%). The importance of glycaemic management as early as possible during diabetes has been further emphasised by results of the Epidemiology of Diabetes Intervention and Complications (EDIC) study. This observational follow-up of the DCCT cohort of patients was observed that the group undergoing glycaemic control continued to exhibit a significantly lower incidence of further progression of their DR severity stage in comparison to the group undergoing conventional treatment¹⁴⁷. These robust clinical results indicate the long-term impact of intensive glycaemic control, highlighting the importance of glycaemia management as early as possible during diabetes.

1.7.2 Prevention by Blood Pressure Control

Blood pressure is another risk factor that can be monitored to help prevent and manage DR. In addition to reducing shear damage to blood vessels resulting from hypertension, blood pressure control can reduce damage to ECs, blood vessels and surrounding tissues by preventing hypoperfusion¹⁴⁸. As with glycaemic control, the clinical evidence for the beneficial effect of controlling

blood pressure on DR development and progression is convincing. In the UKPDS trial on type 2 diabetic patients, a tight blood pressure control group were administered either beta blockers or angiotensin-converting enzyme (ACE) to maintain blood pressure at a level <150/85 mm Hg, whereas the blood pressure of a less tight control group was maintained at a level <180/105 mm Hg. Following the 7-year study, the tight control group showed a 34% reduction in the risk of DR progression, a 47% reduction in vision loss, and a 35% reduction in the need for laser treatment¹⁴⁶. However, unlike glycaemic control, the benefits of blood pressure regulation are lost without ongoing and long-term control.

1.8 Management of Proliferative Diabetic Retinopathy

Interventions using intraocular anti-VEGF agents, panretinal laser photocoagulation (PRP), and vitrectomy can help reduce vision loss resulting from PDR.

1.8.1 Laser Photocoagulation

Since two landmark trials in the 1980s, The Diabetic Retinopathy Study (DRS) and The Early Treatment Diabetic Retinopathy Study (ETDRS), laser therapy has been the gold standard treatment for PDR and DME. The DRS demonstrated a reduced risk of severe vision loss in patients with severe NPDR or PDR, from 33% to 13.9% at 5 years following PRP¹⁴⁹. Similarly, the EDTRS demonstrated a 24% to 12% reduction in the risk of vision loss in patients with clinically significant DME¹⁵⁰.

The primary goal of laser therapy is to preserve patients' useful vision and prevent blindness; reversal of vision loss is uncommon. Treatment by laser for PDR by PRP involves applying many evenly spaced laser spots (typically 1200 to 1600, approximately 500 μ M in size) to the peripheral retina, focally destroying out photoreceptors and RPE. The cells absorb the light and the

resultant heat causes destruction of the outer retina. Treatment for DME differs in that a gentle laser applied to the macula is used to target leaking microaneurysms directly. Although the mechanism of action is not fully understood, one hypothesis is that PRP alleviates hypoxia by improving oxygen supply to areas of the inner retina that had become oxygen-deprived¹⁵¹. This occurs because not only are the choriocapillaris physically closer to the inner retina allowing for diffusion of oxygen from the choroid, but also because the highly metabolically active rods and cones are no longer present to absorb oxygen from the choriocapillaris in the area of the burns. As a result, the improved retinal oxygenation reduces neovascularisation and oedema formation by reducing the production of hypoxia driven VEGF.

However, despite widespread use, laser photocoagulation is associated with significant risk due to its destructive nature. Laser photocoagulation burns and destroys part of the retina which can result in visual symptoms related to the loss of function of the 'burned' part of the retina¹⁵¹. This can include loss of central vision, reduced night vision, decreased ability to focus and induction of a blind spot. In addition, a proportion of patients continue to develop active neovascularisation and vision loss^{152,153}.

1.8.2 Management: Vitrectomy

In 1970 the first successful vitrectomy was performed on a diabetic eye with persistent vitreous haemorrhage. Traditionally, non-clearing vitreous haemorrhage was the main indication for vitrectomy in the diabetic eye. However, advances in surgical techniques and surgical instruments mean that vitrectomy is now also used for the management of retinal detachments and fibrovascular proliferation. With the vitreous body removed there is better access to the retina allowing for a variety of repairs, including the removal of scar tissue to release tractional forces that pull on the retina, removal of opacities such as non-clearing vitreous haemorrhage, laser repair of retinal detachments and to remove the scaffolding into which the neovascularisation

may grow. Since anti-VEGF therapies have become more efficient, safer and more accessible, proliferative neovascularisation and DME are treated less frequently with vitrectomy. Visual outcomes following vitrectomy are better in comparison to the natural course of disease progression, and if initial treatment is successful then long-term stability following surgery is good. However preventative measures such as improved control of glucose levels and timely application of laser treatment are more efficacious than vitrectomy¹⁵⁴.

1.8.3 Anti VEGF-Agents

The VEGF-VEGFR system is one of the most predominant pathways involved in the later stages (DME and PDR) of DR progression. Therefore, most antiangiogenic agents used in clinics for the treatment of DME and PDR with evidence of clinical efficacy currently act by inhibiting VEGF. Unlike laser PRP, anti-VEGF agents have been shown to improve visual acuity and even ocular tissue structure in some cases¹⁵⁵. Currently there are three commonly used agents for the treatment of DME and as an adjunct therapy for PDR, which all work by the inhibiting VEGF.

Bevacizumab (Avastin®) is a full-length humanised antibody targeting all isoforms of VEGF-A. It was initially approved by Food and Drug Administration (FDA) for treatment of metastatic colorectal cancers in February 2004¹⁵⁶ and it has since been approved for the treatment of other solid tumours (non-epithelial lung, breast, ovarian and renal cancers) and glioblastomas¹⁵⁷. It is not approved for any ocular indication however ophthalmologists quickly determined that bevacizumab was also efficacious for the treatment for the diseases with ocular neovascularisation and started to use it 'off label'¹⁵⁸. Ranibizumab is the first approved anti-VEGF agent for ocular diseases and it is a recombinant antibody fragment (Fab) of the humanised anti-VEGF antibody bevacizumab that binds all isoforms of VEGF-A. After multiple trials, ranibizumab was approved by the FDA in 2006 for all stages of diabetic retinopathy. Finally, aflibercept is a recombinant fusion protein that has been constructed by fusing specific

domains from human VEGF-R1 and VEGF-R2 with the Fab fragment of human IgG1. It binds VEGF-A, VEGFB and PlGF to prevent their activation of VEGF-R, and it has been shown to bind VEGF with greater affinity than other anti-VEGF agents.

Despite its clear efficacy, a substantial number of patients are intrinsically refractory to anti-VEGF treatment or may develop resistance over time. It is not surprising since many angiogenic factors jointly contribute to new blood vessel formation²⁸. Indeed, VEGF inhibition in the eye was reported to cause compensatory activation of alternative angiogenic pathways, such as Hepatocyte Growth Factor (HGF)¹⁵⁹ and erythropoietin¹⁶⁰. Furthermore, considering the important neuroprotective effect of VEGF¹⁶¹ and its role in physiological neovascularization¹⁶², long term treatment with VEGF blockades may result in local and systemic side effects¹⁶³⁻¹⁶⁵.

1.9 The Complement System

1.9.1 Complement Activation

The mammalian immune system is a complex choreography of biochemical processes that detect and eliminate pathogens that can cause harm to the host; no small task given the impressive number of pathogens and host processes that are able to cause diseases. One of the most important defence mechanisms of the human body is the complement system. Despite being discovered in the late 1880s, the complement system evolved over 700 million years ago¹⁶⁶ and is an integral part of the innate immune system that acts as a first-line defence to protect the host from invading pathogens and abnormal self-derived components. It is comprised of an army of over 30 different proteins that are mainly synthesised by the liver and circulate in the blood as inactive precursors¹⁶⁷. The identification of a pathogenic surface initiates a proteolytic cascade that leads to three main effector mechanisms: (i) the generation of

potent pro-inflammatory mediators (anaphylatoxins), (ii) opsonisation ('coating') of the pathogenic surface by complement opsonins (e.g. C3b), and (iii) targeted lysis of the pathogenic surface through the assembly of membrane-penetrating pores known as the membrane attack complex (MAC)¹⁶⁸.

In the early stages, the complement cascade can be driven by three distinct pathways (classical, CP; alternative, AP; and lectin, LP). Each pathway of complement activation employs different recognition molecules and initiating serine proteases, however the three pathways all converge at the level of C3 to generate the same set of effector molecules¹⁶⁹ (*please refer **Figure 8** to for a schematic representation of complement activation*). These reactions are known as the 'early' events of complement activation, and consist of triggered-enzyme cascades in which inactive complement proteins are cleaved to yield two fragments, the larger of which is an active serine protease. The active serine protease is retained at the pathogen surface which ensures the next complement protein in the pathway is also cleaved and activated at the pathogen surface. The small peptide fragment (known as an anaphylatoxin) on the other hand, is released from the site of the reaction to act as a potent inflammatory mediator, targeting a broad spectrum of immune and non-immune cells¹⁷⁰. Mechanisms such as this one, where the activation of a small number of complement proteins at the start of the pathway is hugely amplified by each successive step, results in a cascade that rapidly generates a large complement response.

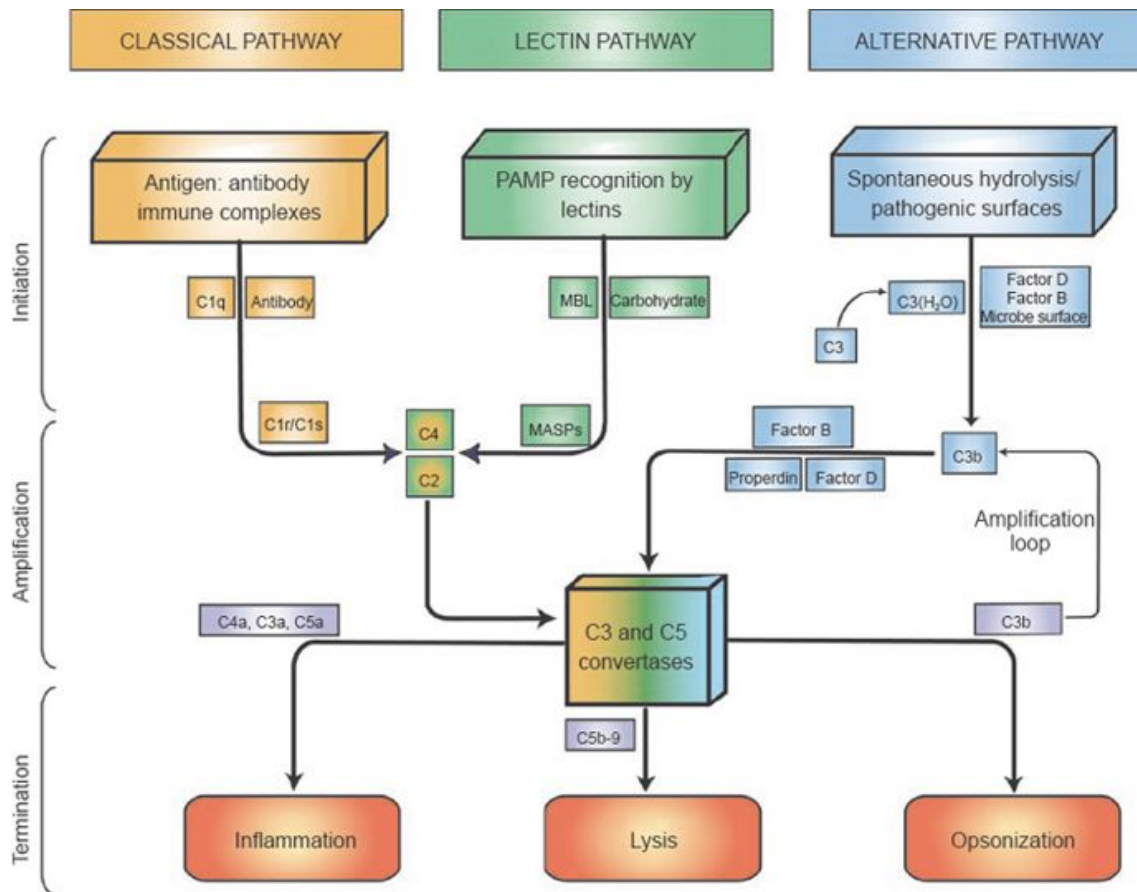


Figure 8: Schematic representation of the three pathways of complement activation.

Activation of C3, the central component of complement, may take place via three pathways: (1) classical, (2) lectin or (3) alternative pathway. The three pathways of complement activation. The CP is initiated by IgM or IgG antibody clusters that are associated with a bound antigen. The CP begins with a large protein complex, C1, which is comprised of three subunits; C1q, C1r and C1s. When the globular heads of the C1q subunit bind to two or more antibodies, C1r is enzymatically activated, which in turn cleaves and activates C1s. Activated C1s potentiates the action of the next protein in the cascade, C4, cleaving it into C4a and C4b. This cleavage exposes a thioester bond, allowing for the covalent deposition of C4b on surfaces in the immediate vicinity of the activation sites. Complement protein C2 can then complex with surface bound C4b, which allows for cleavage by C1s to generate C2a and the CP C3 convertase C4b2b. This convertase can bind and cleave C3 to initiate amplification by forming C3b, which complexes back with C4b2b to form the classical pathway C5 convertase C4b2b3b. The C5 convertase initiates the formation of C5b and the later steps of complement activation. The LP is functionally similar to the CCP but is initiated by mannose-binding lectin (MBL). MBL acts as a pattern recognition molecule that predominantly recognises carbohydrate patterns. MBL is found in a complex with MBL-associated proteases (MASPs); MASP-1, MASP-2 and MASP-3. Binding of MBL to its surface target leads to the activation of Masp-2 which cleaves both C4 and

C2, generating the same C3 convertase as in the classical pathway. The AP is activated when a small fraction of circulating C3 molecules are hydrolysed to form the initial AP C3 convertase, C3(H₂O)Bb, in the presence of Factors B and D, leading to additional C3 cleavage and eventual formation of the AP C3 convertase (C3bBb) and AP C5 convertase (C3bBbC3b). All three pathways culminate in the formation of the convertases, which in turn generate the major effectors of the complement system: anaphylatoxins (C4a/C3a/C5a), the membrane attack complex (MAC), and opsonins (e.g., C3b). Anaphylatoxins are potent proinflammatory molecules derived from the cleavage of C4, C3, and C5. The MAC is a terminal assembly of complement components C5b through C9, which can directly lyse targeted surfaces. C3b induces phagocytosis of opsonized targets and also serves to amplify complement activation through the AP. (Adapted from Cell Research, volume 20, pages 34-50, (15th December 2009)¹⁶⁸).

The CP begins with a large protein complex, C1, which is comprised of three subunits; C1q, C1r and C1s. Initiation of the classical pathway occurs when C1q, binds to the Fc region of complement-fixing antibodies attached to pathogenic surfaces, activating C1r and C1s. Subsequently, activated C1s cleaves C4 and C2 into larger (C4b, C2a) and smaller (C4a, C2b) fragments. The larger fragments associate on pathogenic surfaces to form the complex C4bC2a, which gains the ability to cleave C3 and is termed the C3 convertase¹⁷¹. Generation of the C3 convertase cleaves C3 into the anaphylatoxin C3a and the opsonin C3b, the point at which all complement activation cascades converge. The LP is functionally similar to the CP but is initiated by the serum protein mannose-binding lectin (MBL). MBL acts as a pattern recognition molecule that binds to carbohydrate structures on the surfaces of bacteria or viruses¹⁷². MBL is found in a complex with MBL-associated proteases (MASPs)-1, -2, and -3 which are functionally and structurally similar to C1s and C1r¹⁷³. Binding of MBL to its target leads to the activation of the associated MASP-2, cleavage of C2 and C4, and ultimately generation of the same C3 convertase as in the classical pathway¹⁶⁸. The AP is mechanistically distinct from the CP and LP; activation of the AP occurs in an antibody-independent manner¹⁷¹. It is initiated by the low-level, spontaneous hydrolysis of C3 to form C3(H₂O) in a process known as 'tick-over'¹⁷⁴. CFB binds to C3(H₂O) and this complex is cleaved by the complement factor D

(CFD), generating Ba and Bb fragments. The Bb fragment remains associated with the complex, forming the initial AP C3(H₂O)Bb-convertase, which can cleave additional C3 molecules to generate C3b. Once produced by these means C3b initiates a positive feedback loop, associating with CFB and generating more C3-convertase (please refer to **Figure 9** for a schematic representation of the AP of complement activation).

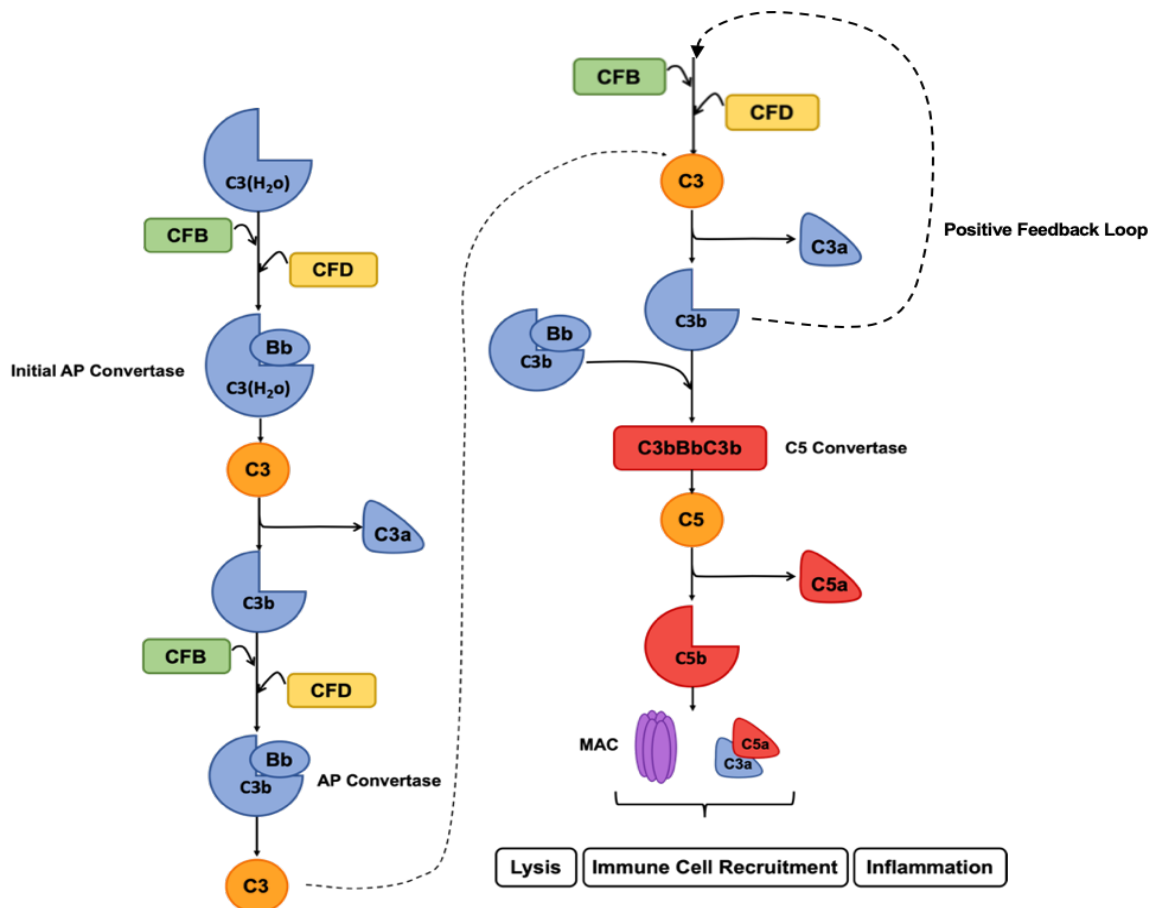


Figure 9: Schematic representation of the alternative pathway of complement activation. It is initiated by the low-level, spontaneous hydrolysis of C3 to form C3(H₂O). C3(H₂O) binds to CFB, and this complex is cleaved by CFD, generating Ba and Bb. The Bb fragment remains associated with the complex, forming the initial AP C3(H₂O)Bb-convertase, which can cleave additional C3 molecules to generate C3b. Once produced by these means C3b initiates a positive feedback loop, associating with CFB and generating more C3-convertase. C3b complexes with the C3-convertase to form the AP c5 convertase (C3bBbc3b).

1.9.2 Effectors of the Complement System

Primarily, as an important branch of first-line defence, complement protects the host from invading pathogens and abnormal self-derived components. This can be achieved through three main mechanisms: (i) direct target lysis after incorporation of the MAC into the cell membrane of the invading pathogen, (ii) alerting and attracting immune cells through by the generation of potent proinflammatory anaphylatoxins, and (iii) opsonisation by complement activation products and engagement of complement receptors on phagocytic cells, such as macrophages and neutrophils. The MAC with its lytic pore is probably the best recognised of these effectors¹⁷⁴. MAC assembly begins with cleavage of C5 into C5a and C5b by a C5 convertase: this cleavage is the final step in the 'early stage' of complement activation, and the first step in the terminal pathway¹⁷⁵. C5b cleavage exposes a binding site for C6, and the subsequent C5bC6 binds reversibly to the targeted surfaces and sequentially recruits C7, creating C5b-7. C5b7 is integrated into the phospholipid membrane bilayer on the target pathogen. This induces the membrane insertion of C8 α and C8 β , forming unstable pores. Finally, C9 binds to C8 α and initiates polymerization of multiple C9 molecules to form stable inserted pores of approximately 10nm in diameter¹⁶⁸. Formation of the fully formed MAC pore leads to targeted lysis of the surface upon which it has assembled¹⁷⁶.

Since certain pathogens have evolved mechanisms that enable them to evade the destructive potential of MAC, it is crucial for complement to engage and recruit other components of the immune system through the generation of potent pro-inflammatory anaphylatoxins (C3a, C4a and C5a). They are constantly released during activation and amplification triggering pro-inflammatory signalling¹⁷⁷. Their functions include many hallmark proinflammatory activities, such as increases in vascular permeability, smooth muscle contraction, leukocyte recruitment, as well as promoting the production and release of other inflammatory mediators (e.g. histamine).

The third and final major effector arm of activated complement lies in the ability of phagocytic cells to recognize, ingest, and eliminate cells coated with opsonins (C3b and C4b). Opsonins are the smaller cleavage fragments produced by complement activation that remain deposited on the target surface. They act as molecular beacons, interacting with receptors on macrophages, monocytes and neutrophils to enable phagocytosis of the target cell¹⁷⁸.

1.9.3 Regulation of the Complement System

Primarily, as an important branch of first-line defence, complement protects the host from invading pathogens and abnormal self-derived components. Despite this, activated complement can be a double-edged sword that not only helps defend the host against pathogens, but also has the potential to inflict damage to self-tissues. To protect from the destructive effects of complement-mediated damage the host is endowed with rigorous complement regulatory proteins (CRegs) that allow for tight regulation of complement activation. In fact, because of its potent pro-inflammatory and destructive capabilities, nearly half of the complement proteins serve in regulation¹⁷⁹. (*Please refer to **Table 2** for a list of the key membrane bound and soluble CRegs*)

Table 2: A table outlining the key membrane bound and soluble complement regulatory proteins.

Membrane Bound	
Regulator	Function
Decay Accelerating Factor (DAF, CD55)	CD55 inhibits the assembly of new C3 convertases and shorten the half-life of preformed convertases, therefore limiting their ability to participate in further complement activation.
Membrane Cofactor Protein (MCP, CD46)	CD46 acts as a co-factor for the proteolytic activity of CFI, helping with non-specific C4b degradation
Complement Receptor 1 (CR1, CD35)	CR1 acts as a co-factor for the proteolytic activity of CFI. This helps with non-specific C3b and C4b degradation ¹⁸⁰ . CRI also has decay-accelerating activity to prevent classical, lectin,

	and alternative pathway C3 convertase formation.
Membrane Inhibitor of Reactive Lysis (MIRL, CD59)	CD59 inhibits the assembly lytic MAC by preventing insertion of the final component C9 into lipid bilayer of the target membrane ¹⁸¹
Soluble Bound	
C1 Inhibitor (C1INH)	C1INH regulates activation of the classical pathway by binding and inactivating C1r and C1s, leading to dissociation of the C1 complex ¹⁶⁷
C4 binding Protein (C4BP)	C4BP acts as a cofactor for the proteolytic activity of CFI, to help prevent non-specific C4b degradation. also has decay-accelerating activity to prevent classical and lectin pathway C3 convertase formation and leads to the catabolism of C4b to its degradation products.
Complement factor H (CFH)	Factor H achieves host-specific protection by binding polyanions, such as sialic acid and heparin, which make up an essential component of eukaryotic, but not prokaryotic, cell surfaces. The functional consequence of this mechanism is that Factor H is preferentially targeted to host surfaces. Here it acts as a cofactor for the proteolytic activity of CFI and in addition, exerts decay-accelerating activities to prevent alternative pathway C3 convertase formation.
Complement Factor I (CFI)	CFI cleaves the opsonins, C3b and C4b, into inactive fragments ¹⁸⁰ .

1.9.4 Complement and Retinal Diseases

Traditionally, complement has been primarily viewed as a first line of defence against microbial intruders, quickly tagging and eliminating them and buying the adaptive immune response time to pick up momentum. There is now a well-established picture of how complement acts as an immune surveillance system to discriminate among healthy host tissue, cellular debris, apoptotic cells and foreign intruders. Underlying the proper functioning of the complement system is a finely balanced, intricate network of effectors, receptors and regulators, and any trigger that tips this delicate balance between complement activation and

regulation can induce self-attack¹⁷⁷. There is now a new perception of complement that reaches far beyond the elimination of pathogens¹⁸². Numerous studies have elaborated on the pathogenic role of complement during immune, inflammatory, neurodegenerative, ischemic and age-related diseases¹⁸³, and it is now widely accepted that the presence and activation of complement plays a crucial role in the pathogenesis of a large number of diseases, inclusive of retinal diseases such as age-related macular degeneration (AMD) and DR¹⁸⁴. The subsequent chapters of this review will be focused of the AP in retinal diseases, and more specifically the role of Complement Factor B.

1.9.4.1 Complement and Age-Related Macular Degeneration

Age-related macular degeneration (AMD) is the progressive degeneration of the macula (central part of the retina). It accounts for 8.7% of blindness worldwide and is the leading cause of irreversible vision loss in the aging population in the Western world¹⁸⁵. With an increasing aging population worldwide its prevalence is only expected to rise: an estimated 288 million people will be affected by AMD by 2040¹⁸⁵. Despite not being the focus of this study, it is worth to briefly visit the role of complement in AMD: AMD and DR both share the same characteristic feature in that they are both driven by inflammation and aberrant angiogenesis and therefore complement involvement in AMD may have cross-over with, and provide insights into the DR pathogenesis. The early stage of AMD is characterised by the formation of extracellular deposits, known as drusen, between the RPE and underlying Bruch's membrane. Late AMD is broadly classified into two advanced clinical forms, a 'dry' form with geographic atrophy (GA) characterised by loss of RPE and outer retinal cells, or a 'wet' form, otherwise known as neovascular AMD (nAMD), characterised by abnormal choroidal neovascularisation (CNV) that extends into the retina generating immature blood vessels that leak and haemorrhage.

There have been considerable advances in the unravelling of the biological bases of AMD, from which have emerged several lines of evidence implicating

activation of the complement cascade, especially the AP, in AMD pathogenesis. Firstly, the major stressors for AMD development, such as aging, smoking, and oxidative stress, have been linked to overactivation of the complement system¹⁸⁶. As mentioned above, drusen are the first signs of early AMD. The observation that drusen contains proteins of the complement system was first made by two independent groups in France and the Netherlands, and then later confirmed by the Hageman group in the U.S. who conducted extensive immunohistochemical studies¹⁸⁷⁻¹⁸⁹. These findings on the molecular composition of drusen implicate local activation of the alternative pathway. In addition, increased levels of various complement components, including C3a, C3b and CFB, have been detected in the plasma from AMD patients¹⁹⁰⁻¹⁹³.

Secondly, genetic studies have revealed highly significant statistical associations between AMD and genetic variants that affect different aspects of the AP. These variations in genes encoding complement proteins suggest that certain individuals may be genetically predisposed to AMD because of local or systemic aberration of the AP. In 2005, several studies were simultaneously published identifying and confirming variation in the complement factor H (CFH gene)¹⁹⁴⁻¹⁹⁷. These genetic studies were then extended by the observation that polymorphisms in other complement genes, notably those coding for CFB are also associated with AMD¹⁹⁸⁻²⁰⁰.

Lastly, a strong argument in support of the involvement of the AP in AMD comes from *in vitro* and *in vivo* experimental data. In a study aimed at elucidating how complement is regulated in the retina, one group reported that CFH, a negative regulator of the AP, is constitutively expressed by RPE cells and that RPE cells are a significant local source of CFH, which is negatively regulated by inflammation²⁰¹. To further investigate the retinal complement regulatory system, they followed on from this by investigating the production and regulation of the central AP activator, CFB. Similarly, they found that CFB is also produced locally in the retina by RPE cells, however unlike CFH, CFB is positively regulated by inflammation²⁰². These results suggest that under

inflammatory conditions, like those that manifest in both AMD and DR, the local production of CFB by RPE cells is increased, resulting in elevated levels of CFB within the retina. The exact biological consequence of elevated CFB is yet to be elucidated, however this data implies a link between the pro-inflammatory pathologies seen in both AMD and DR, and increased CFB levels.

Another approach used to study the role of complement in retinal health is to evaluate and compare the retinal phenotype of mice carrying mutations or deletions of specific complement genes. In one study, the authors characterised the retinas of mice carrying null mutations in the genes of three central components of the AP, $Cfb^{-/-}$, $Cfh^{-/-}$, and $Cfd^{-/-}$ ²⁰³. In addition, they also examined the phenotype of the $Cfb^{-/-}/Cfh^{-/-}$ double knockout mouse retina. The retinae were examined at 12 months to identify signs of retinal abnormalities. They reported that in the first year of life there were no gross anatomical differences in retinal morphology between the genotypes with regard to retinal thickness and number of photoreceptors. Retinal vessel morphology and density was also examined by immunostaining retinal flatmounts. Across all genotypes, the retinal vascular plexus was morphologically comparable to that of wildtype mice including no withering vessels or other vascular abnormalities. This suggests that under physiological conditions the retina is stable and healthy in the absence of a functional alternative pathway²⁰³. However, this study was carried out in the absence of a pathological challenge or environmental stressor, and therefore provides limited insight into how complement contributes to vascular pathology under disease conditions. There are several studies however, that have utilised the mouse model of laser-induced choroidal neovascularisation (CNV) to mimic vascular pathology seen in AMD and explore the role of complement in choroidal angiogenesis. Choroidal neovascularisation (CNV) is the hallmark of neovascular AMD (nAMD) and one of the ways to induce CNV in mice is to rupture the Bruch's membrane with laser photocoagulation. One group who utilised siRNA directed against CFB in C57BL/6 mice, demonstrated a significant reduction in CNV compared to their wild-type controls²⁰⁴. However, this data using siRNA must be

interpreted with caution because it has been reported that that siRNA can suppress angiogenesis and CNV independent of the target gene²⁰⁵. Other studies have used a combination of CNV and complete gene knock-out of CFB in mice to determine which complement pathway is essential for CNV development. They reported that following laser photocoagulation, CFB -/- mice developed smaller CNV lesions and as a result better-preserved retinal function^{206,207}.

1.9.4.2 Complement and Diabetic Retinopathy

DR has a complex pathophysiology characterised by progressive degeneration of the retinal vasculature¹³⁶. Disease pathology begins with the loss of pericytes, hypertrophy of the basement membrane, inflammation, and BRB^{136,208,209}. This is followed by loss of capillaries that become acellular and nonperfused along with both vascular and neural cell apoptosis²⁰⁹. The destruction of retinal vessels leads to ischemia followed by expression of angiogenic growth factors culminating in proliferative neovascularisation and eventually vision loss^{210,211}. Being an immune-privileged organ the retina has its own unique immune regulatory mechanisms and immune defence mechanisms, which when alerted by any kind of noxious signal, starts a cascade of inflammatory events as an adaptive response to restore the homeostatic balance²¹²⁻²¹⁴. These mechanisms not only reduce the risk of infection, but also prevent inappropriate immune responses, consequently reducing the risk of inflammation-mediated retinal damage²¹⁴. Low-level activation of the innate immune mechanisms, specifically the complement system, is required for the homeostatic tissue husbandry necessary for long-term maintenance of the functional and structural integrity of the adult retina²¹⁵. However, this protective mechanism can have a detrimental impact if the insults persist for a sustained period of time, leading to irreversible functional loss²¹².

In comparison to AMD, genetic evidence for the involvement of complement in DR is minimal, however the role of genetic factors in the development of DR

was explored in a 2013 study. This group investigated a possible association of CFH and CFB complement genes in type 2 diabetic patients. By generating tag-single nucleotide polymorphisms (tSNPs) in CFH and CFB, they compared the allelic and genotypic frequencies of a CFH variant and four CFB variants, in type 2 diabetic patients with and without retinopathy. They observed a significant decrease in the frequencies of the A allele and the AA genotype for the CFH variant (rs800292) in patients with DR compared to diabetic controls. On the other hand, the study revealed a significant increase in the frequencies of the A allele and AA genotype for one of the CFB variants (rs1049709) in patients with DR compared to diabetic controls. The results from this study suggest that the mutation in CFH, a regulator of the AP, provides protection against DR whereas a mutation in CFB, an activator of the AP, increases the risk of developing DR²¹⁶. Although these findings further strengthen the concept that the complement system, particularly the AP, is associated with the pathogenesis of DR, this study does not explore the biological function of the mutations and consequently the pathogenic significance of the CFH and CFB polymorphisms remains unclear. The variant in CFB represents a synonymous substitution whereby one base is substituted for another in the exon of the gene. With the mutation situated in the exon of the gene the coded amino acid will not be affected, so the increased risk of developing DR with the CFB mutation is likely to be because the mutation cause changes in CFB gene transcription or changes in tissue specificity of CFB gene expression. However, determining the biological roles of these polymorphisms in DR would require further investigation.

Over the past decade, a body of clinical evidence has emerged that supports a link between the AP and the pathogenesis of DR. Firstly, increased glycosylation that occurs in DM has been implicated in the inactivation of important complement regulatory proteins, such as CD59, which normally serve to prevent self-cells from being targeted by MAC²¹⁷. Evidence comes from the observation that membrane bound inhibitors of complement, CD55 and CD59, expression is significantly depressed or impaired due in part to non-enzymatic

glycation^{218,219}. Several proteomic studies have been carried out to analyse the protein profiles of human vitreous samples from patients with DR. In these studies, vitreous fluid obtained from diabetic patients undergoing vitreoretinal surgery was analysed for protein composition. Results reported that complement factors C3, CFI, CFB, C4, C4b, C2 CFD and CFH were detected in the vitreous of patients with PDR^{89,220-226}. However, there are two confounding factors that mean data reported in these studies should be interpreted with caution. Firstly, vitreous haemorrhage, which often occurs in patients with PDR, can produce a large influx of serum proteins²²⁷. Secondly, the disruption of the blood-retina barrier that occurs in DR also produces an increase in proteins in the vitreous body²²⁷. Both these factors may preclude the usefulness of the vitreous fluid when studying intraocular production of a particular protein, since elevated intravitreal levels of a particular protein does not necessarily indicate an increase in intraocular production, and might simply reflect a non-specific increase in protein levels due diffusion. Immunohistochemistry methods have also reported that activation of the AP system is involved in the pathogenesis of DR. In one study, using a panel of antibodies directed against candidate markers of complement activation, investigators examined the presence of activated complement in donor eyes affected by DR found extensive staining for the terminal complex MAC²²⁸. In the same study, no positive staining was found for C1, C4 or MBL which suggests that the classical and lectin pathways did not participate in complement activation, and the AP of activation seems most likely²²⁸. Although findings in this study implicating the AP in DR bare some relevance, it is worth to note a couple of limitations associated with this study. Firstly, only the posterior poles of diabetic eyes were available for study because in most cases the retinas were detached, and as a result complement activation could only be examined in the choriocapillaries not in the retinal vasculature. Secondly, extensive complement deposition was observed in some diabetic patients without severe retinopathy²²⁸.

Another argument for the involvement of the AP in DR, in particular CFB, comes from *in vivo* experimental data. However, results are somewhat conflicting to

studies in AMD. The mouse model of oxygen-induced retinopathy (OIR) is used to mimic vascular pathology seen in DR, however unlike the mouse model of CNV for AMD, it seems fewer studies have been carried out using OIR to study complement in retinal angiogenesis. The OIR model is a well-defined model associated with late-stage destructive neovascularisation and inflammation. The first phase of OIR involves exposure of mouse pups to hyperoxia, resulting in inhibition of normal retinal vessel growth and dropout of pre-existing vasculature, leaving a centrally avascular retina²²⁹. The second stage of OIR is initiated when mouse pups are placed back into a normal oxygen environment. The initial loss of retinal vasculature, coupled with the increasing metabolic demands of the developing retina, leads to local hypoxia and the up-regulation of angiogenic growth factors. As a consequence, there is an overcompensating vasoproliferative response with the formation of disorganized and leaky neovascular tufts²³⁰. In 2014 one group who used this model to investigate how the AP regulates pathological angiogenesis in the retina reported a link between CFB and retinal vascular pathology following OIR. In order to characterise the role of the AP in pathological retinal neovascularisation the authors induced OIR in CFB deficient mice. They found that OIR treatment in CFB $-/-$ mice resulted in a significant increase in neovascularisation compared with control mice. Since VEGF plays a pivotal role in driving neovessel formation in the OIR model, in seeking to explain the enhanced neovessel formation in CFB $-/-$ mice, the authors first compared VEGF expression between control and CFB $-/-$ retina subjected to OIR. Interestingly the expression levels of VEGF and its type II receptor, VEGFR2, were not affected in the retina of CFB $-/-$ mice subjected to OIR. Another explanation for the increased neovascularisation seen in CFB $-/-$ mice could be enhanced neovessel proliferation. Although the VEGF data suggested no change in growth stimulation it is not a direct reflection of proliferation, so to directly determine this the authors quantitated the amount of EC proliferation by intraperitoneal injection of EdU (a thymidine analogue that intercalates into the DNA of proliferating cells). Consistent with the observation of unchanged VEGF expression, the rate of neovessel proliferation remained unchanged in CFB $-/-$ mice following OIR compared to their control

counterparts. In addition, an increase in CFB gene expression following OIR treatment in the retina of wildtype mice and co-localisation of CFB with neovessels was reported²³¹; both these observations implicate CFB in driving vascular pathology. This led to the idea that the increase in neovascularisation in CFB^{-/-} mice was not a result of higher levels of VEGF or neovessel proliferation, but rather because of a decrease in the removal of neovessels over time. The authors later showed a significant reduction in apoptotic cells in retinal neovessels of OIR treated CFB ^{-/-} mice which suggests that CFB may have a protective role in the development of neovascularisation and exerts its function through mediating cell apoptosis.

1.10 Summary

DR is a major microvascular complication of DM. It can be broadly classified into two stages: NPDR and PDR. Vascular changes in NPDR include vascular basement membrane thickening, the loss of pericytes and the formation of microaneurysms. These progressive functional and structural alterations of retinal vasculature result in capillary degeneration and retinal ischemia, which subsequently trigger an adverse compensatory neovascularisation response: the hallmark of PDR. These newly formed blood vessels are fragile and more liable to bleed. Total or partial vision loss can occur when abnormal blood vessels breach the inner limiting membrane of the retina and grow into the vitreous causing vitreous haemorrhage, retinal detachment and eventually vision loss²³². For many decades, laser photocoagulation has been the gold standard treatment for PDR and although effective at preserving central visual acuity, patients often suffer the loss of peripheral vision^{233 234,235}. Recent advances in elucidating the molecular mechanisms of angiogenesis have led to the development of potentially disease-modifying treatments for PDR²³⁶. Pharmacological agents that inhibit VEGF, a key causative factor associated with PDR pathologies, are now increasingly used as adjuvant treatment to laser photocoagulation. Despite being highly effective at inhibiting neovascularization and preventing further vision loss, anti-VEGF treatment is not able to relieve

ischemic stress caused by vascular degeneration, and so neovascularization is likely to reoccur once the treatment is stopped. Consequently, long-term repetitive treatment is necessary, and not only does this place a significant burden upon healthcare systems, chronic VEGF suppression also raises concerns regarding potential adverse effects due to the loss of its important neuro-trophic and protective role^{237,238}. Furthermore, around 50% of patients are not responsive to anti-VEGF treatment or develop resistance over time, which is not surprising as angiogenesis is regulated by multiple angiogenic pathways²⁸. Targeting VEGF may also lead to compensatory activation of alternative angiogenic pathways. Therefore, effective management of PDR remains a significant unmet medical worldwide. Consequently, the development of new therapies capable of preventing or slowing the onset and progression of DR remains a priority²³⁹ and this underpins the need for continuing efforts to fully elucidate the mechanisms involved in the pathogenesis of DR. Although DR has long been considered a vascular disease, evidence shows that poorly controlled complement activation, in particular the AP, is associated vascular pathologies in the eye²⁴⁰. Investigating the role of the complement in retinal angiogenesis could provide a better insight into the cellular and molecular mechanisms underlying DR, which may facilitate the development of alternative or complementary treatment to current anti-VEGF therapeutics.

1.11 Aims and Objectives

Genetic, clinical and experimental based evidence, including that obtained from studies on AMD, strongly implicates the AP of complement, in particular CFB, in the development of DR. Unfortunately, the exact pathogenic significance of this association remains unclear. As a result, investigating the biological function of CFB within the retina will help link complement activation to specific molecular events in order to determine the pathologic effects of complement activity in DR. Therefore, the overarching aim of this project is to explore the role of one of the key components of the AP, CFB, in DR. We hypothesise that CFB plays a causative role in DR by promoting diabetes-associated retinal

neovascularisation. In order to satisfy this aim, the specific objectives are threefold:

- 1) To characterise the expression level of CFB in rodent models of PDR, and human PDR patient samples.
- 2) To investigate the role of CFB in retinal vascular endothelial cell behaviour and angiogenesis.
- 3) To elucidate the mechanism through which CFB contributes to vascular pathology in DR.

2 Materials and Methods

2.1 Human Patient Samples

Aqueous humor samples were collected from patients referred to Tan Tock Seng Hospital, Singapore for vitreoretinal surgery to treat PDR. Samples were obtained from patients who provided written-informed consent. The study was in accordance with the Declaration of Helsinki for Human Research, and with guidelines from the Health Sciences Authority of Singapore. Study protocols for allocation and biochemical analysis of specimens were approved by the SingHealth Centralised Institutional Review Board.

2.2 Animal Husbandry

All procedures were performed according to the Responsible Care and Use of Laboratory Animals (RCULA) guidelines and approved by the Institutional Animal Care and Use Committees (IACUC) in Nanyang Technological University, Singapore. Mice were maintained at the designated animal facility under a 12-hour dark-light cycle at $23^{\circ}\text{C} \pm 2^{\circ}\text{C}$ and given standard mouse chow and water ad libitum.

2.3 STZ Diabetic Mouse Model

Diabetes was induced by subcutaneous injection of 50 mg/kg Streptozotocin (STZ) for five consecutive days²⁴¹. 6-week male mice were weighed and subjected for basal fasting blood glucose (FBG) test using a point-of care glucometer following a 16-h starvation period. Mice with body weight >20g and FBG <100mg/dl or >250mg/dl were used for the induction of diabetes. Mice were then starved for 6-h each day before being subjected to intraperitoneal (IP) injection of 50mg/kg of freshly prepared STZ solution for 5 consecutive days. The STZ solution was freshly prepared just before injection by

reconstituting STZ powder into 0.1 M citrate buffer (please refer to **Appendix Table 6** for composition of the sodium citrate buffer) at pH 4.5. Mice were subjected to measurement of FBG 4- and 8-week post-injection. Mice with FBG levels ≥ 250 mg/dl at both time points were considered diabetic. Mice that did not develop hyperglycemia at 4-weeks post-induction were subject to a second cycle of STZ-injection. Those with FBG levels of ≥ 250 mg/dl at both the 4- and 8-week post-injection time-points were included in downstream studies.

2.4 Oxygen-Induced Retinopathy (OIR) Mouse Model

Nursing mothers and neonatal mice were kept at room air from birth through to postnatal day (P)7. At P7 mouse litters were placed in a 75% oxygen chamber for 5 days until P12. The mice were then returned to room air until at P12 until P17. Retina were harvested for RNA and protein isolation (please refer **Figure 10** for a schematic representation of the OIR mouse model)

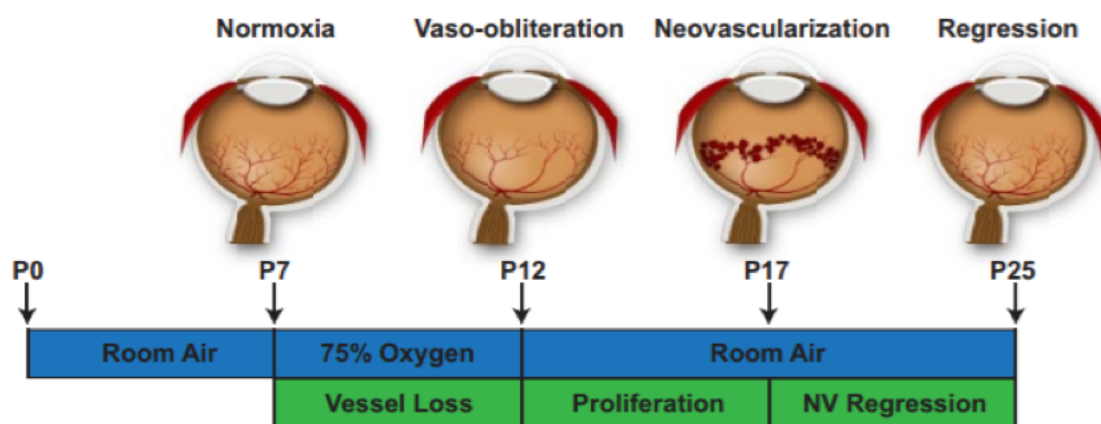


Figure 10: Schematic of the mouse model of OIR. From P7 to P12 mice are exposed to 75% oxygen for 5 days, which inhibits retinal vessel growth and causes significant vessel loss, leading to a central zone of vaso-obliteration. At P12, when the mice are returned to room air, the central avascular retina becomes hypoxic, triggering pathological neovascular growth, which reaches its maximum severity at P17. Between P17 and P25 neovascularisation begins to regress. (Adapted from Nature Protocols, Volume 4, Pages 1565-1573 (8th October 2009)²⁴²)

2.5 Protein Isolation from Retinal Tissue

Eyes were enucleated by placing 45° forceps under the eyeball. Eyes were transferred to a 1.5 mL Eppendorf tube containing 1 mL 1X PBS and kept on ice until all remaining eyes had been harvested. Enucleated eyes were transferred to a 9 mm petri dish and submerged in 1X PBS. The retinae were dissected under using Leica M165 FC Stereo Microscope. Forceps were used to grip the optic nerve and gently rotate the eye such that the front (cornea and lens) were facing upwards. Whilst maintaining a grip on the eye an 18-gauge needle was used to make a small incision on the ora serrata, the serrated junction between the retina and ciliary body. Micro-dissection scissors were placed within the puncture and used to cut around the circumference of the ora serrata as the eye was gently rotated using the forceps gripping the optic nerve. After finishing the cut, the cornea, iris, and lens could be removed, leaving behind the posterior section of the eye. Two pairs of straight micro-forceps were then used to free the retina by peeling it away from the eyecup (RPE/Choroid). To do so, one pair of forceps was used to grip tightly between the eyecup and the retina. A second pair of forceps was placed loosely between the eyecup and the retina. The first pair of forceps were slowly pulled such that it caused the second pair of forceps to slide along the eye, detaching the retina from the eyecup (the action is similar to grasping a piece of paper between the thumb and forefinger of one hand and gently pulling it through the grasp with the other hand). Once the retinae had been separated from the eyecup they were transferred into a new 1.5 mL eppendorf tube, snap-frozen in liquid nitrogen and stored at -80°C.

Retina were homogenised before adding 30 µL of cold RIPA lysis buffer (*please refer to **Appendix Table 6** for RIPA buffer composition*). Samples were incubated on ice for 10 minutes before being snap-frozen in liquid nitrogen, thawed in a water bath and vortexed for 10 seconds. This freeze-thaw cycle was repeated three times before samples were centrifuged at 13,000 RPM for 10 minutes to remove cell debris. The supernatant for each sample was

transferred into a new 1.5 mL and protein concentration was determined by Bradford Assay.

2.6 Sodium Dodecyl Sulphate Polyacrylamide Gel Electrophoresis (SDS-PAGE)

After calculating protein concentration using the Bradford assay, samples were diluted in Laemmli loading buffer (*please refer to **Appendix Table 6** for Laemmli buffer composition*) so that an equal amount of protein for each sample was loaded onto the gel. Each sample was prepared in 20 μ L volume and denatured by incubating at 100°C for 5 minutes. All samples, including a molecular weight marker, were loaded into the wells of a 10% SDS-PAGE gel (*please refer to **Appendix Table 22** for SDS-PAGE gel composition*). The gel was placed into a Mini Trans-Blot® Cell (**Appendix Table 3**) and topped up with running buffer before securing the lid and ensuring the terminals were correctly aligned (red to red and black to black). The gel was run at 80 V for 30 minutes to allow samples to pass through the stacking gel. After which the voltage was increased to 110 V for 2 hours (or until the loading dye had run off the end of the gel).

2.7 Western Blotting: Wet Transfer

Following electrophoresis, proteins were blotted onto a polyvinylidene fluoride (PVDF) membrane (**Appendix Table 4**) using a wet blotting system. Sponges and filter paper were soaked in transfer buffer before being assembled in gel/membrane sandwich in the blotting cassette as follows; sponge, 2 x filter paper, PVDF membrane (pre-soaked in methanol), 2 x filter paper. A roller was used to remove any bubbles between layers. The blotting cassette was clamped tightly together and placed into a Mini Trans-Blot® Cell along with an ice pack. The tank was topped up with transfer buffer (*please refer to **Appendix Table 6** for transfer buffer composition*) to the fill level and the lid secured,

ensuring the terminals were correctly aligned. The transfer was run at 90V for 90 minutes. Once complete, the blotting cassette was disassembled, and the membrane was removed for target protein detection.

2.8 Target Detection

After transferring, the membrane was blocked in 5% milk solution for 1h at room temperature under gentle agitation. The membrane was washed 3 X 15 minutes in TBS-T followed by overnight incubation at 4°C with primary antibody (**Table 10**) diluted in 5% BSA (*please refer to **Appendix Table 6** for 5% milk solution, 5% BSA blocking buffer, and TBS-T composition*). Gentle agitation was applied to ensure homogenous covering of the membrane by antibody containing blocking buffer. The following morning, the membrane was washed 3 X 15 minutes in TBS-T to remove residual primary antibody and then incubated with blocking buffer containing appropriate Horse Radish Peroxidase (HRP) conjugated secondary antibody (**Appendix, Table 11**) for 2h at room temperature. After incubation the membrane was washed with TBS-T 3-4 times for 2h at room temperature with gentle agitation to remove residual secondary antibody.

Chemiluminescence was used to visualize targets of interest. Firstly, excess TBS-T was removed from the membrane by blotting gently on a paper towel. Equal volumes of solution A (fixation agent) and solution B (development agent) of SuperSignal™ West Pico PLUS Substrate (**Appendix, Table 3**) were mixed together and applied directly onto the membrane. The membrane was then placed between two plastic sheets inside a developing cassette with protein side facing upwards. All subsequent steps were carried out in a dark room. The light sensitive X-Ray film was removed from its packaging, cut to size and placed over the membrane. The cassette lid was closed, and the film exposed to the membrane. After exposure the film was developed.

2.9 Western Blot Stripping

To re-probe the membrane for the detection of other protein targets, the membrane was first washed three times in TBS-T to remove the staining. The primary and secondary antibodies were removed by incubating the membrane in stripping buffer for 10 minutes at room temperature under gentle agitation, washed under running tap water to remove stripping buffer followed by blocking in 5% (w/v) fat free milk solution in TBS-T for 1h at room temperature. After the membrane was probed with new primary antibody and as described above.

2.10 RNA Isolation from Retinal Tissue

Retina were dissected as previously described (*please refer to methods section 2.5*). To isolate RNA from retinal tissue 500 μ L RNAzol®RT was added directly to each dissected retina in a 1.5 mL eppendorf tube and homogenised using a 23 and 26G needle. 200 μ L of RNAase free dH₂O was added to the tissue homogenate. The resulting mixture was shaken vigorously for 15 seconds, incubated at room temperature for 10 minutes before centrifuging at 12,000G for 15 minutes. Following centrifugation, DNA, proteins, and most polysaccharides form a semisolid pellet at the bottom of the tube, whereas the RNA remains soluble in the supernatant. Approximately 550 μ L of the supernatant (75% of the total supernatant volume) was transferred to a new tube leaving a layer of the supernatant above the DNA/protein pellet. To precipitate the RNA, 200 μ L of 75% ethanol was added to the supernatant and samples were stored at -20°C overnight. The following day, samples were centrifuged at 12,000g for 8 minutes, after which the RNA precipitate formed a white pellet at the bottom of the tube. The pellet was washed a further 2-3 times using 75% ethanol and centrifuging at 8,000g for 3 minutes. After the final wash, the RNA pellet was air-dried for 5 minutes and then dissolved in 20 μ L of RNAase free dH₂O. Extracted mRNA was quantified using a NanoDrop ND-1000 Spectrophotometer. Purity was determined using 260/280 and 260/230

ratios; only samples with values over 1.8 were used for gene expression studies. RNA samples were stored at -80°C.

2.11 Quantification of DNA and RNA by Spectroscopy

DNA and RNA preparations were quantified using the NanoDrop™ 2000c. Following background correction with μL of dH_2O , 1 μL of DNA was quantified by measuring the absorbance at 260nm. A conversion factor of 50 for DNA and 40 for RNA for every unit of absorbance represents an estimated 50 $\mu\text{g}/\text{L}$ and 40 $\mu\text{g}/\mu\text{L}$ respectively.

2.12 First Strand cDNA Synthesis

First strand cDNA was synthesised from RNA using 5X qScript® cDNA SuperMix Kit. 1 μg of RNA was added into a RNase free 0.2 mL tube, along with 4 μL of 5X qScript® cDNA SuperMix and RNase free dH_2O . The reaction volume per RNA template was 20 μL (refer to **Table 17** for the composition of the qScript® cDNA SuperMix).

2.13 SYBR® Green Real-Time PCR

The cDNA was subject to quantitative real time polymerase chain reaction (RT-qPCR). Each reaction was performed in a 20 μL volume containing cDNA, forward and reverse primers, nuclease free dH_2O and iTaq™ Universal Synergy Brands (SYBR®) Green Supermix. Reactions were performed in experimental duplicates and read from a 96-well plate. All RT-qPCR components were thawed on ice. A master-mix for each target gene was prepared by combining forward and reverse primers (*please refer to **Appendix Table 18** and **Table 19** for primer sequences*), nuclease free dH_2O and SYBR® Green supermix in a 1.5 mL eppendorf tube on ice (*please refer to **Appendix Table 20** for SYBR® reaction volume composition*). The 96-well RT-qPCR plate was placed on ice

and 19 μL of the master-mix was added to the wells, followed by the addition of 1 μL of sample cDNA. The 96-well plate was briefly centrifuged to ensure all components were collected at the bottom of each well. RT-qPCR was performed using Applied Biosystems StepOnePlus™ Real Time PCR System (please refer to **Appendix Table 21** for RT-qPCR cycling conditions).

Relative gene expression was quantified using the $\Delta\Delta\text{CT}$ method to calculate fold change, normalising against the housekeeping gene β -actin, as described in the equation below.

Relative Expression:

$$2^{-\Delta\Delta\text{CT}}$$

Where:

$$\Delta\Delta\text{CT} = \Delta\text{CT}_{\text{sample}} - \Delta\text{CT}_{\text{control}}$$

$$\Delta\text{CT} = \text{CT}_{\text{gene of interest}} - \Delta\text{CT}_{\text{housekeeping gene}}$$

2.14 Cell Culture Basics

All cell culture was performed in sterile conditions in an Airstream® (ESCO) Class II biological safety cabinet. All materials and equipment to be used in the biological safety cabinets were either sterilised with 70% IMS or autoclaved. All cell culture plastic-ware was bought pre-sterilised. Any liquids were bought pre-sterilised or were sterile filtered using a 0.22 μM filter in the biological safety cabinets. Cells were cultured in an incubator in humidified conditions at 37°C and 5% CO₂. All cell culture media was pre-warmed in a 37°C water bath for 30 minutes prior to cell culture.

2.15 Thawing Cells

Prior to thawing, a T25 tissue culture flask was coated with Quick Coating Solution for 5 minutes. Cryopreserved cells (1ml per cryovial) were defrosted rapidly in a 37°C water bath and transferred to a 15 mL universal tube

containing 9ml of appropriate cell growth media. The cell suspension was then placed into a centrifuge and spun at 1300 rpm for 5 minutes. After pelleting, the supernatant was removed and the cells re-suspended in 5 mL appropriate cell growth media. The quick coat solution was removed from the T25 flask and the cell suspension was transferred from the 15 mL universal. Media was replaced the following day and every 2-3 days thereafter until cells were 80-90% confluent.

2.16 Counting Cells

To count the number of cells in a cell suspension, a glass haemocytometer was used. The haemocytometer and coverslip were cleaned with 70% ethanol prior to use. The coverslip was moistened with water to affix to the haemocytometer. Cells were re-suspended in 1ml of the appropriate culture medium. 10 μ l of the cell suspension was pipetted into the haemocytometer tip at the edge of the chambers, allowing capillary action to draw the suspension from the pipette. The haemocytometer was viewed under an inverted microscope at 10x objective and phase contrast was used to visualise cells. A hand tally counter was used to count the total number of cells within a one set of 16 squares occupying a volume of 1×10^{-4} ml. To avoid counting cells more than once, cells were only counted when they were set within a square or on the left-hand or top boundary line. Counting was repeated for the remaining 3 sets of 16 squares to obtain an average cell number. The calculation outlined below was used to calculate the total number of cells per mL of cell suspension.

Number of cells/mL:

$$(X / D) * Y$$

Where:

X = Number of live cells counted

D = Dilution Factor

Y = 1mL/volume of 1 haemocytometer corner square

e.g. (240 live cells/4 squares) $\times 10^4$
= 6×10^5 cells/mL

Calculation for cell seeding:

$$(A/B) * N = Tc$$

Where:

A = Number of cells needed

B = Number of cells counted/mL

N = Number of wells/flasks to be seeded

Tc = Total volume of cell suspension

$$Tv - Tc = Tm$$

Where:

Tv = Total final volume of all wells/flasks

Tm = Total respective media required

2.17 Primary Cells: Culture and Sub-Cultivation

Human Retinal Microvascular Endothelial Cells (HRECs) isolated from normal human retinal tissue were purchased as a cryopreserved stock of 5×10^5 cells per vial at passage 3. Upon thawing, HRECs were plated onto a T25 tissue culture flask coated with Quick Coating Solution and maintained in Endothelial Growth Medium (EGM-2™). EGM-2™ was made from a kit comprised of Endothelial Basal Media (EBM-2™) and Endothelial Growth Supplement Mix. To prepare the culture medium the contents of the supplement mix were added to 500 ml of EBM-2™ in a class II biological safety cabinet. In addition, 1% penicillin/streptomycin was added (*please refer to **Appendix Table 12** for the specification of EBM-2™ media composition*).

Cultures were grown at 37°C in 5% CO₂ with media replaced every 2-3 days. Upon reaching 80-90% confluence cells were passaged to allow for cellular proliferation to expand the number of cells available for experimentation. To passage cells, media was removed from the T25 flask and washed once with 2.5 mL of 1X phosphate buffered saline (PBS) to remove any residual serum proteins. Flasks were then incubated with 1 mL of trypsin EDTA at room temperature for 2-3 minutes. To counteract the action of trypsin 2.5 mL of EGM-2™ was added and the cell suspension was transferred into a 15 mL universal tube. The cell suspension was centrifuged at 1300 rpm for 5 minutes before re-suspending in 1 ml of culture medium. Cells were either plated at the desired

density for experiments or re-plated for continued cell culture. HRECs were split in the ratio of 1:3. HRECs were used until passage 12 in this study.

2.18 Primary Cells: Cryopreservation

When cells had reached 90% confluency, they were trypsinised. Cells were resuspended in 1 mL of cell freezing media (*please refer to **Appendix Table 5** for cell freezing medium details*) and counted. Cells were re-suspended further to a concentration of 1×10^6 cells per mL. The cell suspension was added to 1 mL cryovials labelled with cell type, cell passage number, cell concentration and date of cryopreservation. Cryovials were cooled on ice for 10 minutes and then transferred to a freezing container that enabled cells to be cooled at a rate of -1 °C per minute. The container was placed into a -80 °C freezer overnight before transferring the cryovials to a liquid nitrogen dewar for long-term storage.

2.19 Freestyle 293-F Cells: Culture and Sub Cultivation

Freestyle 293-F cells were purchased as a cryopreserved stock of 1×10^7 cells in 1 mL 90% Freestyle Expression Medium (FEM) and 10% DMSO. Prior to thawing, a 125 mL shaker flask was filled with 30 mL of pre-warmed freestyle 293 culture media. Cryopreserved cells were removed from liquid nitrogen storage and defrosted rapidly in a 37 °C water bath. Just before cells were completely thawed, the outside of the vial was decontaminated with 70% IMS and the entire contents of the cryovial was then transferred directly to the 125 mL shaker flask. Cells were incubated in a 37 °C incubator containing a humidified atmosphere of 8% CO_2 on an orbital shaker platform rotating at 125 rpm. To allow oxygenation/aeration the cap of the flask was loosened a quarter turn from snug.

Cells were sub-cultured once the cell density had reached greater than $2-3 \times 10^6$ cells/mL (typically 3 to 5 days). After determining the total cell number, the cell suspension was transferred aseptically from the 125 mL shaker flask into a 50 mL universal tube and spun at 100 G for 5 minutes. Cells were resuspended in the appropriate volume of pre-warmed FEM to give a cell density of 3×10^5 cells/ mL. Either 125- or 250-mL shaker flasks containing 30- or 50-mL total working volume of cell suspension, respectively were used.

2.20 Freestyle 293-F Cells: Cryopreservation

Freezing medium was prepared immediately before use. In a sterile 15 mL universal the following reagents were mixed together for every 1 mL of freezing medium needed: 0.9 mL FEM and 0.1 mL DMSO. The freezing medium was filter sterilised using a 0.22 μ M filter unit and then placed on ice until use. Any remaining freezing medium was discarded after use.

The Freestyle 293-F cells were counted to determine the total cell number. After determining the total cell number, the cell suspension was transferred aseptically from the 125 mL shaker flask into a 50 mL universal tube and spun at 100 G for 5 minutes. Cells were resuspended in the required volume of freezing medium to give a final cell density of $5-8 \times 10^6$ cells/mL. 1 mL of the cell suspension was aliquoted into a cryovial labelled with the cell type, cell passage number, cell concentration and date of cryopreservation. Cryovials were cooled on ice for 10 minutes, transferred to a freezing container and placed into a -80 °C freezer for at 24hours before transferring the cryovials to a liquid nitrogen dewar for long-term storage.

2.21 Molecular Cloning of CFB Sequence

The coding sequence human CFB (NM_001710.5) carrying a 6XHis tag at the 3' end and Kozak consensus sequence at the 5' end was cloned into pcDNA3.1 at the AFLII/XbaL sites to form pcDNA-CFB-His (*please refer to **Figure 11***).

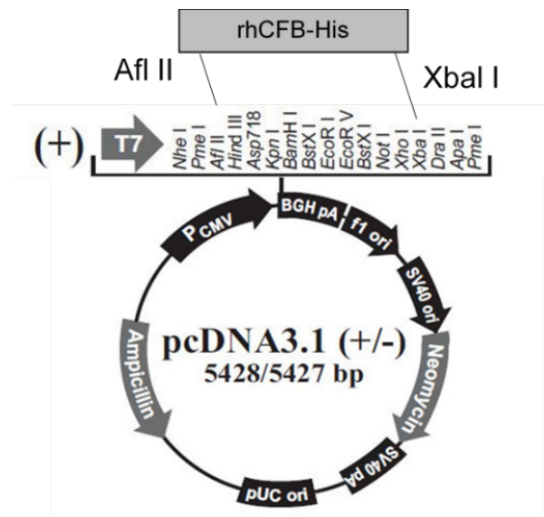


Figure 11: Schematic outline of the rhCFB cloning strategy. The coding sequence of human CFB (NM_001710.5) with a 6 X His tag at the 3' end was cloned into pcDNA3.1 expression vector at the Afl II/ Xba I sites to form pcDNA-rhCFB-His.

2.22 Polymerase Chain Reaction (PCR)

The coding sequence of human CFB (NM_001710.5) was amplified from sequence-verified cDNA clone MGC:1795 IMAGE:2959705 (Dharmacon), using Q5® High-Fidelity DNA Polymerase. All reaction components were assembled on ice in a 0.2mL PCR strip tube (*please refer to **Appendix Table 15** for the final PCR Mastermix composition*). The reaction was gently mixed, followed by a pulse spin to collect all liquid to the bottom of the tube, before transferring the PCR tubes to the PCR machine for thermocycling (*please refer to **Appendix Table 16** for the PCR amplification thermocycling conditions*).

2.23 Agarose Gel Electrophoresis

PCR products were separated and analysed for reaction quality by gel electrophoresis using a 1% agarose gel. 1% (w/v) agarose was prepared by mixing 1g agarose powder in 100 mL 1 X TBE buffer and microwaving at full power for 2 minutes. The solution was cooled before adding 10 µL GelRed®

nucleic acid gel stain (**Appendix Table 5**) to visualise DNA using ultraviolet (UV) light. Gels were poured into Sub® Cell GT electrophoresis chambers (**Appendix, Table 3**) and allowed to set before being placed into gel box and flooding with 1 X TBE buffer. PCR samples were mixed with GelPilot® DNA loading dye and loaded into the wells of the agarose gel. Samples were run next to GeneRuler 1 kb DNA ladder for approximate size calculation. Gels were run at 120V for 1.5 hour and then removed from the tank and placed onto a Dark Reader™ blue light transilluminator to visualise the bands of stained nucleic acid.

2.24 PCR Product Purification

PCR product was purified using QIAquick PCR purification kit (**Appendix, Table 9**) to remove unincorporated primers, left over dNTPs, salts, and other impurities from PCR amplicons. The method was carried out in accordance with the manufacturers protocol. DNA concentration was measured using the NanoDrop™ 2000c

2.25 Restriction Digestion

Restriction enzyme digestion of plasmid DNA (pcDNA3.1 vector and CFB insert) was performed with AFLII and XbaL restriction endonucleases (**Appendix, Table 9**) in FastDigest buffer (**Appendix, Table 9**). Restriction enzyme digests were performed using the buffer system with time and temperature according to manufacturer's instruction. Briefly, 20 units of enzyme was used in a reaction mixture containing the FastDigest buffer, 1 µg plasmid DNA, and incubated at 37°C for 1-2 hours in a water bath.

2.26 Agarose Gel Purification

The digested DNA product was separated in 0.8% agarose gel. The DNA fragment with appropriate size was excised from the gel using a clean scalpel. Purification proceeded using the QIAquick Gel Extraction Kit (**Appendix, Table 9**) in accordance with the manufacturers protocol. DNA concentration was measured using the NanoDrop™ 2000c.

2.27 Ligation

DNA ligation was carried out in a 20 µL reaction volume by combining 50 ng vector DNA (pcDNA3.1) in a 3:1 molar ratio with insert DNA (CFB) and Quick Ligation™ Kit components in a microcentrifuge tube on ice (*please refer to Appendix Table 14 for the Quick Ligation reaction components*). The online NEBicalculator was used to calculate molar ratios. The reaction was mixed by gentle pipetting before incubating at room temperature for 5 minutes. The ligation reaction mixture was chilled on ice before transforming into 50 µL of competent cells.

2.28 Transformation

Microbiological Luria-Bertani (LB) agar plates were used for growing bacterial cells. To make 200 mL (enough for approximately 20 plates), 7g of Agar powder (**Appendix, Table 5**) was added to 200 mL dH₂O in a glass Duran. The mixture was shaken briefly to free the powder from the bottom of the bottle and remove major clumps, before autoclaving to sterilise. After autoclaving the mixture was cooled slightly (not below 45-50°C) and 25 µg/mL Chloramphenicol antibiotic (**Appendix, Table 5**) was added. Approximately 10 mL of LB agar was poured into each plate.

Bacterial strains were grown in LB medium (**Appendix, Table 5**) with antibiotic selection from a single colony. Stocks of bacteria were stored at -80°C in cryovials in a minimum of 10% glycerol. For each transformation, 5 µL of the ligation reaction was mixed with 50 µL of chemically competent cells by gentle pipetting and incubated on ice for 30 minutes, followed by heat shock at 42°C for 30 seconds. The cells were allowed to recover in 950 µL of room temperature media (without antibiotic) and then incubated for 60 minutes at 37°C with shaking at 250 rpm. Cells were plated on LB-agar plates containing 25 µg/mL chloramphenicol antibiotic and incubated statically at 37°C overnight.

2.29 Mini-Prep

After overnight incubation, a single colony was picked up using a sterile pipette tip and cultured with 4 mL of LB media containing and cultured overnight at 37°C on an orbital shaker at 190-225 rpm. The bacteria were pelleted and lysed for plasmid DNA isolation using QIAprep Spin Miniprep Kit (**Appendix, Table 9**) in accordance with manufactures protocol. The plasmid DNA was then adsorbed on a QIAprep membrane, washed then eluted with nuclease free H₂O. The DNA was quantified using the NanoDrop™ 2000c.

2.30 Freestyle 293-F Transfection

Over-expression of CFB in Freestyle 293-F cells was achieved using a transient transfection method. Transfection experiments were performed in a 30 mL volume with a total cell count of 3×10^7 cells. The day before transfection Freestyle 293-F cells were counted to determine the total cell number. After determining the total cell number, the cell suspension was transferred aseptically from the 125 mL shaker flask into a 50 mL universal tube and spun at 100 G for 5 minutes. Cells were resuspended in the required volume of pre-warmed FEM to give a final cell density of $6-7 \times 10^5$ cells/mL.

The following day, cells were counted again as described in to determine the total cell count and cell viability. For optimal transfection cells needed to be in a single cell suspension with viability of over 90%. The volume of cell suspension containing 3×10^7 cells was calculated and transferred into a new 125 mL shaker flask. The volume was topped up to 30 mL with fresh pre-warmed FEM. The shaker flask was incubated in a 37°C incubator containing a humidified atmosphere of 8% CO₂ on an orbital shaker platform rotating at 125 rpm whilst the transfection reagent mix was prepared. For the transfection of one 125 mL flask containing 3×10^7 cells in 30 mL FEM, 112.5 µL OptiMEM containing 37.5 µL of lipofectamine 2000 was added to 150 µL Opti-MEM® containing 37.5 µg of pCFB in a 1.5 mL eppendorf tube and incubated at room temperature for 20 minutes to allow the DNA-lipofectamine complexes to form. After incubation, the transfection reagent mix was added dropwise to the 125 mL shaker flask prepared earlier. The shaker flask was incubated in a 37°C incubator containing a humidified atmosphere of 8% CO₂ on an orbital shaker platform rotating at 125 rpm. Samples of conditioned media were harvested every 24h to check for recombinant protein expression.

Approximately 72h after transfection, cells were counted to determine the total cell number. After determining the total cell number, the cell suspension was transferred aseptically from the 125 mL shaker flask into a 50 mL universal tube and spun at 100 G for 5 minutes. The conditioned media was collected into a new 50 mL universal and stored at -80°C until downstream protein purification was to be carried out.

2.31 Protein Purification

2.31.1 Buffer Preparation

0.1M Sodium Phosphate Buffer

To prepare 50mL 1M stock solutions of $\text{NaH}_2\text{PO}_4 \cdot \text{H}_2\text{O}$ (monobasic) and $\text{Na}_2\text{HPO}_4 \cdot \text{H}_2\text{O}$ (dibasic), 6.9 g and 8.9 g were dissolved in dH_2O respectively (Table 7). To prepare 500mL of 0.1M sodium phosphate buffer at pH 7.4 (from 1M stock), 11.3 mL NaH_2PO_4 and 38.7 mL Na_2HPO_4 were diluted to 1L (final volume) with dH_2O .

Elution and Binding Buffers

To prepare stock buffer 1 and stock buffer 2, buffer components were dissolved in 400 mL dH_2O . The solutions were cooled at 4°C and the pH was adjusted to pH 7.4 before diluting to a final volume of 500mL with dH_2O . Working 50 mL stocks of elution and binding buffers were prepared by mixing the correct volumes of stock buffer 1 and stock buffer 2 (Table 8). Elution and binding buffers were passed through a $0.22 \mu\text{M}$ filter before use.

2.31.2 Protein Concentration

Conditioned media collected from 239-F cells was thawed overnight on ice. After centrifuging at 100 G for 5 minutes, the supernatant was filtered using a $0.22 \mu\text{M}$ filter before being concentrated using an Amicon® Pro Affinity concentrator spun at 4000 G for 30 minutes at 4°C . After each spin the flow-through was discarded and the conditioned media in the reservoir was topped up. Conditioned media was concentrated to 100 X the starting volume.

2.31.3 Buffer Exchange

After concentration, the conditioned media was equilibrated with binding buffer. The concentrated media was gently resuspended using a pipette and the reservoir was topped up with binding buffer before centrifuging at 4000 G for 30 minutes or until the sample was concentrated to 10 X the starting volume. The flow through was discarded and the reservoir topped up to 10 mL with binding buffer. This step was repeated three times.

2.31.4 Protein Binding

Ni Sepharose high performance nickel-charged immobilised metal ion affinity chromatography (IMAC) resin was used to purify the rhCFB. 600 μ L of Nickel beads were transferred to a 15 mL falcon tube, topped up to 5 mL with cold sterile PBS and centrifuged at 800 G for 5 minutes. This washing step was repeated twice with PBS and a final time with binding buffer. After buffer exchange the concentrated protein solution was gently re-suspended before being transferred to the 15 mL falcon with Ni beads. The tube was topped up to 10 mL with binding buffer and incubated on the roller at 4°C overnight.

2.31.5 Elution

After overnight incubation the Ni beads were centrifuged at 800 G for 5 minutes. The supernatant was removed, and the beads were incubated with 10 mL cold binding buffer on the roller at 4°C for 10 minutes, before being centrifuged at 800 G for five minutes. This washing step was repeated three times. After the final wash, Ni beads were incubated with 2 mL of elution buffer on the roller at 4°C and incubated for 10 minutes before being spun at 800 G for 5 minutes. The eluent was collected, and the protein concentration was evaluated using Bradford reagent (180 μ l 1 \times Bradford + 20 μ l eluent) and checking for a colour change by eye. The elution steps were repeated until a colour change could no

longer be observed using the Bradford reagent. The eluent was then concentrated using Amicon Ultra 2 mL centrifugal filters. The membrane was washed first by adding 500 μ L of cold PBS and spun at 4000 G for approximately 10 minutes (or until all of the PBS has passed through). After washing the membrane was spun at 4000 G for 10-15 minutes or until the sample was concentrated to 4 X the starting volume. The flow through was discarded and the reservoir topped up to 2 mL with eluent. This step was repeated, each time topping up the reservoir once the level of eluent drops, until the eluent was concentrated to approximately 500 μ L. The the protein concentration was evaluated using Bradford reagent.

2.31.6 Dialysis

To remove imidazole from the concentrated protein solution dialysis was carried out using a 15 mL Scientific Slide-A-Lyzer MINI Dialysis Device. The Slide-A-Lyzer MINI Dialysis Device was removed from the conical tube, being careful to not touch the dialysis membrane so to avoid contamination. 14 mL of cold PBS buffer was added to the conical tube. 500 μ L of the concentrated protein sample was added to the device, which was then placed slowly into the conical tube containing the buffer, making sure the membrane was in contact with the buffer and no air bubbles had been introduced. The conical tube was placed in the 4°C cold room on an orbital shaker set at 200 rpm. The dialysis procedure was as follows: dialyze for 2h; change the dialysis buffer and dialyze overnight. After overnight dialysis, the device was removed from the conical tube and the sample collected using a pipette. The protein concentration of the sample was measured, and the protein purity was confirmed by InstantBlue™ protein stain solution (Concentrated protein was aliquot into smaller volumes in 1.5 mL eppendorf tubes, and stored at -80°C).

2.31.7 Protein Purity

Gels were prepared and run as described (*please refer to section 2.23*). Following electrophoresis gels were removed from cassettes and transferred directly into the InstantBlue™ staining solution, making sure the gel was able to move freely within the solution to allow for diffusion. Protein bands were allowed to develop for 15 minutes at room temperature with gentle agitation.

2.32 Primary Cell Transfection: Small Interfering RNA (siRNA) Silencing

10 nM pooled CFB siRNA was briefly centrifuged to ensure that the pellet was collected at the bottom of the tube before resuspending in 100 µL of RNase-free dH₂O to obtain a stock solution with a concentration of 100 µM. The tube was securely sealed with and placed onto an orbital shaker for 30 minutes at room temperature. siRNA was briefly centrifuged again to ensure that the solution was collected at the bottom of the tube before being aliquoted into smaller 5 µL volumes to limit the number of freeze-thaw cycles. Resuspended siRNA was stored at -20°C. After thawing, storage at 4°C was suitable for up to 6 weeks.

Knockdown of CFB in primary cells was achieved using a transient transfection method. HRECs were seeded in EGM-2™ overnight at a density of 2×10^5 cells per 6-well so that the following day they were approximately 70-90% confluent before transfection. For transfection of one well, 150 µL OptiMEM® containing 6 µL of lipofectamine 3000 was added to 150 µL OptiMEM® containing 1µL of 100 µM stock CFB siRNA in a 1.5 mL eppendorf tube and incubated at room temperature for 20 minutes. 1.2 mL of fresh OptiMEM® was added to the 300 µL transfection reagent mix giving a final concentration of 66nM. HRECs were washed once with Opti-MEM® before adding the transfection mix. HRECs were incubated with the transfection mix

for 6h at 37°C and 5% CO₂. After 6h, the transfection reagent mix was removed and replaced with 1.5 mL fresh EGM-2™. Cells were incubated for a further 24h-48h before they were used for downstream experiments. CFB knockdown was confirmed by qRT-PCR.

2.33 Primary Cell Transfection: CFB Over-expression

Over-expression of CFB was achieved using a transient transfection method (*please refer to section 2.21 for molecular cloning of CFB*). HRECs were seeded in EGM-2™ overnight at a density of 2X10⁵ cells per 6-well so that the following day they were approximately 70-90% confluent before transfection. For the transfection of one well, 150 µL OptiMEM® containing 2 µL of lipofectamine 3000 was added to 150 µL Opti-MEM® containing 1 µg of pCFB and 2 µL p3000 in a 1.5 mL eppendorf tube and incubated at room temperature for 20 minutes. After incubation 1.2 mL of fresh Opti-MEM® was added to the 300 µL transfection reagent mix. HRECs were washed once with Opti-MEM® before adding the transfection mix. HRECs were incubated with the transfection mix for 6h at 37°C and 5% CO₂. After 6h, the transfection reagent mix was removed and replaced with 1.5 mL fresh EGM-2™. Cells were incubated for a further 24-48h before they were used for downstream experiments. CFB over-expression was confirmed by qRT-PCR.

2.34 Growth factors and Inhibitor Treatments

Recombinant human CFB (rhCFB) was expressed in FreeStyle™233-F cells and purified as described (*please refer to section 2.31 for transfection protocol*). For all *in vitro* and *ex vivo* assays rhCFB was used at a concentration of 100 µg/mL. The multi-targeted tyrosine kinase inhibitor, Linifanib, was used in the Matrigel® network formation assay at a concentration of 5nM.

2.35 Cell Viability Assay

Cell viability of cultured cells was evaluated over 2 days using the colorimetric MTS tetrazolium assay in a 96-well tissue culture plate. Prior to cell seeding, the number of individual wells required for the assay were calculated and each well was coated with 50 μL of Quick Coating Solution for 5 minutes. To evaluate HREC viability after rhCFB treatment, cells were seeded at 1000 cells per 96-well in 100 μL EGM-2™ and cultured for 24 hours. After 24h culture cells were washed once with 1X PBS and cultured in EBM-2™ for 3h. Following this, EBM-2™ media was aspirated from the wells and replaced with EGM-2™ containing either 100 $\mu\text{g}/\text{mL}$ rhCFB or equivalent vehicle control. The day 0 time point was taken immediately after adding treatments. To evaluate HREC viability after CFB knockdown or over-expression, cells were transfected as described (*please refer to section 2.32 and 2.33*) and harvested after 48h. Cells were seeded at 1500 cells per 96-well in 100 μL EGM-2™ and cultured for 4h to allow cells to settle and adhere. After cells had adhered the EGM-2™ was aspirated, cells were rinsed once with 1X PBS and cultured for 3h in EBM-2™. Following this EBM-2™ was aspirated from the wells and replaced with EGM-2™. The day 0 time point was taken immediately after adding fresh EGM-2™.

Cell viability was measured at the following time points: day 0, day 1, and day 2. An equivalent group of EGM-2™ without any cells was included in parallel for use as a media blank. At each time point, 10 μL of MTS reagent was added into the corresponding wells and incubated for 2h at 37°C in 5% CO_2 . After incubation the absorbance of formazan product was measured using a plate reader at the wavelength of 490 nm. The final value was obtained by subtracting the absorbance reading of the media blank control. Each time point was measured in triplicate per group and control.

2.36 Cell Proliferation Assay

Cell proliferation of cultured cells was evaluated by immunofluorescence staining of the nuclear marker Ki67. Cell proliferation was evaluated in a 48-well plate. Prior to cell seeding, the number of individual wells required for the assay was calculated and each well was coated with 500 μ L of Quick Coating Solution for 5 minutes. To evaluate HREC proliferation after rhCFB treatment, cells were seeded at 10,000 cells per 48-well in 500 μ L EGM-2™ and cultured for 24 hours. Following this, fresh EGM-2™ containing either 100 μ g/mL rhCFB or equivalent PBS control was added to the HRECs and cultured for 24h. To evaluate HREC viability after CFB knockdown or over-expression cells were transfected as described (*please refer to section 2.32 and 2.33*) and harvested after 48h. Cells were seeded at 12,000 cells per 48-well in 500 μ L EGM-2™ and Transfected HRECs were cultured for a further 24h.

At the assay endpoint culture media was removed and cells were washed three times with sterile 1x PBS before fixation in 4% paraformaldehyde (PFA) for 15 minutes. Once the cells had been fixed, subsequent work was carried out in non-sterile conditions on the laboratory bench. 4% PFA was aspirated from the wells and cells were washed three times with 1X PBS before being blocked and permeabilised in 1X blocking buffer (*please refer to **Appendix Table 6** for the composition of blocking 1 X buffer*) for 45 minutes at room temperature. After blocking, cells were incubated with primary rabbit anti- Ki67 antibody (*please refer to **Appendix Table 10** for primary antibody details*) diluted in 1x blocking buffer at 4°C overnight. After overnight incubation, cells were washed three times with 1x blocking buffer to remove excess primary antibody before incubating with Alexa Fluo® 594 conjugated goat anti-rabbit IgG secondary antibody (*please refer to **Appendix Table 11** for secondary antibody details*) diluted in 1x blocking buffer, for 2h in the dark at room temperature. Excess secondary antibody was removed by washing three times with 1X PBS followed by incubation with DAPI dye diluted in 1x PBS, for 10 minutes in the dark at room temperature. A final three washes with 1x PBS was carried out before

imaging. Fluorescent images were captured using an Eclipse Ti-E Inverted Research Microscope (Nikon, Japan). Images were captured across five fields of view per well and the total number of cell nuclei and the total number of Ki-67⁺ cell nuclei were manually counted. The cell proliferation rate was calculated as a percentage Ki-67⁺ cells. The average of the five fields of view was taken to give a final proliferation rate per well.

2.37 Matrigel® Network Formation

The day prior to conducting the tube formation assay, growth factor reduced Corning® Matrigel® Matrix was thawed overnight on ice at 4°C. 60ul of completely thawed Matrigel® was plated into each well of a pre-cooled 96-well plate and allowed to polymerise for 30 minutes at 37°C.

To evaluate HREC network formation after rhCFB treatment, cells were seeded onto the polymerised Matrigel® at 12,000 cells per well of a 96-well plate in 100 µL EGM-2™ medium containing either 100 µg/mL rhCFB or equivalent volume of PBS control and cultured overnight for 16 hours. To evaluate HREC tube formation after CFB knockdown or over-expression, cells were transfected as previously described (*please refer to section 2.32 and 2.33*) and harvested after 48h before being seeded at 15,000 cells per well of a 96-well plate in 100 µL EGM-2™ medium and cultured overnight for 16 hours.

After incubation, the vasculature was imaged using Eclipse Ti-E Inverted Research Microscope (Nikon, USA) at 4x magnification. Quantification of the vascular network was analysed using Image J (National Institute of Health, USA) for total number of junctions, total vessel length and total branching length per well. The values for each parameter were normalised to the control group (untreated control, scrambled control or pcDNA control) for statistical analysis.

2.38 Transwell Migration Assay

HREC migration was evaluated using Transwell migration inserts. The day prior to conducting the migration assay, 8 μ M Transwell® 24-Well Plate Inserts were coated with 1 mL Quick Coating Solution for 5 minutes and then allowed to dry thoroughly overnight.

To evaluate HREC migration after rhCFB treatment, cells were seeded in a 6-well plate in EGM-2™ at a density of 2×10^5 cells per well and cultured for 24h. The following day cells were rinsed once with 1x PBS and pre-treated with EBM-2™ containing either 100 μ g/mL rhCFB or equivalent volume of PBS for 24h. After pre-treatment, cells were harvested and seeded into the upper chamber of the 8 μ M Transwell® inserts at a density of 30,000 cells per well of a 24-well plate in 200 μ L EBM-2™. In the lower chamber of the inserts, EBM2 containing 5% foetal bovine serum (FBS) was used as a chemoattractant.

To evaluate HREC tube formation after CFB knockdown or over-expression cells were transfected as previously described (*please refer to section 2.32 and 2.33*), and harvested after 48h. Cells were seeded into the upper chamber of the 8 μ M Transwell® inserts at a density of 40,000 cells per 24-well in 200 μ L EBM-2™. In the lower chamber of the I inserts, 600 μ L EBM2 containing 5% FBS was used as a chemoattractant.

After 4h of incubation media was removed from both the upper and lower chambers and inserts were washed three times in 1x PBS. To fix cells, 1 mL 1% PFA was added to each insert for 10 minutes followed by washing three times with 1x PBS. Cells were permeabilised with 0.2% Triton-X 100 for 10 minutes and non-migrated cells on the upper side of inserts were gently removed using cotton swabs. Inserts were washed a further three times with 1x PBS before migrated cells on the underside of the inserts were incubated with the nuclear stain DAPI, diluted in 1x PBS for 10 minutes in the dark at room temperature. A final three washes with 1x PBS was carried out to remove excess DAPI. Images

were captured across five fields of view per well using an Eclipse Ti-E Inverted Research Microscope (Nikon, USA). The total number of cell nuclei per field of view were counted manually using Image J (National Institutes of Health, USA). The five fields of view were averaged to give a total number of migrated cells per well.

2.39 Aortic Ring Sprouting Assay

All dissection instruments were sterilised before use and kept in 70% industrial methylated spirit (IMS) during the procedure to maintain sterility. The C57BL/6 mouse strain was used for this assay.

The thoracic aortas were dissected from wild type postnatal day 3 (P3) mouse pups. After surface-sterilising the mouse by spraying with 70% industrial IMS, it was lay back-down on a dissecting board with pins used to fix the legs in place. Dissection scissors were used to make a single cut in the ventral skin and blunt dissection was used to peel back the skin. To open the thoracic cavity dissection scissors were used to cut through and along the sternum, and around the ribcage. The heart and lungs were removed to expose the aorta which is visible as a fat-covered blood vessel tracking down along the spine. Forceps were used to grasp the anterior end of the aorta in one hand. Using a closed pair of sharp forceps in the other hand, the aorta was detached from the spinal column by blunt dissection. running the instrument between the aorta and spine all the way down toward the posterior end before the artery branches into the iliacs in the abdomen. Once the aorta was separated from the spine it was cut once near the abdominal branch and once near the anterior end and transferred into a petri dish containing aortic ring media (*please refer to **Appendix Table 13** for the composition of aortic ring media*) Under the Leica M165 FC Stereo microscope dissection microscope all extraneous fat, tissue and branching vessels were removed with forceps and a scalpel. Using a scalpel, the aorta was then cut into rings approximately 0.5 mm in width and

transferred to a new petri dish containing ARM. On average, a total of 5-10 rings can be obtained from each P3 aorta.

Following dissection, the aortic ring explants were embedded in collagen. Type I collagen was prepared to a final concentration of 1mg/mL in ARM and the pH was adjusted to pH 7 by adding 1-N NaOH dropwise into the collagen solution. One aortic ring was embedded per well of a 96-well plate and 8-10 aortic rings were used per treatment group. For embedding, 60 μ L of collagen was added to each well of a 96-well plate and aortic rings were carefully transferred from the petri dish using forceps, ensuring that they were completely submerged in the collagen, and placed so that the luminal axis was parallel to the bottom of the well. The plate was left undisturbed for 10-15 minutes at room temperature followed by incubation for 30 minutes at 37°C and 5% CO₂ to ensure the collagen gel was fully polymerised. After incubation, 100 μ L of ARM without treatment was added to all the aortic rings and they were cultured for 24h. The following day, media was carefully removed from the wells and replaced with ARM containing either 100 μ g/mL rhCFB or equivalent volume of PBS. The media was changed every other day for 5-7 days.

At the conclusion of the culture period, culture media was carefully removed, and the aortic rings were washed once with 200 μ L 1X PBS before being fixed with 100 μ L of 4% PFA for 20 minutes at room temperature. Aortic rings were then washed three times with 200 μ L 1X PBS and submerged in 100 μ L of 1% blocking buffer for 1 hour at room temperature. After blocking, aortic rings were incubated in 50 μ L of 1% blocking buffer containing biotinylated primary anti-GSL I-B₄ Isolectin antibody to stain ECs, and primary rabbit-anti NG2-antibody to stain supporting cells overnight at 4°C in the dark (*please refer to **Appendix Table 10** for primary antibody details*). After incubation, aortic rings were washed with 200 μ L 1% blocking buffer three times to remove excess antibody, followed by incubation with 50 μ L 1X PBS containing DAPI dye in the dark at room temperature. A final three washes with 1X PBS were carried out to remove excess DAPI. After immunofluorescence staining of aortic rings, they

were visualised under the Nikon Eclipse Ti Inverted Fluorescence Microscope. To quantify, starting from a specific point on the ring (e.g. the 12 o'clock position), each micro-vessel emerging from the main ring as a sprout and then individual branches arising from it as separate vessels, were counted. The focus was adjusted manually whilst moving around the ring to ensure that vessels sprouting in different planes were counted. Quantification was carried for the mean number of microvessels per ring. A mean of ≥ 8 aortic rings being analysed for each treatment. Representative images were captured and were processed In Adobe Photoshop to mask for presentation purposes.

2.40 Fetal Metatarsal Sprouting Assay

The fetal metatarsal sprouting assay was carried out as described²⁴³. The C57BL/6 mouse strain was used for this assay. Time-mating was performed to achieve an accurate prediction of the embryonic stages of the foetuses. In brief, a male and two other females were placed in the same cage. Thereafter, the females were examined for a copulatory plug every morning. The plugged female was transferred into a new cage and the gestation stage was considered to be E0.5. Embryos between E16.5 to E18 were sacrificed and metatarsal bones were dissected under a stereomicroscope and maintained in ice-cold dissection media (*please refer to **Appendix Table 13** for the composition of metatarsal dissection media*). Individual metatarsals were mounted onto a 24-well coated with 0.1% gelatin and left to adhere for 5 minutes. Next, 200 μ L of metatarsal growth media was added to each mounted metatarsal (*please refer to **Table 13** for the composition of metatarsal growth media*). The explants were incubated for 48 hours to allow for fibroblast migration out from the metatarsal bones. Any explants lacking fibroblast sprouting were classed as non-viable and were discounted from the assay. Those with visible fibroblast sprouting were subject to further treatments. The explants were treated with 300 μ L of fresh metatarsal growth media containing either 100 μ g/mL rhCFB or equivalent volume of PBS. The media was changed every other day for 10-12 days.

At the conclusion of the culture period culture media was carefully removed, and the metatarsal explants were washed once with 200 μ L 1X PBS before being fixed with 100 μ L of 4% PFA for 20 minutes at room temperature. Metatarsal explants were then washed three times with 200 μ L 1X PBS and submerged in 200 μ L of 1X blocking buffer for 1 hour at room temperature. After blocking, metatarsal explants were incubated with primary rabbit anti-CD31 antibody diluted in 1x blocking buffer at 4°C overnight (*please refer to **Appendix Table 10** for primary antibody details*). After overnight incubation metatarsal explants were washed three times with 200 μ L of 1X blocking buffer to remove excess primary antibody before incubating with Alexa Fluo® 594 conjugated goat anti-rabbit IgG secondary antibody diluted in 1x blocking buffer, for 2h in the dark at room temperature (*please refer to **Appendix Table 11** for secondary antibody details*). Excess secondary antibody was removed by washing three times with 1X PBS followed by incubation with DAPI dye diluted in 1x PBS, for 10 minutes in the dark at room temperature. A final three washes with 1x PBS was carried out before imaging. Explants were imaged directly in the 24-well plate using the Nikon Eclipse Ti Inverted Fluorescence Microscope. The raw images were processed in Adobe Photoshop CS4 to mask for quantification purposes. The total area of the masked image was normalised to the bone area to give the percentage of sprouting area.

2.41 RNA Isolation from Cell Lines

For RNA isolation, all pipetting was carried using filter pipette tips and all centrifugation steps were performed at 4°C. Cell culture media was removed, and cells were washed once with 1X PBS. After washing, 500 μ l RNAzol®RT was added to each well and incubated for five minutes at room temperature to lyse the cells. Following incubation, the lysate was passed through a pipette several times and added to 200 μ L of RNAase free dH₂O in a 1.5 mL eppendorf tube. The resulting mixture was shaken vigorously for 15 seconds, incubated at room temperature for 10 minutes before centrifuging at 12,000G for 15 minutes.

Following centrifugation, DNA, proteins, and most polysaccharides form a semisolid pellet at the bottom of the tube, whereas the RNA remains soluble in the supernatant. Approximately 550 μ L of the supernatant (75% of the total supernatant volume) was transferred to a new tube leaving a layer of the supernatant above the DNA/protein pellet. To precipitate the RNA, 200 μ L of 75% ethanol was added to the supernatant and samples were stored at -20°C overnight. The following day, samples were centrifuged at 12,000g for 8 minutes, after which the RNA precipitate formed a white pellet at the bottom of the tube. The pellet was washed a further 2-3 times using 75% ethanol and centrifuging at 8,000g for 3 minutes. After the final wash, the RNA pellet was air-dried for 5 minutes and then dissolved in 20 μ L of RNAase free dH₂O. Extracted mRNA was quantified using a NanoDrop ND-1000 Spectrophotometer. Purity was determined using 260/280 and 260/230 ratios; only samples with values over 1.8 were used for gene expression studies. RNA samples were stored at -80°C.

and the samples were then processed as described (*please refer to section 2.40*). RNA concentration was determined using the NanoDrop™2000c.

2.42 Biochemical Methods

2.42.1 Protein Isolation from Cell Lysates

Cell culture media was removed, and cells were washed once with 1X PBS before adding 25 μ L of cold RIPA lysis buffer containing 1X protease inhibitor and 1X phosphatase inhibitor to each well of a 6-well plate. A cell scraper was used to dissociate the cells from the bottom of the well and samples were pipetted into 1.5 mL eppendorf tubes and incubated on ice for 10 minutes. After incubation, samples were snap-frozen in liquid nitrogen, thawed in a water bath and vortexed for 10 seconds. This freeze-thaw cycle was repeated three times before samples were centrifuged at 13,000 RPM for 10 minutes to remove cell debris. The supernatant for each sample was transferred into a new 1.5 mL and protein concentration was determined by Bradford Assay.

2.43 Statistical Analysis

Statistical analysis was performed using GraphPad Prism software (GraphPad Software, Inc.). Results are depicted as mean \pm standard deviation (SD). Prior to running any statistical analysis, the Shapiro-Wilk normality test was carried out. If data was found to have normal distribution, for experiments with $n \geq 3$, statistical analysis was performed using unpaired, two-tailed t-test, or one-way analysis of variance (ANOVA) followed by Turkey's multiple comparisons test. If data was not normally distributed, for experiments with $n \geq 3$, statistical analysis was performed using the Mann-Whitney test. Differences were deemed statistically significant for p-values < 0.05 . For gene expression data where all control values are represented as 1, statistical significance was determined on raw delta-CT values by unpaired two-tailed students' t-test.

3 Results

3.1 Characterising the Expression of Complement Factor B Using Rodent Models and Human Patient Samples

CFB, a 95-kDa serine protease, is the crucial catalytic element of the AP that acts as a C3 convertase in the presence of factor D. In addition to its role in activating the alternative pathway, previous studies have shown a link between the CFB and DR pathogenesis (*please refer to chapter 1.9.4.*) To begin with the expression of CFB was characterised using a chemically induced mouse model of diabetes, established by subcutaneous streptozotocin (STZ) injection. To investigate the association between CFB and diabetes, CFB gene and protein expression in the retina of STZ-induced diabetic mice was analysed by RT-qPCR and western blot. No significant differences were observed in either CFB gene or CFB protein expression between the buffer-injected controls and STZ mice (**Figure 12**). Following on from this, CFB protein expression in the serum and aqueous humor of diabetic patients at various stages of DR progression was analysed by western blot. No significant differences were observed in serum samples from diabetic patients with no DR, NPDR and PDR as compared to the non-diabetic control group (**Figure 13**). In the aqueous samples, an up-regulation of CFB protein expression was observed in both diabetic patients with NPDR and PDR, respectively, when compared to diabetic patients with no DR (**Figure 14**).

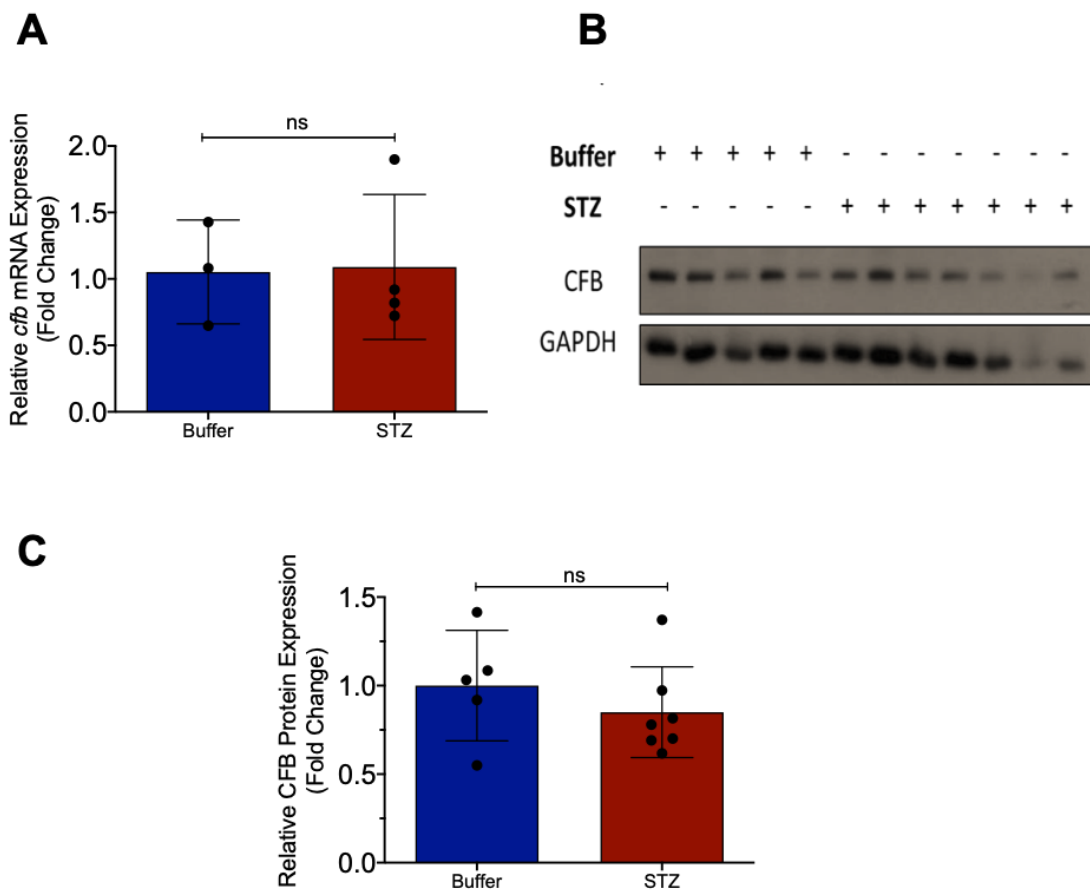


Figure 12: CFB expression in the retina of STZ-induced diabetic mice. Diabetes was induced by Streptozotocin injection. The retinae were harvested for the analysis of CFB mRNA and protein expression. The changes in gene expression were calculated using fold change ($-2(\Delta\Delta Ct)$). The changes in protein expression were detected by western blot **A**, RT-qPCR analysis of CFB transcript levels in the retina of STZ injected mice, represented as fold change normalised to wildtype buffer, **B**, Representative western blot of CFB protein levels in the retina of wildtype buffer and STZ injected mice, GAPDH was used as a loading control. **C**, Densitometry quantification of western blot. CFB was first normalised to the internal control GAPDH. Quantification is represented as fold change normalised to wildtype buffer. Results represent the mean \pm SD. Differences were not statistically significant as tested by Student's t-test: $n \geq 3$

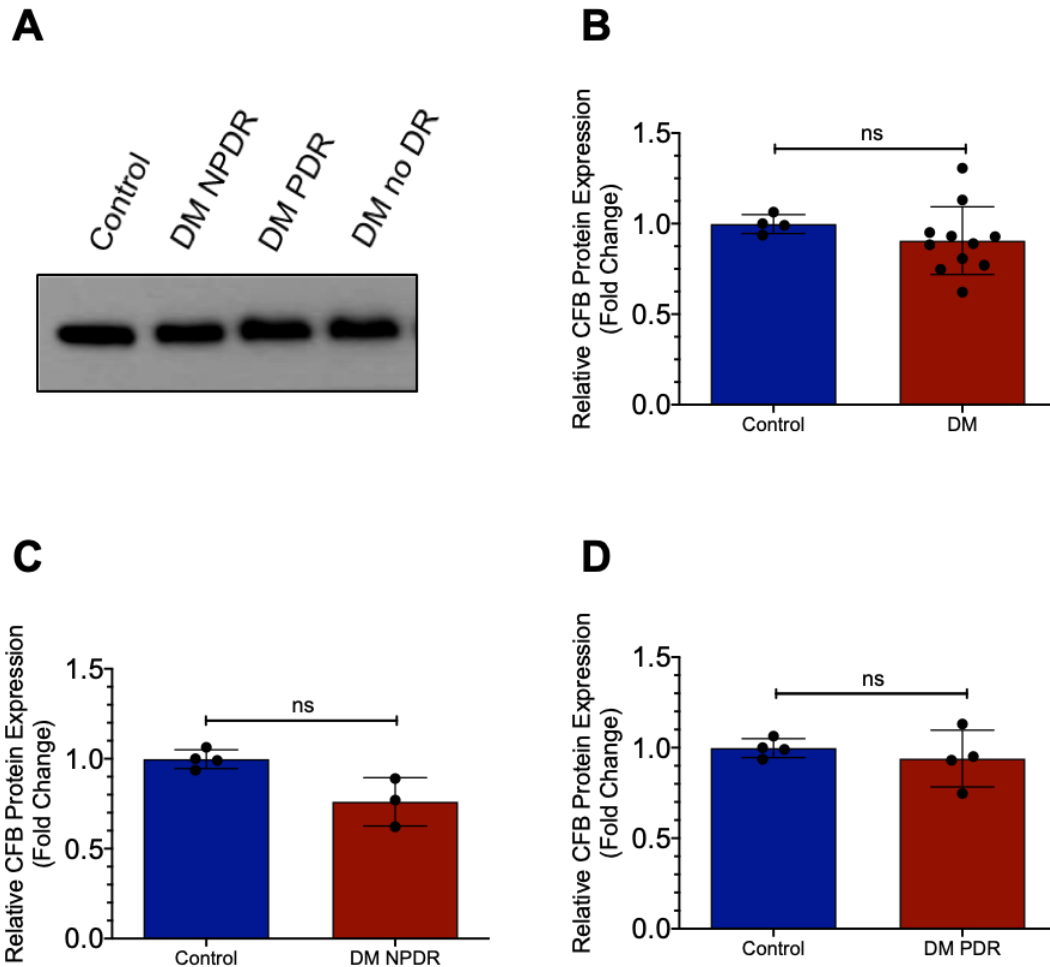


Figure 13: CFB expression in human patient serum samples. Human serum samples from patients with varying severity of DM and DR were analysed for CFB protein expression. The changes in protein expression were detected by western blot. **A**, Representative western blot of CFB. **B-D** Densitometry quantification of western blot. Quantification is represented as fold change normalised to control patient samples. Results represent the mean \pm SD. Differences were not statistically significant as tested by Student's t-test: $n \geq 3$.

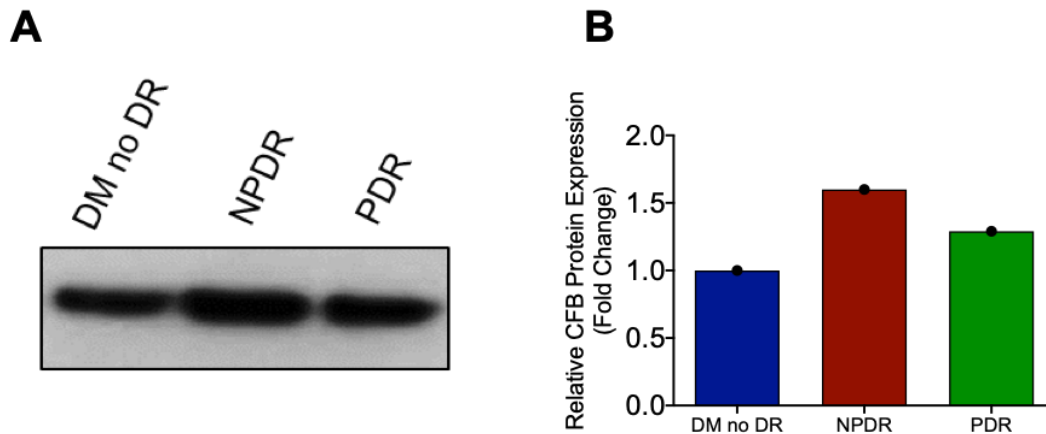


Figure 14: CFB expression in human patient aqueous samples. Human aqueous humor samples from patients with varying severity of DM and DR were analysed for CFB protein expression. The changes in protein expression were detected by western blot. **A**, Representative western blot of CFB. **B**, Densitometry quantification of western blot. Quantification is represented as fold change normalised to DM no DR patient samples. No statistical test was performed: n =1

To study the role of CFB in pathological neovascularisation, the well-established model of oxygen-induced retinopathy (OIR) was used. The OIR model of pathological neovascularization is used to mimic the clinical features of proliferative retinopathies²³⁰. Briefly, neonatal mice were exposed to hyperoxic (75%) conditions from postnatal day (P) 7-12. This abundance of oxygen prevents further vessel growth and causes already formed immature vessels to regress. From P12-17 the mice are returned to normoxic conditions (21%) and the avascular retina become hypoxic triggering exuberant neovascularization^{230,244}. Using the OIR model, retinae were harvested at P12 and P17 for RT-pPCR analysis of CFB gene expression. At P12 there was a significant reduction in CFB gene expression ($*p < 0.05$) in OIR retina when compared to retina in the normal oxygen control group. On the other hand, at P17 there is a significant increase in CFB expression ($*p < 0.01$) in OIR retina when compared to the normal oxygen control group (**Figure 15**).

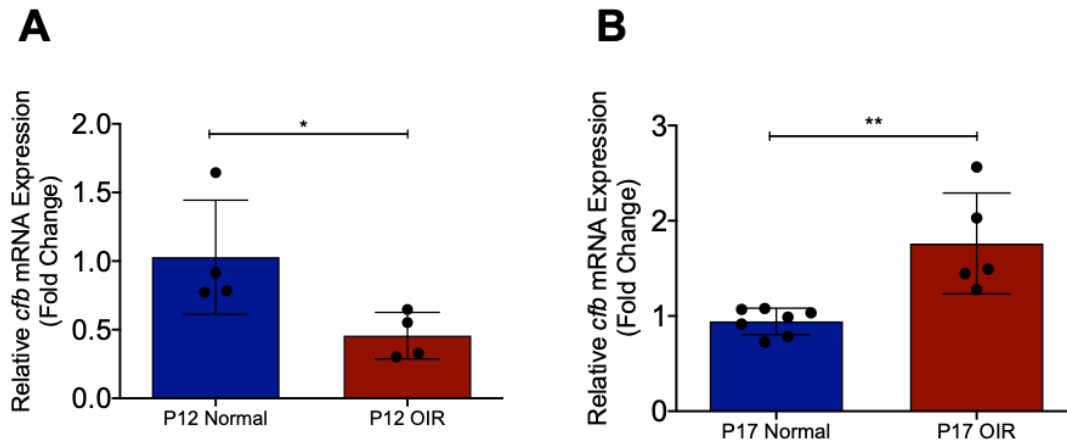


Figure 15: CFB gene expression in the retina of OIR mice. C57BL/6 mice were subject to OIR to induce pathological neovascularisation. Retina were harvested at P12 and P17 for analysis of CFB mRNA expression. The changes in CFB gene expression were calculated using fold change ($-2(\Delta\Delta cT)$). **A**, RT-qPCR analysis of CFB transcript levels in the retina of P12 OIR mice, represented as fold change normalised to the normal oxygen control. **B**, RT-qPCR analysis of CFB transcript levels in the retina of P17 OIR mice, represented as fold change normalised to the normal oxygen control. Results represent the mean \pm SD. Statistical significance was determined by unpaired two-tailed students' t-test; $n \geq 3$, *: $p < 0.05$, **: $p < 0.01$.

3.2 The Role of CFB in Regulating Retinal Angiogenesis

The progression of DR is a complex process resulting from chronic and sustained hyperglycaemia, which culminates in a series of pathological events that result in vascular dysfunction and eventually blindness²⁴⁵. The formation of new blood vessels in the retina as a result of aberrant angiogenesis is a hallmark feature of the advanced stage of the disease, PDR. Retinal ECs are one of the primary cells involved in retinal angiogenesis: they line the blood vessels and are involved in each of the angiogenic processes; basement membrane disruption, migration, proliferation, stabilisation and maturation¹⁴². We set out to evaluate the angiogenic potential of CFB, by studying its impact on retinal EC behaviour using *in vitro* angiogenesis assays following recombinant CFB treatment, CFB over-expression and CFB knockdown. Firstly,

we attempted to demonstrate the pro-angiogenic effects of CFB using standard cell viability and proliferation assays, on an organ specific EC cell line, HRECs. The effect of CFB was assed using rhCFB treatment, CFB over-expression (pCFB) or CFB knockdown using siRNA (siCFB). For recombinant protein treatment cells were treated with 100µg/mL rhCFB and the effects of rhCFB were compared to the PBS control group. CFB has been reported to have an approximate plasma concentration of 200 µg/mL²⁰⁷ The pre-determined dose of rhCFB at 100 µg/mL was chosen based on this reported concentration. For CFB over-expression cells were transfected with 1µg pCFB or 1µg pcDNA control. Similarly, for CFB knowckdown cells were transfected with 1µg siCFB or 1µg siRNA. The effects of CFB over-expression and CFB knockdown were compared the pcDNA and siContol groups, respectively (*for confirmation of successful knockdown and overexpression please refer to **Figure 34** and **Figure 35** in the **supplementary figures** for CFB mRNA expression following CFB knockdown and over-expression*).

HREC viability was evaluated using the colorimetric MTS assay. MTS assay indirectly measures the capacity of metabolically active healthy cells to convert the tetrazolium reagent into a coloured formazan end-product. The assay is a surrogate means to estimate the number of metabolically-viable ECs upon rhCFB treatment. Given the treatment conditions, rhCFB significantly promoted the viability of HRECs. Compared with the untreated control, 100 µg/mL rhCFB significantly increased the viability of HREC on Day 1(* $P < 0.05$) and Day 2 (** $P < 0.0001$) (**Figure 16**). Similarly, pCFB increased HREC viability on Day 1(*ns*) and with a significant increase on Day 2 (**** $P < 0.0001$), in comparison to the pcDNA control group (**Figure 17**). Compared with siControl, siCFB significantly reduced HREC viability on Day 1 (** $P < 0.01$) and Day 2(*** $P < 0.001$) (**Figure 18**).

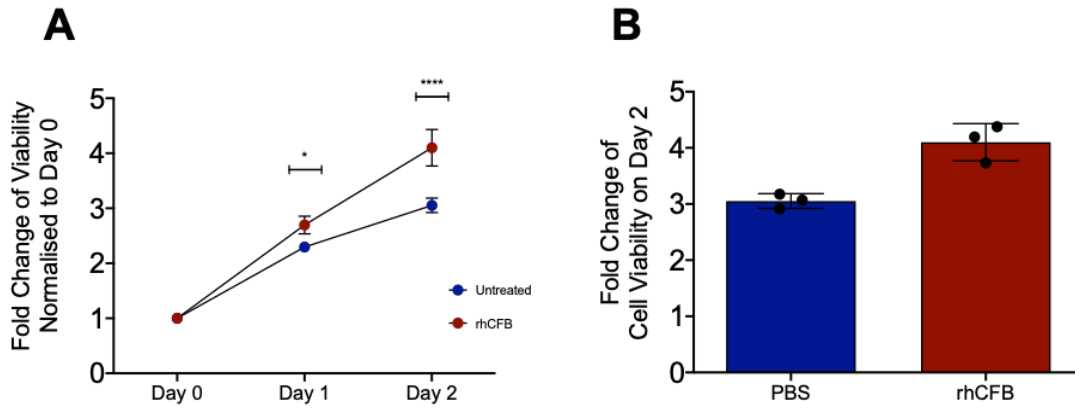


Figure 16: rhCFB treatment promotes HREC viability. Primary HRECs were treated with 100 $\mu\text{g/mL}$ rhCFB or equivalent PBS control and functional change was measured as quantitative changes in cell viability on day 1 and day 2. **A**, HREC growth curve measured by MTS assay. **B**, Cell viability of HRECs on day 2. Results were presented as fold change normalised to PBS control. Results represent the mean \pm SD. Statistical significance was determined using two-way ANOVA followed by post-hoc Sidak's multiple comparisons test; $n=3$, *: $p < 0.05$, **** $p < 0.0001$.

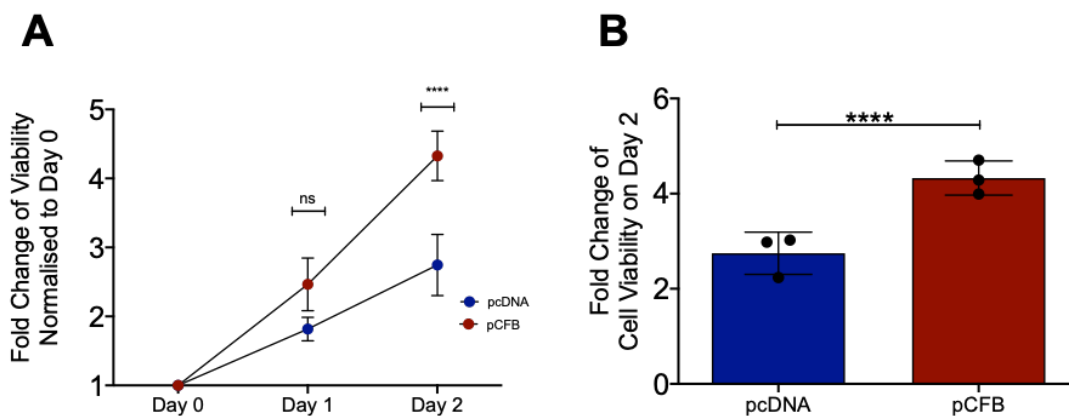


Figure 17: CFB overexpression increases HREC viability. Primary HRECs were transfected with 1 μg pCFB or 1 μg pcDNA control and functional change was measured as quantitative changes in cell viability on day 1 and day 2. **A**, HREC growth curve measured by MTS assay. **B**, Cell viability of HRECs on day 2. Results were presented as fold change normalised to pcDNA control. Results represent the mean \pm SD. Statistical significance was determined using two-way ANOVA followed by post-hoc Sidak's multiple comparisons test; $n=3$, **: $p < 0.0001$.

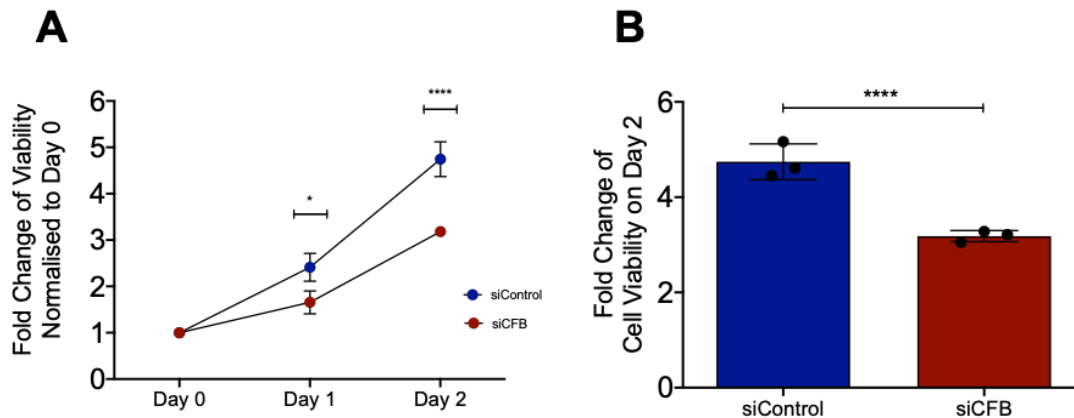


Figure 18: 1 CFB silencing reduces HREC viability. Primary HRECs were transfected with 66nM siCFB or 66nM siRNA control and functional change was measured as quantitative changes in cell viability on day 1 and day 2 **A**, HREC growth curve measured by MTS assay. **B**, Cell viability of HRECs on day 2. Results were presented as fold change normalised to siRNA control. Results represent the mean \pm SD. Statistical significance was determined using two-way ANOVA followed by post-hoc Sidak's multiple comparisons test; $n=3$, **: $p < 0.01$, ****: $p < 0.0001$

Notably, the overall cell viability is regulated by a balance between the rate of cell proliferation and cell death. Hence, to improve our understanding in the CFB-regulated cell viability, its impact on cell proliferation was examined by staining HRECs with an antibody specific to Ki-67, a human nuclear protein that is strictly associated with cell proliferation. The total number of cell nuclei and the total number of Ki-67⁺ cell nuclei (*please refer to the white arrows on **Figure 19, Figure 20 and Figure 21***) were manually counted and the cell proliferation rate was calculated as a percentage Ki-67⁺ cells. Consistent with the observation in HREC viability, rhCFB treatment resulted in a significant increase in cell proliferation. Compared with the PBS control, treatment with 100 $\mu\text{g}/\text{mL}$ rhCFB significantly increased the percentage of Ki67⁺ cells (** $P < 0.001$) compared to the PBS control, (**Figure 19**). Similarly, pCFB significantly increased cell proliferation (** $P < 0.001$) in comparison to the pcDNA control, (**Figure 20**). On the other hand, compared with siControl, siCFB significantly attenuated cell proliferation, (** $P < 0.05$) (**Figure 21**).

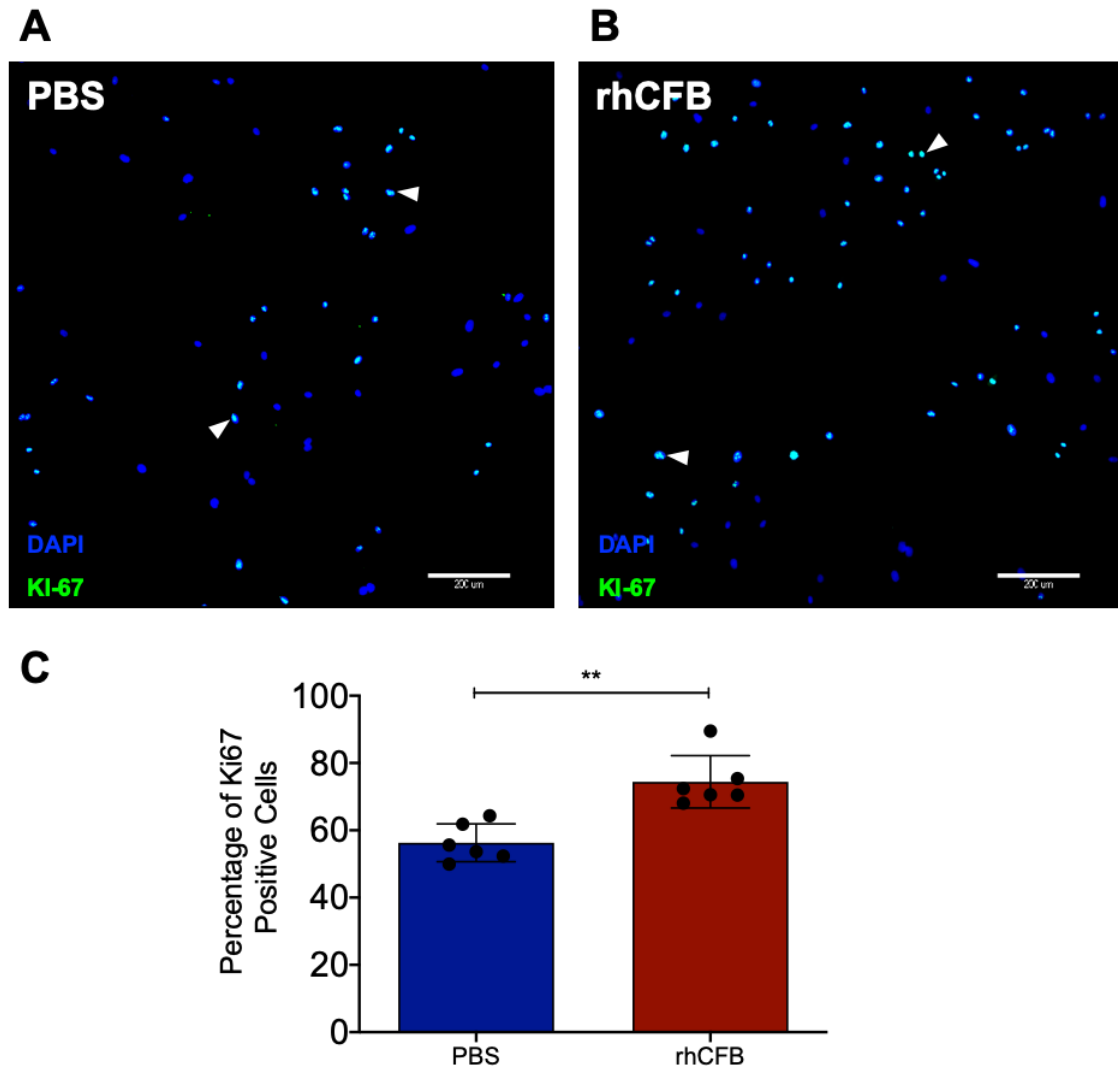


Figure 19: Recombinant CFB treatment promotes HREC proliferation. Primary HRECs were treated with 100 μ g/mL rhCFB or equivalent PBS control and functional change was measured as a change in cellular proliferation after 24h. Changes in cell proliferation was demonstrated using Ki-67 proliferation marker (green) localised in the cell nucleus (blue). **A-B**, Representative images of Ki-67 staining. Scale bar: 200 μ M. **C**, Quantification of proliferating cells reported as the percentage of Ki-67⁺ nucleus. Results represent the mean \pm SD of three experiments per treatment performed in duplicate (the symbols representing the technical repeats). Statistical significance was determined by unpaired, two-tailed students' t-test; n=6, **: p< 0.01.

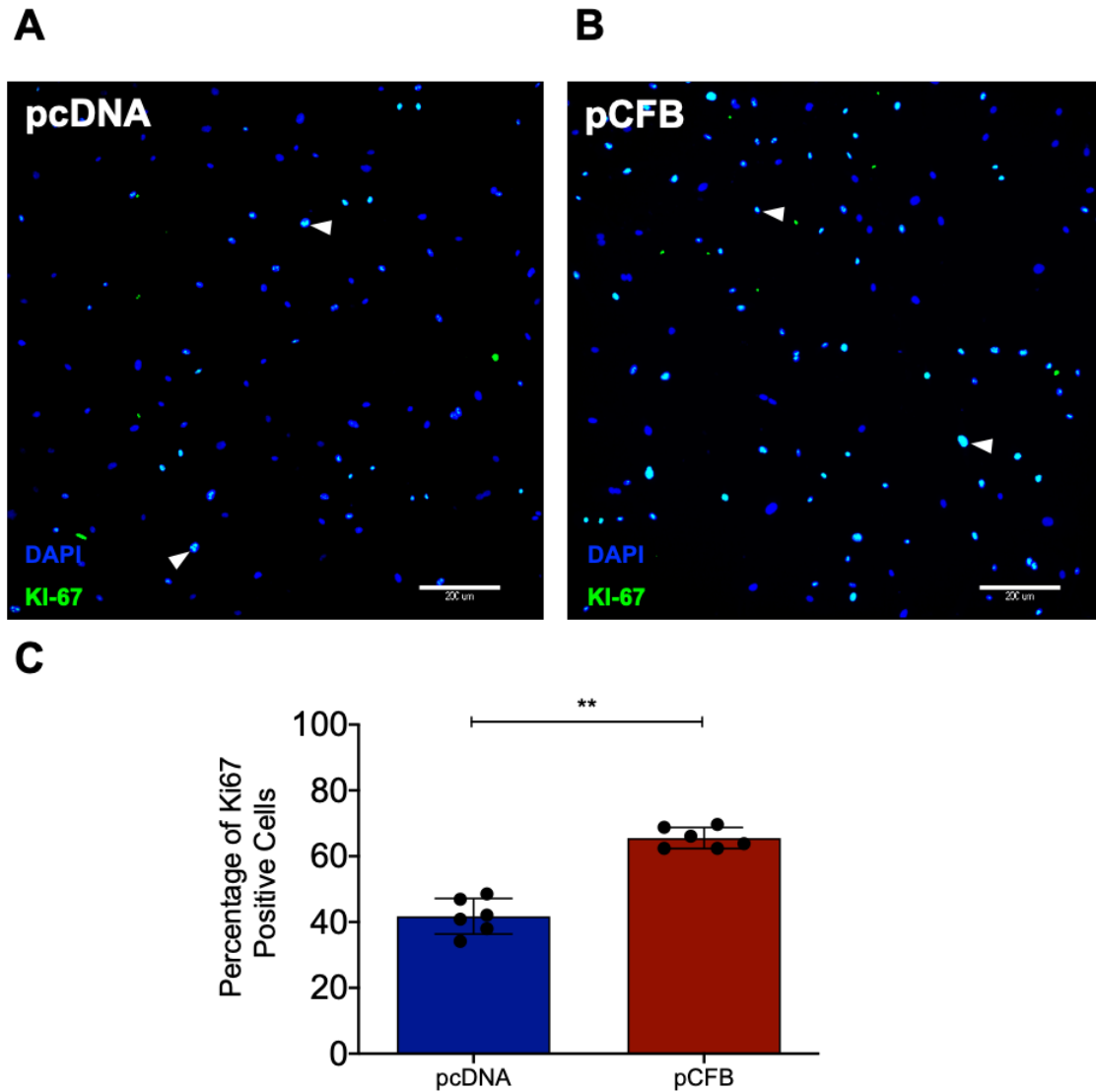


Figure 20: CFB overexpression promotes HREC proliferation. Primary HRECs were transfected with 1 μ g pCFB or 1 μ g pcDNA control and functional change was measured as a change in cellular proliferation after 24h. Changes in cell proliferation was demonstrated using Ki-67 proliferation marker (green) localised in the cell nucleus (blue). **A-B**, Representative images of Ki-67 staining. Scale bar: 200 μ M. **C**, Quantification of proliferating cells reported as the percentage of Ki-67⁺ nucleus. Results represent the mean \pm SD of three experiments per treatment performed in duplicate (the symbols representing the technical repeats). Statistical significance was determined by unpaired, two-tailed students' t-test; n=6, **: p < 0.01.

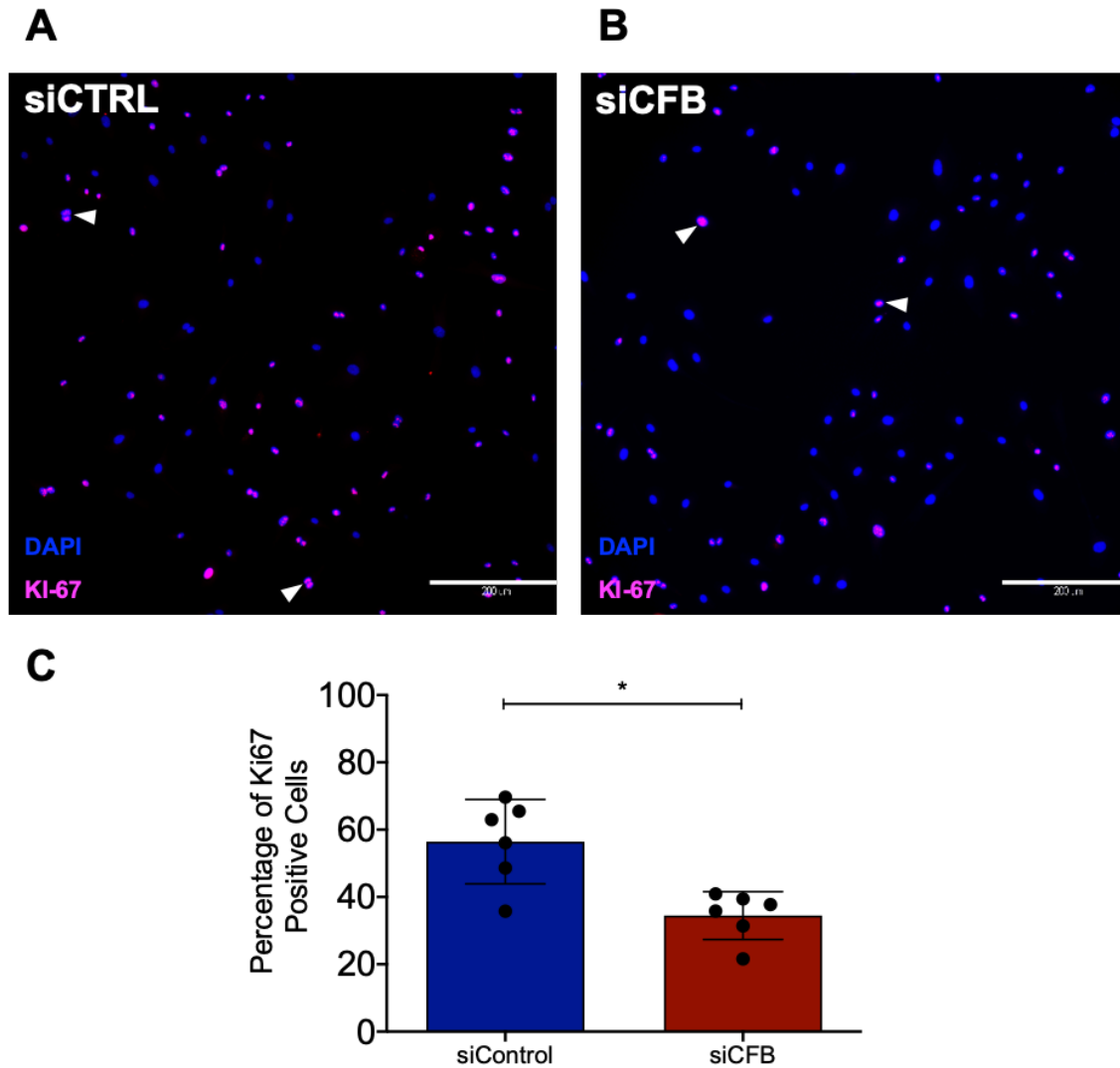


Figure 21: CFB knockdown reduces HREC proliferation. Primary HRECs were transfected with 66nM siCFB or 66nM siRNA control and the functional change was measured as a change in cellular proliferation after 24h. Changes in cell proliferation was demonstrated using Ki-67 proliferation marker (pink) localised in the cell nucleus (blue). **A-B**, Representative images of Ki-67 staining. Scale bar: 200 μ M. **C**, Quantification of proliferating cells reported as the percentage of Ki-67⁺ nucleus. Results represent the mean \pm SD of three experiments per treatment performed in duplicate (the symbols representing the technical repeats). Statistical significance was determined by unpaired, two-tailed students' t-test; n=6, *: p < 0.05.

As mentioned, angiogenesis is a highly dynamic process. In response to local angiogenic cues, ECs degrade the basement membrane and migrate along chemical gradients established by angiogenic factors. The transwell migration assay, also known as the Boyden chamber assay, was chosen to evaluate CFB's effect on HREC migration. Given the experimental setup (*please refer to 2.38*) the directional migration was induced by the FBS gradient, in which cells migrated across a 0.8 μ M porous filter membrane, from the upper well (containing 0% FBS) to the bottom side of the well (containing 2% FBS). Following a five-hour incubation period the number of transmigrated DAPI⁺ cell nuclei were manually counted. Compared with the untreated control, treatment with 100 μ g/mL rhCFB significantly increased HREC migration (*****P<0.0001*) (**Figure 22**). On the other hand, compared with siControl, siCFB significantly attenuated HREC migration, (*****P<0.0001*) (**Figure 23**).

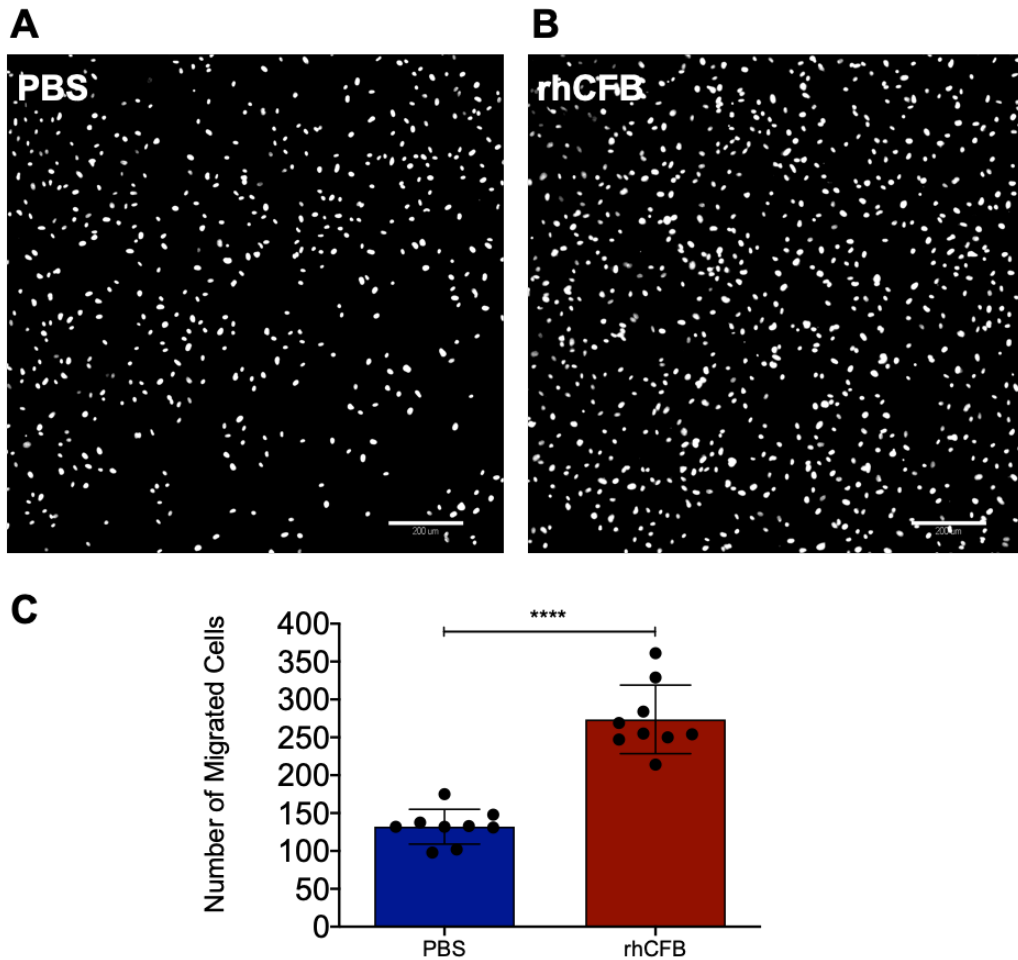


Figure 22: Recombinant CFB treatment promotes HREC transwell migration. Primary HRECs were treated with 100 $\mu\text{g}/\text{mL}$ rhCFB or equivalent PBS control and the functional change was measured as a change in cellular trans-migration after 5 hours. **A-B**, Representative images of migrated HRECs. Scale bar: 200 μM **C**, Quantification of migrated cells reported as the number of migrated DAPI⁺ cell nuclei. Results represent the mean \pm SD of three experiments per treatment performed in triplicate (the symbols representing the technical repeats). Statistical significance was determined by unpaired, two-tailed students' t-test; $n=9$, ****: $p < 0.0001$.

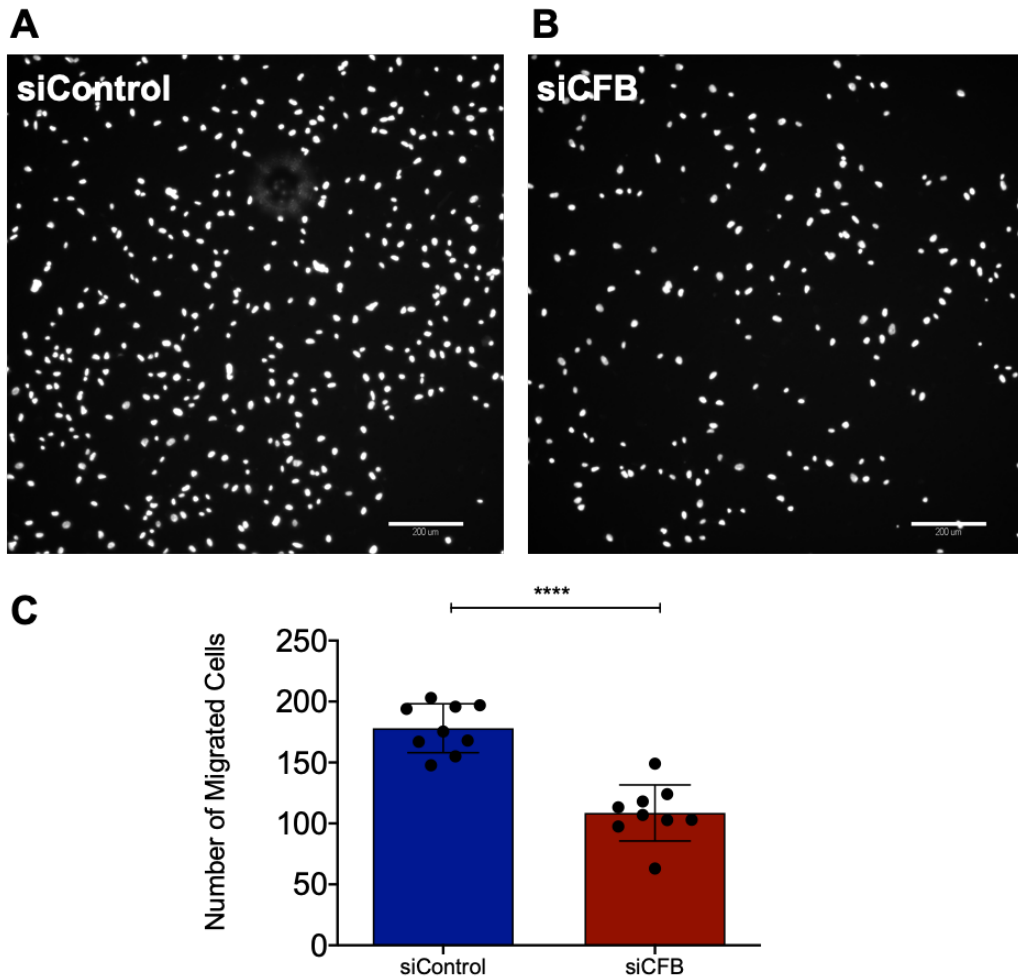


Figure 23: CFB silencing reduces HREC transwell migration. Primary HRECs were transfected with 66nM siCFB or 66nM siRNA control and functional change was measured as changes in cellular trans-migration after 5 hours. **A-B**, Representative images of migrated HRECs after transfection with 66nM control siRNA or 66nM CFB siRNA. Scale bar: 200 μ M. **C**, Quantification of migrated cells reported as the number of migrated DAPI⁺ cell nuclei. Results represent the mean \pm SD of three experiments per treatment performed in triplicate (the symbols representing the technical repeats). Statistical significance was determined by unpaired, two-tailed students' t-test; n=9, ****: p< 0.0001

The innate ability of ECs to spontaneously assemble into tubular structures is a critical step during sprouting angiogenesis. Growth factor-reduced Matrigel® is a specially formulated ECM that supports cells to form two-dimensional vascular networks. HRECs were seeded onto solidified GFR Matrigel® for 16 hours to form stable tubule-like structures. The extent of network formation was analysed using the Angiogenesis Analyzer plugin in Image J to quantify the number of junctions and total tubule length. Compared with the untreated control, 100 µg/mL rhCFB was able to promote HREC network formation, as demonstrated by a significant increase in the number of junctions ($****P<0.0001$), and total tube length ($****P<0.0001$), respectively (**Figure 24**). Similarly, pCFB induced HREC network formation, with a significant increase in number of junctions ($****P<0.0001$), and total tube length ($****P<0.0001$), respectively (**Figure 25**). Compared with siControl, siCFB significantly attenuated HREC network formation with a reduction in number of junctions and total tube length, respectively (**Figure 26**).

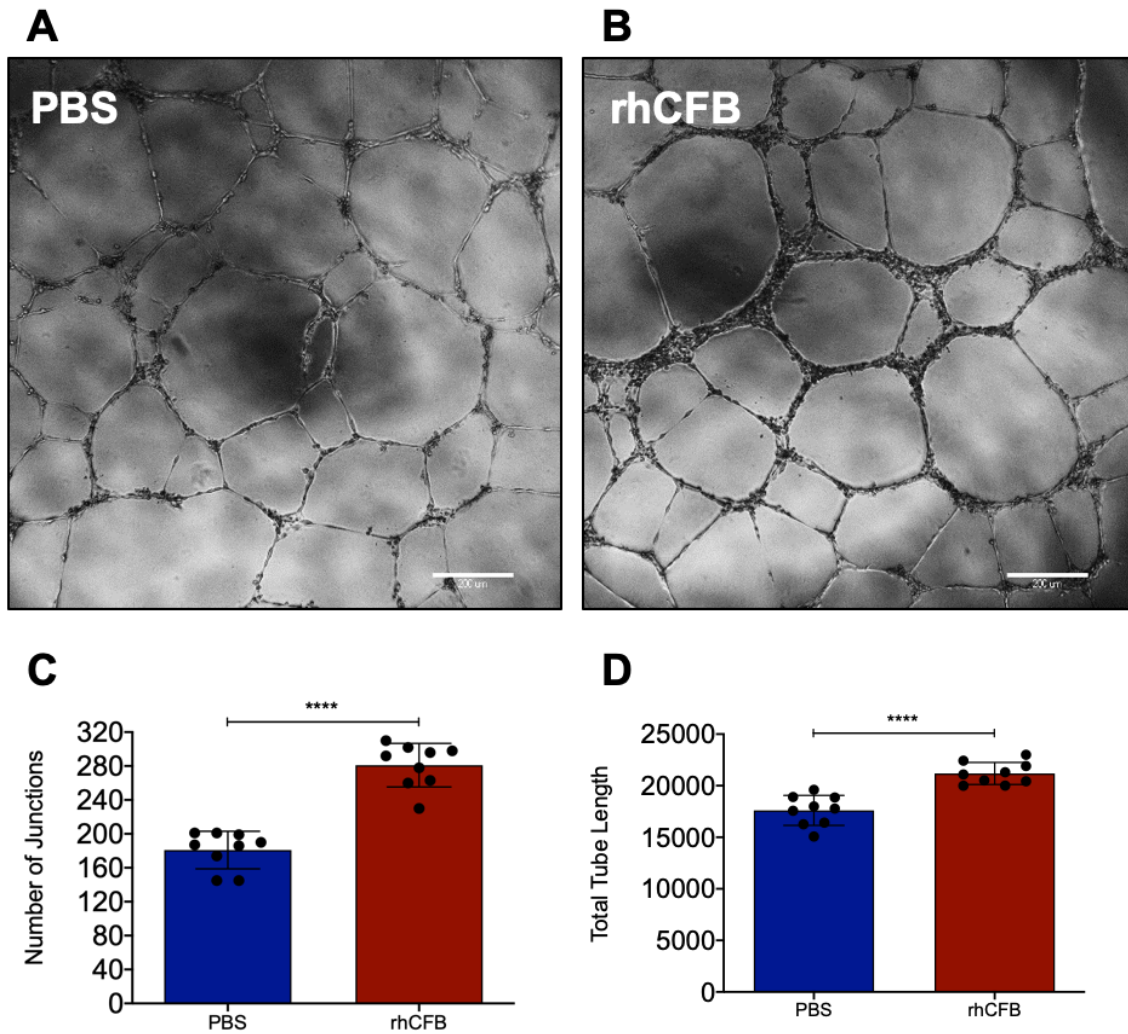


Figure 24: Recombinant CFB treatment promotes HREC network formation. Primary HRECs were treated with 100 $\mu\text{g}/\text{mL}$ rhCFB or equivalent PBS control and the functional changes were measured as changes in EC network formation after 16 hours incubation. **A-B**, Representative images of the Matrigel® network formation assay. Scale bar: 200 μM **C-D**, Quantification of HREC Matrigel® network formation reported as the total number of junctions and total tubule length. Results represent the mean \pm SD of three experiments per treatment performed in triplicate (the symbols representing the technical repeats). Statistical significance was determined by unpaired, two-tailed students' t-test; $n=9$, ****: $p < 0.0001$.

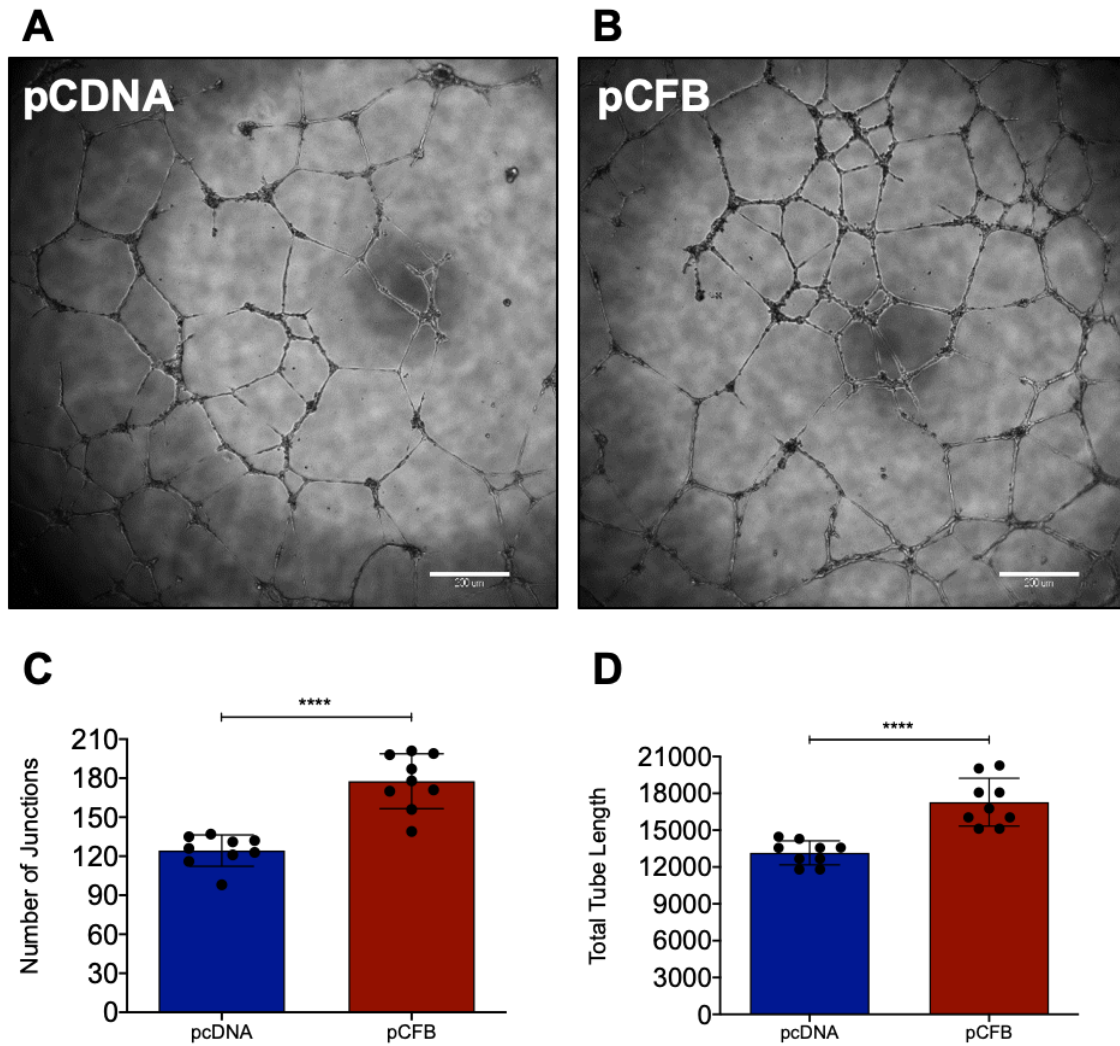


Figure 25: CFB overexpression promotes HREC network formation. Primary HRECs were transfected with 1 μ g pCFB or 1 μ g pcDNA and the functional changes were measured as changes in EC network formation after 16 hours incubation. **A-B**, Representative images of the Matrigel® network formation assay. Scale bar: 200 μ m **C-D**, Quantification of HREC Matrigel® network formation reported as the total number of junctions and total tubule length. Results represent the mean \pm SD of three experiments per treatment performed in triplicate (the symbols representing the technical repeats). Statistical significance was determined by unpaired, two-tailed students' t-test; n=9, ****. p< 0.0001.

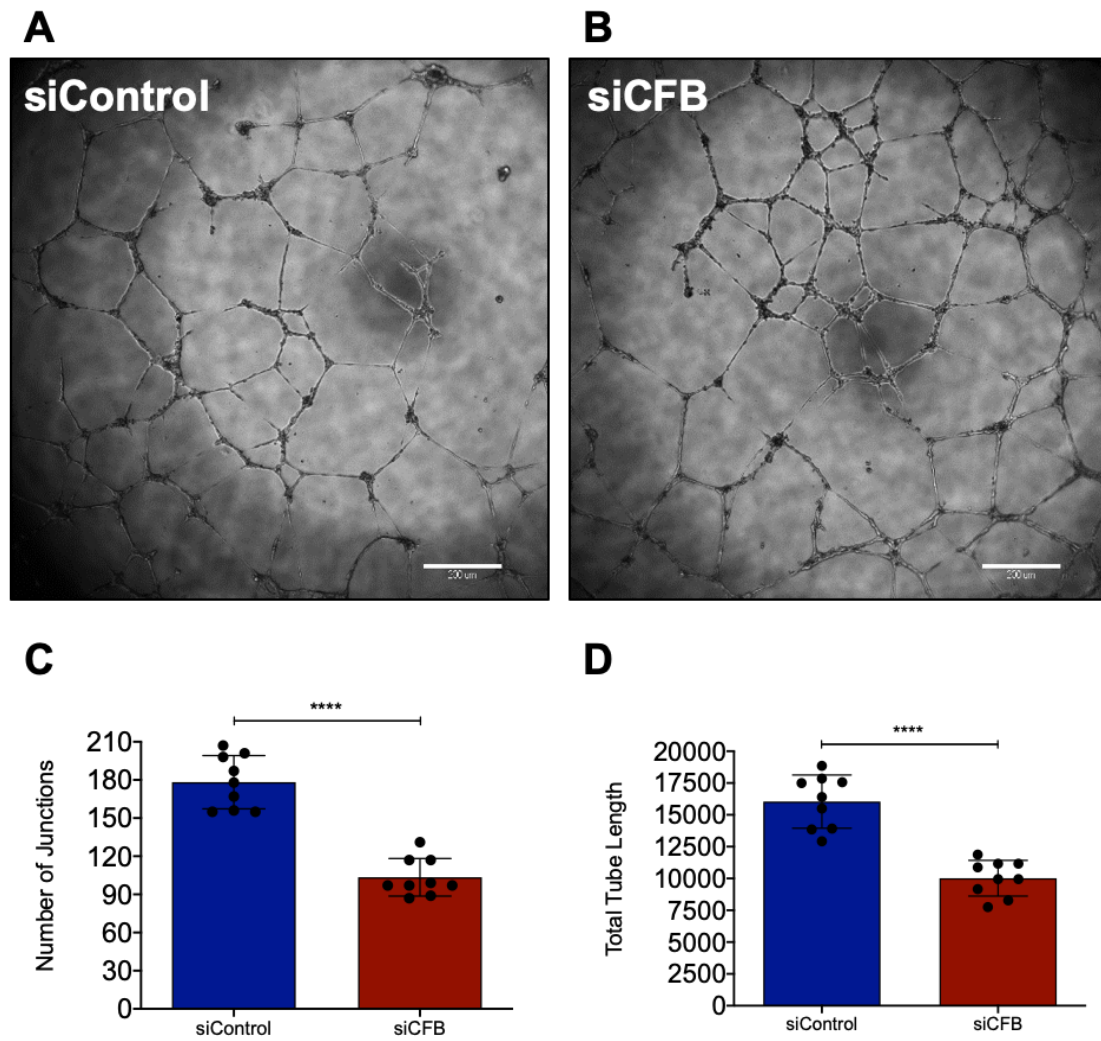


Figure 26: CFB silencing reduces HREC network formation. Primary HRECs were transfected with 66nM siCFB or 66nM siRNA control and the functional changes were measured as changes in EC network formation after 16 hours incubation. **A-B**, Representative images of the Matrigel® network formation assay. Scale bar: 200 μ M **C-D**, Quantification of HREC Matrigel® network formation reported as the total number of junctions and total tubule length. Results represent the mean \pm SD of three experiments per treatment performed in triplicate (the symbols representing the technical repeats). Statistical significance was determined by unpaired, two-tailed students' t-test; n=9, ****: p < 0.0001.

Angiogenesis is a complex process involving multiple cell types and extracellular components²⁴⁶. Apart from ECs, perivascular cells, non-vascular cells, inflammatory cells, and ECM components also actively participate in the angiogenic process^{247,248}. Hence, *ex vivo* angiogenesis assays provide unique opportunity to study the interplay of the multiple cell types subjected to the same microenvironment. Two different *ex vivo* angiogenesis assays were used to confirm the role of CFB in a more complex experimental setup. Both the fetal metatarsal and aortic ring assays were chosen to evaluate microvascular outgrowth, a phenomenon that models the physiologically angiogenic process in a more accurate way²⁴³. Dissected aortic ring explants were embedded in a collagen matrix and cultured in aortic ring media containing 100µg/mL rhCFB for an extended period of 7 days. Its impact on microvessel outgrowth was examined by staining explants with I-B₄ Iseoelectin, an antibody specific to ECs, and quantified by manually counting the number of microvessels that grew from each aortic ring explant. Consistent with previous findings, rhCFB significantly promoted the number of microvessel sprouts per explant (******** $P < 0.0001$), in comparison to the PBS control (**Figure 27**). In the fetal metatarsal assay, dissected metatarsal bones were embedded onto pre-coated plates and cultured in metatarsal growth media containing 100µg/mL rhCFB for an extended period of 12 days. Its impact on microvessel outgrowth was examined by staining explants with CD-31, an antibody specific to ECs, and quantified using Adobe Photoshop CS6 software to calculate the sprouting area per explant. As with the aortic ring assay, rhCFB significantly induced the sprouting area of the metatarsal explants (******** $P < 0.0001$), in comparison to the PBS control (**Figure 28**).

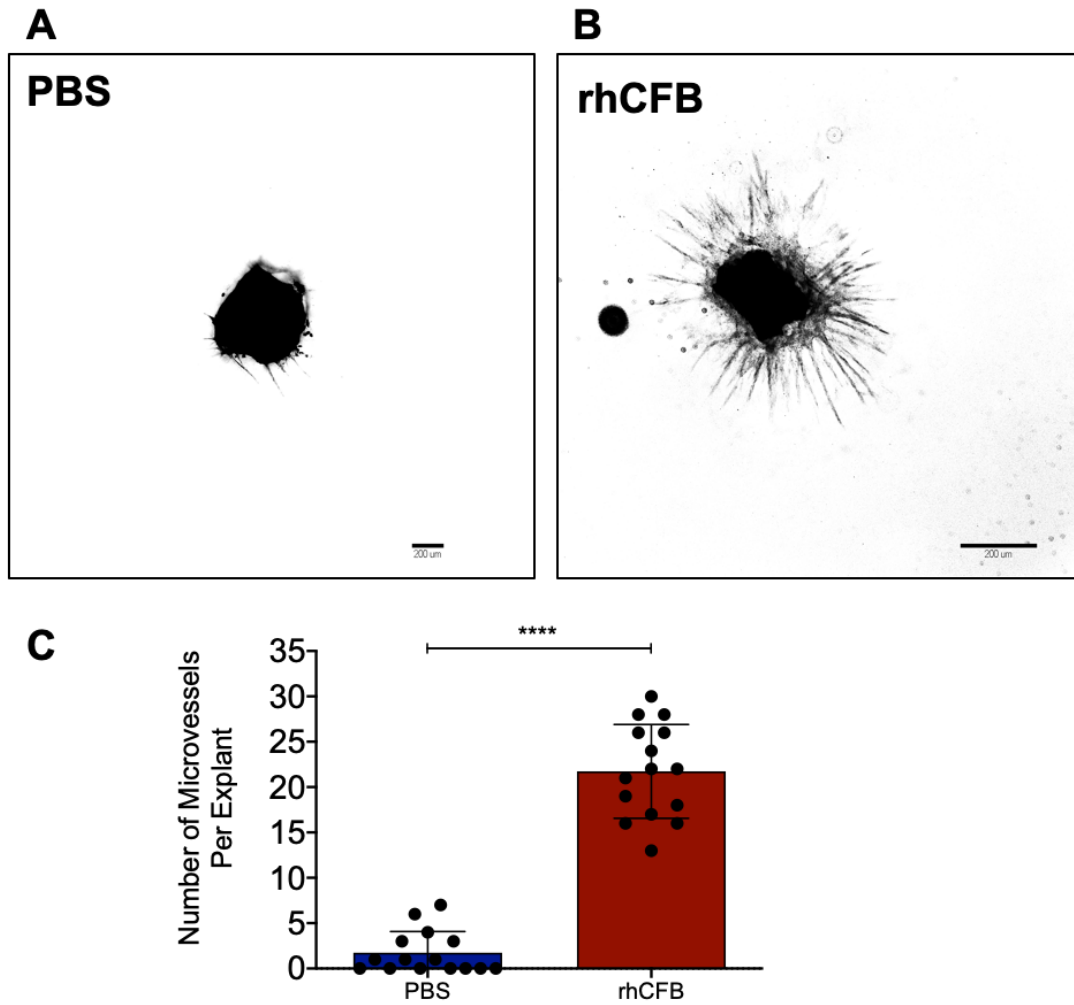


Figure 27: Recombinant CFB treatment promotes vessel outgrowth in the aortic ring explant assay. Aortic ring explants were dissected, embedded into collagen and cultured in aortic ring media with the addition of 100 μ g/mL rhCFB for 7 days. The resultant microvessel outgrowth was stained with I-B₄ Isolectin and quantified manually by counting the number of microvessels growing from each explant. **A-B**, Representative images of aortic ring microvessel outgrowth **C**, Quantification of microvesel outgrowth reported as the number of microvessels per explant. Results represent the mean \pm SD of 15 explants per treatment. Statistical significance was determined by unpaired, two-tailed students' t-test; n =15 PBS, n = 14, rhCFB ****: p< 0.0001

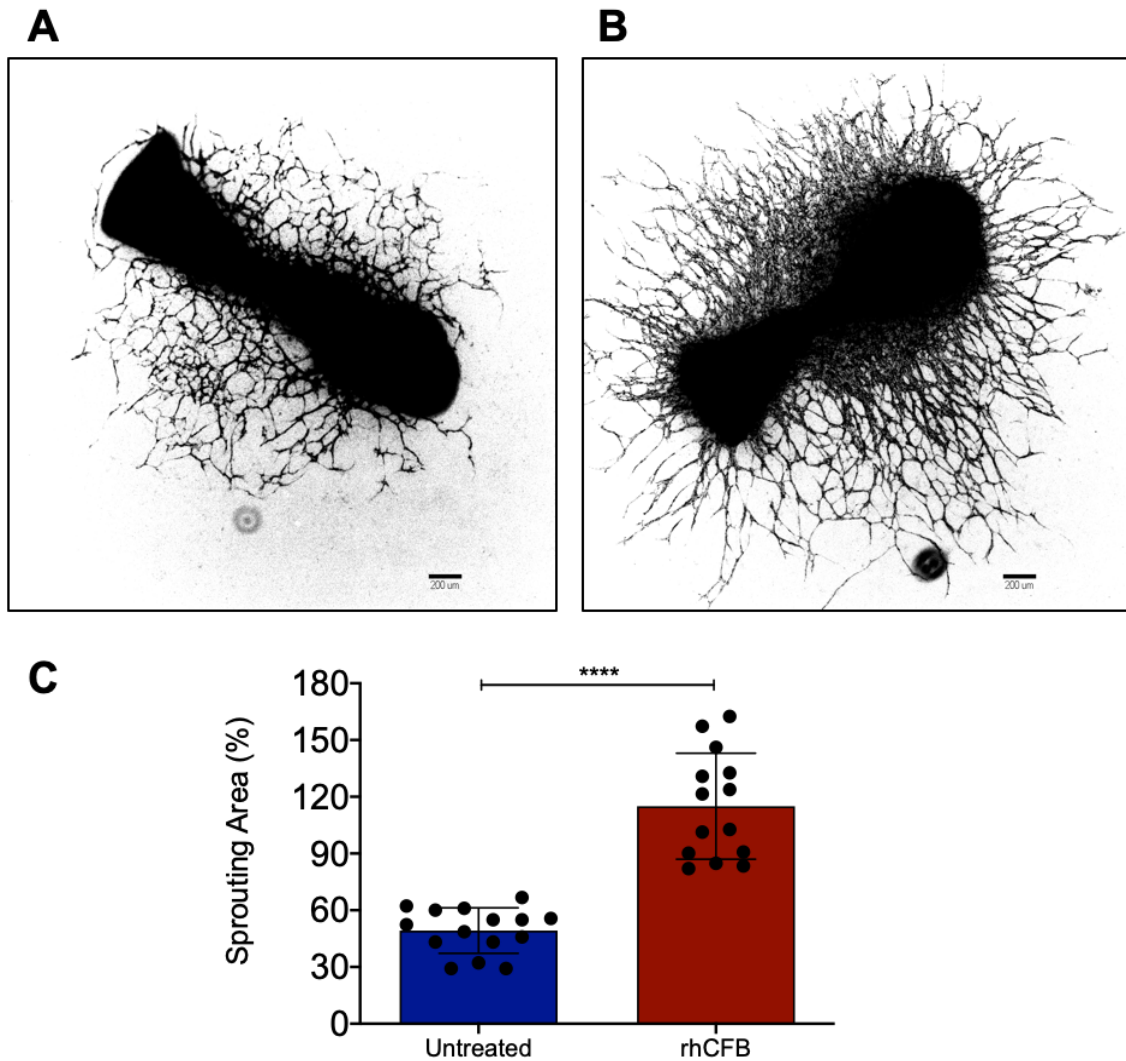


Figure 28: Recombinant CFB treatment promotes vessel outgrowth in the aortic ring explant assay. Metatarsal explants were dissected and mounted onto culture dishes and cultured in metatarsal growth media with the addition of 100 μ g/mL rhCFB for 12 days. The resultant microvessel outgrowth was stained with CD31 and quantified using Adobe Photoshop CS6 software. **A-B**, Representative images of metatarsal sprouting microvessel outgrowth **C**, Quantification of microvessel outgrowth reported as the percentage of sprouting area normalised to the metatarsal area. Results represent the mean \pm SD of 15 explants per treatment. Statistical significance was determined by unpaired, two-tailed students' t-test; $n > 14$, ****: $p < 0.0001$.

3.3 Investigating the relationship between Complement Factor B and VEGF-A and VEGFR2

In the previous chapter, a pro-angiogenic effect of CFB in both cultured HRECs and *ex vivo* models of angiogenesis was established. To follow on from this we sought to find a plausible mechanism that integrated CFB into the angiogenic signalling network underlying PDR pathology. Retinal angiogenesis is a highly complex biological process that involves a delicate balance between angiogenic and anti-angiogenic factors, each regulated by multiple control systems¹⁴¹. Among the cytokines involved in pathological angiogenesis in the retina, VEGF serves as the most potent angiogenic stimulator¹⁴¹. A link between complement, angiogenesis and VEGF has been established in the pathogenesis of tumour angiogenesis, where activation of the AP was shown to stimulate cells to produce VEGF, which promoted angiogenesis of ECs²⁴⁹. Understandably the relevance of this study is questionable since its focus was the role of complement in cancer, and the impact of the AP on angiogenesis was examined *in vitro* using bone osteosarcoma epithelial cells. Having said that, angiogenesis is a characteristic feature of many pathologies, including both tumour growth and diabetic retinopathy, where it aberrantly contributes to disease progression. Some of the mechanisms that underlie pathological angiogenesis in the retina and tumour angiogenesis are similar, and consequently complement involvement in tumour angiogenesis may have cross-over with, and provide insights into DR pathogenesis. There are also a number of studies that report a link between complement components and VEGF in the context of AMD. In these studies, complement components are able to induce VEGF expression both *in vitro* and *in vivo*. However, it is important to note here that the complement components examined in these studies are C3a²⁵⁰, C5a²⁵⁰, and MAC²⁵¹, and they could have different mechanisms of action to CFB. One group that focused specifically on CFB, used short hairpin RNA (shRNA) to knockdown CFB in rats. They reported a significant inhibition of the formation and development of CNV *in vivo* following CFB knockdown which was attributed to a reduction of VEGF expression in the

RPE and choroidal tissues²⁵². In a separate study by a different group, CFB was knocked down in mice using siRNA. Similarly, they reported significant attenuation on the development of laser-induced CNV as well as reduced VEGF expression²⁰⁴. Although not directly relevant to this project, these studies bare more relevance than the aforementioned cancer study, because, as previously mentioned, AMD and DR share the same characteristic feature in that they are driven by aberrant angiogenesis, and it is possible that similar mechanisms may be involved in the pathophysiology of both AMD and DR. Given that proteins and receptors of the VEGF family are important drivers of pathological angiogenesis in PDR, the possibility that CFB contributes to dysregulation of the VEGF-VEGFR2 signalling cascade was considered. To query whether CFB regulates VEGF expression, and gain an understanding of the molecular mechanisms regulating the CFB mediated induction of angiogenesis in HRECs, RT-qPCR was used to identify the changes in gene transcripts associated with the gain-of-function or the loss-of-function of CFB using rhCFB treatment or CFB knockdown using siRNA (siCFB). For recombinant protein treatment cells were treated with 100 μ g/mL rhCFB and the effects of rhCFB were compared to the PBS control group. For CFB knowckdown cells were transfected with 66nM siCFB or 66nM siRNA. The effects of CFB knockdown were compared the siContol groups, respectively (*for confirmation of successful knockdown please refer to **Figure 35** in the **supplementary figures** for CFB mRNA expression following CFB knockdown*). Compared with the untreated control, 100 μ g/mL rhCFB significantly increased the gene expression of both VEGF-A (** $p < 0.01$) and VEGFR2 (** $p < 0.01$). In contrast, siCFB significantly decreased the gene expression of both VEGF-A (** $p < 0.01$) and VEGFR2 ($p < 0.05$) compared with siControl (**Figure 29**).

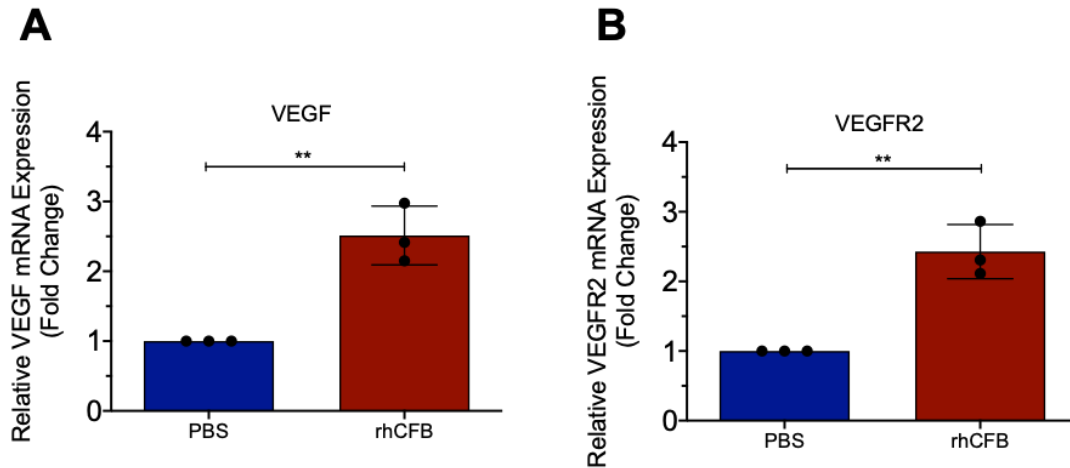


Figure 29: Recombinant CFB treatment induces VEGF-A and VEGFR2 mRNA expression.

Primary HRECs were treated with 100 $\mu\text{g}/\text{mL}$ rhCFB and changes in VEGF and VEGFR2 mRNA levels were analysed after 48 hours incubation. The changes in gene expression were calculated using fold change ($-2(\Delta\Delta\text{CT})$). **A-B**, RT-qPCR analysis of VEGF and VEGFR2 transcript levels represented as fold change normalised to PBS control. Results represent the mean \pm SD. Statistical significance was determined on raw delta-CT values by unpaired two-tailed students' t-test; $n=3$, **: $p < 0.01$.

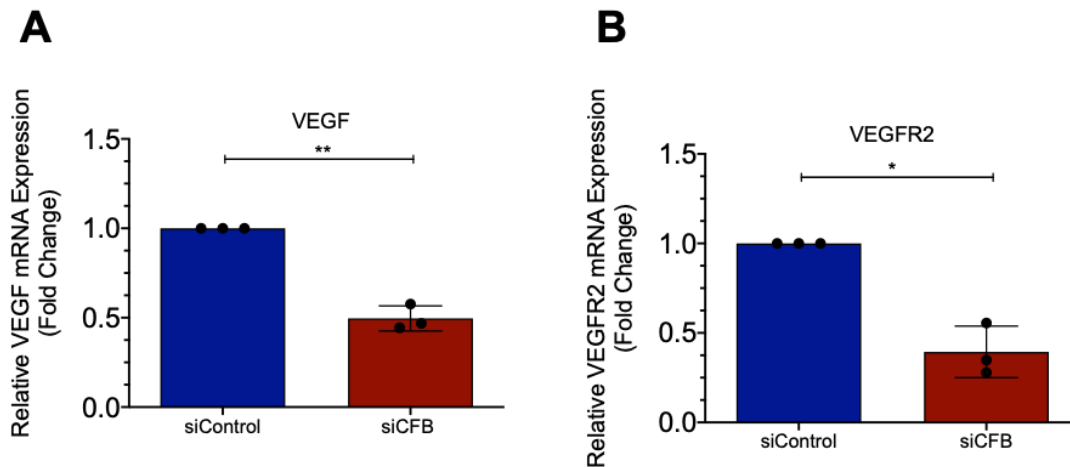


Figure 30: CFB silencing reduces VEGF-A and VEGFR2 mRNA expression.

Primary HRECs were transfected with 66nM siCFB or 66nM siRNA control and changes in VEGF and VEGFR2 mRNA levels were analysed after 48 hours transfection. The changes in gene expression were calculated using fold change ($-2(\Delta\Delta\text{CT})$). **A-B**, RT-qPCR analysis of VEGF and VEGFR2 transcript levels represented as fold change normalised to siControl. Results represent the mean \pm SD. Statistical significance was determined on raw delta-CT values by unpaired two-tailed students' t-test; $n=3$, *: $p < 0.05$, **: $p < 0.01$.

Having observed CFB mediated changes in VEGF-A and VEGFR2 gene expression, western blot analysis was used to identify the changes in protein expression associated with the loss-of-function of CFB. CFB knockdown was first confirmed ($*p < 0.05$). There were no significant changes in VEGF-A protein expression following CFB knockdown. However, in line with the observation of VEGFR2 gene expression, a significant decrease of VEGFR2 protein expression ($*p < 0.05$) was observed alongside the downregulation of CFB, when compared to siControl (**Figure 31**).

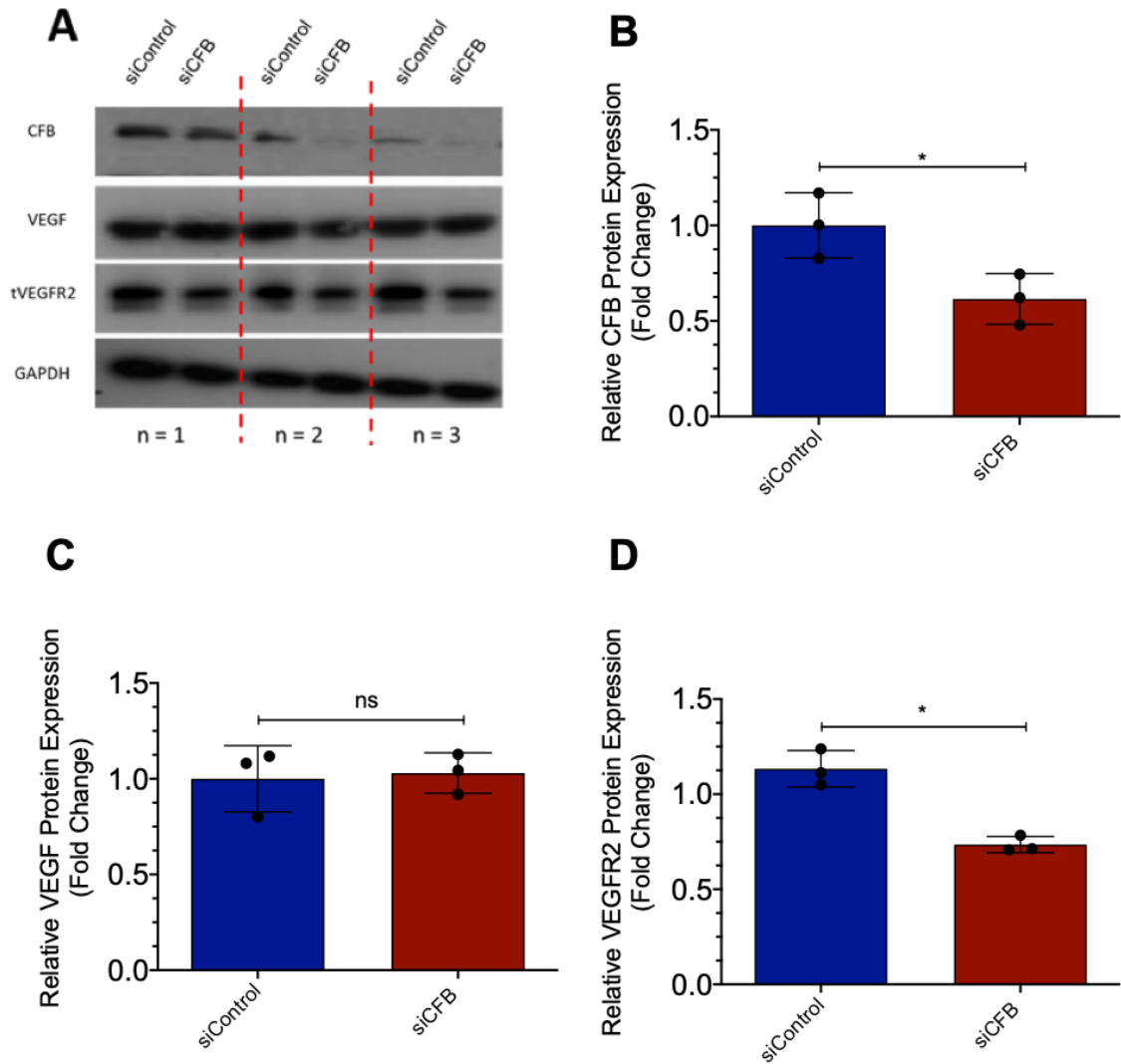


Figure 31: CFB silencing reduces VEGFR2 but not VEGF-A protein expression. Primary HRECs were transfected with 66nM siCFB or 66nM siRNA control and changes in VEGF and VEGFR2 protein expression were analysed after 48h of transfection. The changes in protein expression were detected by western blot. **A**, Representative western blot of CFB, VEGF, VEGFR2. GAPDH was used as a loading control. **B-D**, Densitometry quantification of western blot. CFB, VEGF and VEGFR2 were first normalised to the internal control GAPDH. Quantification is represented as fold change normalised to siControl. Data are expressed as mean \pm SD. Statistical significance was determined by unpaired, two-tailed students' t-test; n=3, *: $p < 0.05$.

Moving on, to further investigate if the CFB-regulated changes in VEGFR2 protein expression has functional consequence on the angiogenic potential of HRECs, the Matrigel® network formation assay was conducted using HRECs treated with rhCFB treatment in the absence and presence of a VEGFR2 small molecule inhibitor Linifanib. (*Please refer to **Figure 36** in the **supplementary figures** for Linifanib concentration optimisation*). Compared with the PBS control, 100 µg/mL rhCFB was able to promote HREC tube formation, indicated by a significant increase in number of junctions ($****p < 0.0001$) and total tube length ($****p < 0.0001$) (**Figure 32**). The presence of 5nM Linifanib attenuated HREC tube formation, observed by a significant decrease in number of junctions and total tube length for both the PBS ($****p < 0.0001$) and rhCFB group ($****p < 0.0001$).

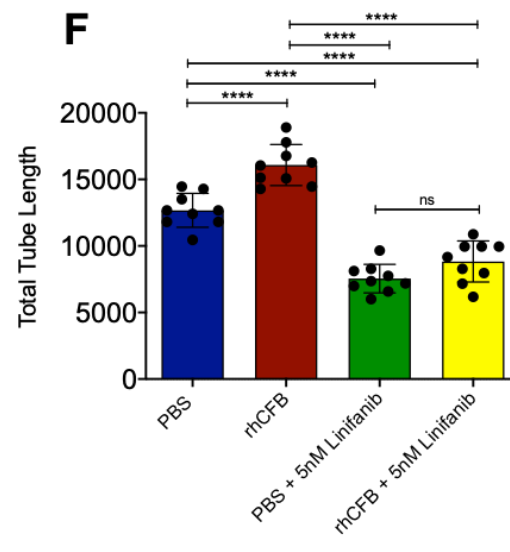
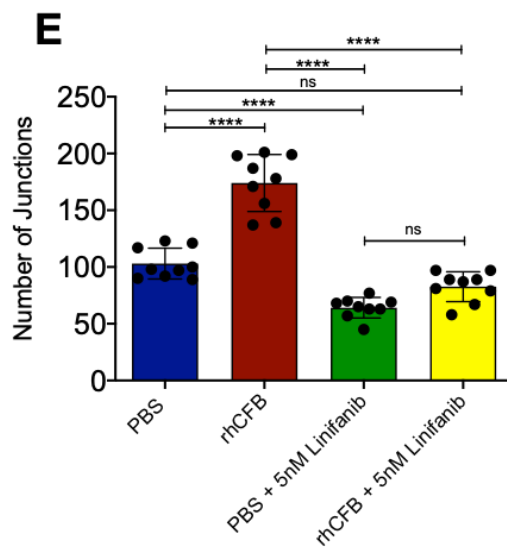
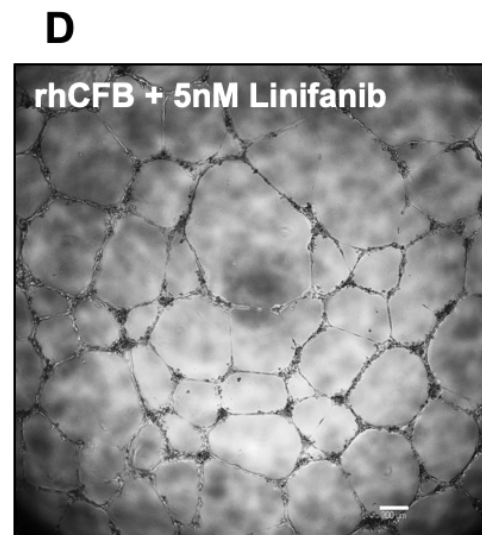
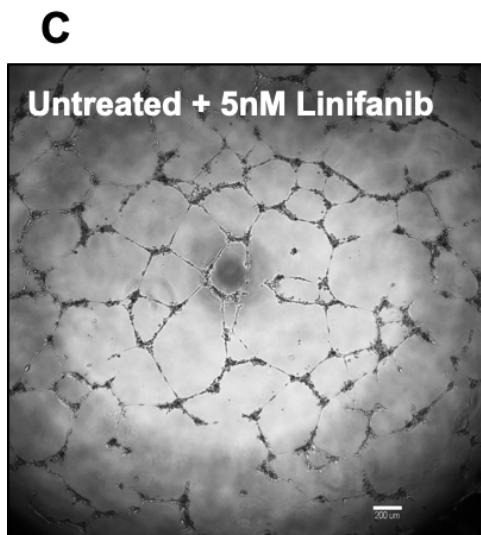
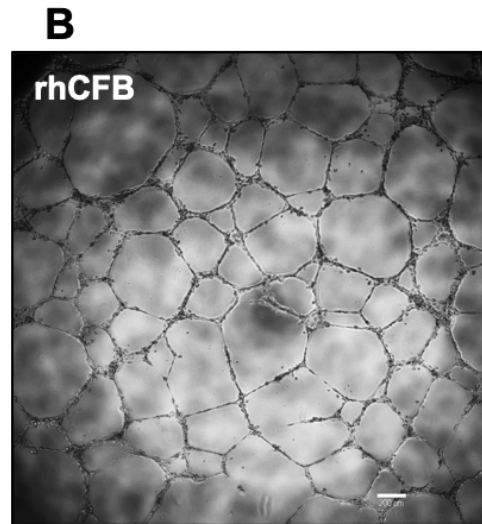
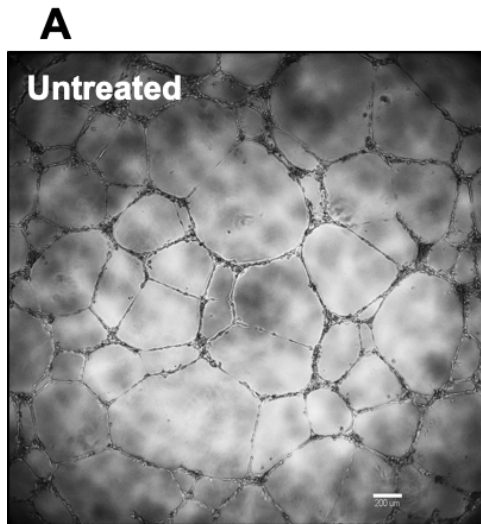


Figure 32: Linifanib attenuates CFB induced HREC network formation. Primary HRECs were treated with 100 $\mu\text{g}/\text{mL}$ rhCFB or equivalent PBS control with the presence or absence of 5nM VEGFR2 inhibitor, Linifanib. Functional changes were measured as changes in EC network formation after 16 hours incubation **A-D**, Representative images of Matrigel® network formation. **E-F**, Quantification of HREC Matrigel® network formation reported as the total number of junctions and total tubule length. Results represent the mean \pm SD of three experiments per treatment performed in triplicate (the symbols representing the technical repeats). Statistical significance was determined by unpaired, two-tailed students' t-test; n=9, ****: $p < 0.0001$.

4 Discussion

The function of the systemic complement system in innate immune defence has been extensively characterised; it is well known to perform homeostatic functions that include opsonisation for phagocytosis, formation of the terminal complex MAC, and recruitment of immune cells. As a crucial mediator of the innate immune response, the complement system has for a long time only been perceived as a front-line surveillance system in host defence. This still holds true; however, it is now becoming clear that the complement system also has functions that reach far beyond immune surveillance. The presence of complement proteins and a complement regulatory system in the retina is widely accepted¹⁰¹, and since the retina is an immune-privileged tissue, its local complement system is independent of the systemic complement components typically produced by the liver²⁵³. DR, characterised by pathological retinal angiogenesis is a major cause of irreversible vision loss worldwide and although the involvement of the complement components in the progression of DR has been recognised¹⁰¹ (*please refer to section 1.9.4*) there is still a great deal more to be uncovered. Previous studies addressing the influence of complement on retinal neovascularisation have revealed contradictory results. For instance, a pro-angiogenic function of CFB has been implicated in the model of laser-induced CNV, which represents a model of angiogenesis during the wet form of AMD^{206,207,254}. Moreover, CFH and CFB polymorphisms have been associated with neovascular AMD^{198,199,255}. In contrast, another study reported that CFB -/- mice demonstrated significantly more neovascularisation following OIR treatment, and suggested that CFB has a protective role in DR by aiding in the clearance of pathological neo-vessels²³¹. It is clear that the mechanisms involved in the crosstalk between CFB and neovascularisation remains ambiguous, and as a result the main focus of this study was to investigate the involvement of CFB in the neovascular pathology of DR.

4.1 Characterising the Expression of Complement Factor B Using Rodent Models and Human Patient Samples

Dysregulation of the complement system is now a recognised characteristic of patients with DR. However, DR is a multifactorial disease and isolating the specific contributions of individual complement proteins to disease pathology is not straightforward. One approach, adopted by Williams *et al* in 2016, to studying the role of the complement system in the maintenance of retinal health was to characterise the retinal phenotype of mice carrying deletions of specific complement genes. After 12 months, they reported that the retinal morphology and retinal vasculature did not appear different across the genotypes. Although these results suggest that under physiological conditions the retina is stable and healthy even with the absence of a functional AP, it doesn't mean to say that these genotypes do not contribute to pathological retinal vascular changes. This study was carried out in the absence of a pathological challenge or environmental stressor, and therefore provides limited insight into how complement contributes to vascular pathology under the disease conditions that manifest in DR. This project aimed to address this by using human patient samples from diabetic patients with retinopathy, and rodent models that better mimic the pathology that manifests in DR.

Most complement proteins and complement regulatory proteins are synthesised in the liver by hepatocytes and released into the blood for distribution²⁵⁶, therefore to begin with CFB expression was first examined in human patient serum samples at different stages of retinopathy. Unsurprisingly, there was no difference in human patient serum CFB levels between control and diabetic patients at different stages of retinopathy. A major problem associated with using serum to detect changes in protein expression is the fact that the detection of low abundant proteins is largely hidden by a vast amount of high abundant proteins such as albumin and IgGs and therefore it might be difficult to detect changes in CFB expression in serum above a high background.

The retina is segregated from the circulation by the BRB and is considered to be an immune privileged²⁵⁷. However, it is now well established that an extrahepatic system of complement biosynthesis exists within the retina to compensate for the restricted entry of bloodborne proteins normally excluded by the BRB.²⁵⁸ Since the retina is an immune privileged organ and is protected from exposure to systemic circulation, human patient serum samples are not a true representation of the retinal microenvironment and may not reflect changes in ocular CFB expression. As a result local concentrations are likely to be more indicative²²⁷. In terms of DM-induced microvascular complications, the shift from a healthy state to pathology can influence protein constituents and/or protein abundance in the ocular fluids. As a result, levels of proteins in the ocular fluids can be used to indicate the health status of blood vessels and/or tissue, and indirectly explore the pathophysiologic events that take place. The vitreous is the largest component structure of the eye. In its normal state, it is a clear gelatinous matrix between the lens and retina, that is primarily composed of water, collagen, glycosaminoglycans, and proteoglycans²⁵⁹. In addition to optical functions, the vitreous also contains a whole host of factors that can influence retinal physiology.⁸⁹ The metabolic and functional alterations that occur in DR can result in molecular changes in the vitreous. In turn, alterations of the vitreous exert pathological effects on the diabetic retina, resulting in a viscous cycle that contributes to disease progression²⁶⁰. Consequently, vitreous samples obtained from diabetic patients undergoing vitreoretinal surgery are currently used to indirectly explore mediators involved in the development of DR²²⁷. Several proteomic studies have been²⁶¹ carried out to analyse the protein profiles of human vitreous samples from patients with DR. In these studies, complement factors including CFB were found to be increased in the vitreous of patients with PDR^{226,261}. Protein levels in the vitreous may be a better indication of retinal health status than other ocular due to the close proximity between the vitreous and retina²⁶². However, surgical harvesting of vitreous fluid is associated with a risk of vitreous haemorrhage, retinal tears, and retinal detachment, and it is difficult to obtain vitreous samples for diagnostic or investigative purpose²⁶³. The aqueous humor (AH) is a

transparent extracellular fluid that is secreted by the non-pigmented ciliary body epithelium of the eye. The AH helps to maintain intraocular pressure and the globe shape of the eye, and supplies oxygen and nutrients to the avascular cornea and lens. In comparison to vitreous samples, obtaining aqueous samples is a far easier and less risky procedure. In the AH of human eyes, a number of growth factors have been detected, such as basic fibroblast growth factor (bFGF), epidermal growth factor (EGF), TGF- β , insulin-like growth factor (IGF)-1, platelet-derived growth factor (PDGF), VEGF, hepatocyte growth factor (HGF), and interleukin (IL)-6, the composition of which changes dramatically with different conditions²⁶⁴. Previous studies have linked elevated cytokine levels in aqueous humor to vitreous fluid levels and to the progression of DR²⁶⁵. Consequently, the AH may act as a powerful tool in understanding the pathophysiology of DR and serve as biomarkers for predicting the development of the disease²⁶⁶. In this regard AH samples obtained from diabetic patients undergoing vitreoretinal surgery were used to evaluate ocular CFB levels. CFB levels were higher in aqueous samples of diabetic patients with retinopathy. In theory, checking CFB expression both systemically in serum and locally in aqueous samples allows comparison between the two. This could help determine if any changes of CFB levels in the aqueous are a localised effect rather than a non-specific, additive effect due to serum diffusion. As no changes in CFB expression were detected in the human serum samples, this observed up-regulated expression of CFB in the aqueous samples from DR patients may be caused by local changes in the eye. However, it is worthy to note that this observation was based on 1 aqueous sample from each patient group and should be confirmed in a larger cohort of patients.

Enhanced expression of complement components have also been observed in the retina of STZ-induced diabetic rats^{219,267}. However, the expression of CFB at both RNA and protein levels remain unchanged in the retina of mice suffering from STZ-induced diabetes. This is likely due to the mild retinal vascular changes in these mice: inducing diabetes in this manner reproduces early symptoms of DR, such as loss of retinal pericytes and capillaries, BM thickening

and increased vascular permeability, however advanced proliferative changes characteristic of PDR do not develop²⁶⁸. The lack of pathological neovascularization in STZ mice may explain the flat CFB expression.

The mouse OIR model is a well-established technique used to mimic pathological retinal neovascularisation seen in PDR. The OIR model consists of 2 distinct phases. In the first phase, P7 through P12, mice are placed in a high-oxygen environment that results in vasoobliteration of the developing vasculature. The second phase begins when the mice are returned to atmospheric oxygen at P12. The relatively low oxygen concentration causes the central avascular zone to become hypoxic, inducing the expression proangiogenic mediators such as VEGF. Although these pathways stimulate the growth of normal vessels, they also cause the formation of pathological vessels which sprout from the superficial retinal vasculature resembling the pathological neovascularization seen in humans with DR. In this study, it has been demonstrated that CFB mRNA expression correlated with the neovascularisation progression in OIR in a similar manner to that reported for VEGF²⁶⁹. In P12 mice when the high oxygen exposure suppresses vascular growth and causes retinal vaso-obliteration, CFB gene expression is lower in the OIR retina compared to normal oxygen control. In P17 mice, upon return to normoxic conditions when the retina becomes hypoxic and there is aberrant angiogenesis, CFB gene expression is significantly increased. The correspondence of increased CFB expression to the phase in which neovascularisation occurs in the OIR model suggests an association of CFB with retinal neo-vessel formation. These results are supported by data from Sweigard *et al* who not only reported an increase in both CFB mRNA and protein expression following OIR, but who also demonstrated CFB deposition on retinal neo-vessels by immunofluorescence staining²³¹. In addition, these results are also in line with a previous study in which authors reported an induction of CFB expression in the pathological retinal blood vessels of several mouse models that exhibit marked remodelling of the retinal vasculature²⁷⁰. By conducting genome-wide transcriptional analysis of retinal microvessel

fragments isolated from the retinal degeneration 1 (*rd1*) mouse very low-density lipoprotein receptor (VLDLR) knockout mouse (*Vldlr*^{-/-}), the *Grhl3*^{ct/J} curly tail mouse and appropriate wild-type controls, they found 62 genes that were differentially regulated but common to all three models. When ranked according to fold change, CFB was one of most significantly up-regulated genes across all three models.

Despite there being no changes in human serum CFB levels or in the retina of STZ mice, higher CFB in aqueous samples of diabetic patients with retinopathy, alongside the increase of CFB expression in OIR retina, indicates a possible role of CFB in driving DR. It suggests that CFB might not only contribute to the innate defence mechanism of the AP but might also contribute to DR pathology through functional crosstalk with other cellular networks. Whilst this characterisation suggests CFB may contribute to DR, the function of this protein has yet to be determined.

4.2 The Role of CFB in Regulating Retinal Angiogenesis

Angiogenesis is a highly complex and tightly regulated process that results in the establishment of a vasculature that supports vital systems of the body. However, when misdirected, angiogenesis manifests in numerous pathologies including diabetic microvascular complications. A defining feature of PDR is the formation of destructive neovascularisation, and the balance between this new vessel formation and regression determines the progression to blindness²³¹. Results discussed in the previous section suggest an association of CFB with neovascular formation and so to understand the more precise function of CFB, several *in vitro* and *ex vivo* angiogenesis assays were conducted.

In vitro assays of angiogenesis are an indispensable tool to gain a better understanding of this process. They represent a rapid, defined and efficient experimental strategy to gain understanding of complex molecular events that occur during angiogenesis; they can be used for modelling pathological

conditions as well as provide a platform for the investigation of biochemical factors that have the potential to be used as therapeutic agents for the treatment of angiogenesis related diseases. An ideal assay would allow for the assessment of multiple parameters, providing reliable and reproducible results that can be related to those found in the clinic²⁷¹. Currently, there is no 'gold standard' assay that accurately represents the process in its entirety and so to provide a comprehensive overview of the angiogenic process, the effect of CFB was evaluated in retinal-specific EC line using a number of *in vitro* and *ex vivo* assays. Results revealed a promoting effect of CFB on HREC survival, proliferation, migration, and the ability to assemble into tubular networks. Despite providing important observations regarding EC behaviour, *in vitro* assays are unable to fully recapitulate blood vessel formation *in vivo*. To overcome these limitations and supplement findings from the cell-based studies, two *ex vivo* assays were carried out: the aortic ring and fetal metatarsal explant assays. Consistent with observations from the *in vitro* studies, in both *ex vivo* assays, vessel outgrowth from explanted tissue was significantly increased after the addition of exogenous CFB. These assays provided a more physiologically relevant platform to study angiogenesis, since explants developed lumenised blood vessels with surrounding supporting cells in a timescale similar to that observed *in vivo*⁴⁶.

Although this data strongly implicates a pro-angiogenic effect of CFB, it is contradictory to a previous report by Sweigard *et al.* Despite reporting an increase in CFB gene and protein expression, and co-localisation of CFB on retinal neo-vessels following OIR, they found that OIR mice deficient in CFB had a significant increase in neovascularisation after exposure to OIR, in comparison to their wildtype counterparts²³¹. They concluded that the increase in neovascularisation was not a consequence of increased stimulation but rather a result of reduced neo-vessel removal, and CFB a protective effect by facilitating with neo-vessel clearance. One reason for these conflicting observations could be down to the use of either *in vitro* or *in vivo* experimental settings to investigate the angiogenic potential of CFB. The main findings from

this study are based on *in vitro* experiments where the effect of CFB was explored in an isolated, and controlled manner using a single cell type. However, it is important to highlight that angiogenesis is a highly context dependent process and the response of different cell types to certain angiogenic stimuli can be significantly different. It is possible that *in vitro*, CFB exerts a promoting effect on HRECs, but when translated *in vivo*, CFB acts on other retinal cell types that mediate its anti-angiogenic effects. In the context of DR, anti-angiogenesis may be the predominant action of CFB, overriding the promoting effect of CFB on HRECs alone. One particular study that supports this idea found that the anti-angiogenic effect of complement was in fact not mediated by endothelial cells, but rather by macrophages²⁷². In addition, Sweigard *et al* conducted their study using knockout mice that had been generated by conventional gene disruption using homologous recombination. This means the knockout manifests itself in all cells of the organism. Since the retina possesses its own complement regulatory system and it has been reported that RPE cells are the major extrahepatic source of CFB in the retina, it WOULD be interesting to investigate the effect of inducing the CFB gene defect in a tissue specific manner. Tissue specific knockdown of CFB in the RPE means the mice would possess a normal complement system in all other tissues and so it is possible that the increase in neovascularisation observed in the CFB deficient mice following OIR could be attenuated by depleting CFB only within the retina.

In summary, results revealed that CFB can exert pro-angiogenic activity in cultured HRECs and in *ex vivo* models of angiogenesis. This novel function is distinct from CFB's well-established role within the AP and indicates an association between systems and pathways that otherwise would be considered as unrelated and antithetical.

4.3. Investigating the relationship between Complement Factor B and VEGF-A and VEGFR2

The previous chapter reported a pro-angiogenic effect of CFB in both cultured HRECs and in *ex vivo* models of angiogenesis, however the mechanisms underlying the regulation of angiogenesis by CFB remain to be elucidated. This leaves an important question unanswered: how does CFB exert this pro-angiogenic function?

The VEGF signalling pathway is one of the most potent angiogenic mediators and VEGF is well established as the main agent responsible for vascular leakage and angiogenesis in the diabetic retina²⁷³. Some VEGF makes its way to the retina from systemic sources and some is produced locally in the eye²⁷³: ECs, pericytes, Muller cells, microglia, astrocytes, RPE cells, and neurons have all been known to produce VEGF in retinal disease²⁷⁴. Additionally, VEGF has a well-established role in promoting neovascularisation in the OIR model²⁷⁵ and as demonstrated by this study, CFB mRNA expression correlated with the neovascularisation progression in a similar manner to that reported for VEGF²⁶⁹. Therefore, a plausible explanation for the pro-angiogenic effect of CFB could be because of increased VEGF signalling. Since increased VEGF signalling could not only be a consequence of increased ligand expression, but also due to increased receptor expression, the mRNA and protein expression of both VEGF-A and VEGFR2 by cultured HRECs was examined. The ability of exogenous CFB to increase VEGF-A and VEGFR2 mRNA expression in HRECs suggests that CFB is able to mediate both VEGF-A and VEGFR2 at the transcript level. The promoting effect of CFB observed in the *in vitro* angiogenesis assays may be driven by the increased mRNA expression of the VEGF signalling pathway components. This effect was confirmed by CFB silencing, where the opposite trend was observed and VEGF-A and VEGFR2 mRNA expression was attenuated. The decrease in angiogenic potential of HRECs observed in the *in vitro* assays after CFB silencing, could be a result of reduced expression of VEGF-A and VEGFR2 mRNA. Looking at changes in

mRNA expression helps gives an indication of functional protein changes, however this is not necessarily always the case. So, to confirm this observation, the effect of CFB on VEGF-A and VEGFR2 protein expression in HRECs was also investigated. Despite the significant suppression of both VEGF-A and VEGFR2 at the mRNA level, VEGFR2 protein level but not VEGF-A was significantly reduced in HRECs subject to treatment with CFB siRNA. This could be due to different rates of translation of VEGF-A and VEGFR2, meaning the duration of the experiment was long enough to capture changes in receptor but not ligand expression. Nevertheless, there is a significant suppression of VEGFR2 protein expression following siRNA treatment. These results are in fact supported by a recent study that investigated the role of CFB in CNV. By using short hairpin RNA (shRNA) to knockdown CFB, they observed a significant inhibition in the formation and development of CNV by reducing the expression of VEGF²⁵². Another study, although not looking specifically at CFB, also showed that VEGF expression was reduced following specific inhibition of the alternative pathway²⁷⁶. In spite of the fact that these results implicate a link between CFB and VEGF, they are in conflict with a previous report by Sweigard *et al.* After observing reduced neovascularisation in CFB deficient mice exposed to OIR they wanted to determine if this increase was a result of VEGF expression, and so they proceeded to check the mRNA expression of three different VEGF isoforms (including VEGF-A), and VEGFR2 in wildtype and CFB^{-/-} mice following exposure to OIR. Surprisingly, they reported no differences in the expression levels of either VEGF or VEGFR2. These conflicting results could again be attributed to the use of either *in vitro* or *in vivo* experimental settings to investigate the possible mechanism of CFB. In this study the effect of CFB on VEGF expression was analysed *in vitro* using only a single cell type. It is possible that in a controlled, well-defined *in vitro* microenvironment comprising of only a single cell type, CFB promotes VEGF expression in HRECs. However, the *in vivo* microenvironment is complex and is comprised of a multitude of cell types. Since VEGF expression was conducted on whole retinal tissue (not isolated cell types) it is not possible to rule out the possibility that the unchanged VEGF expression reported by Sweigard *et al* may

be because CFB has opposing effects on VEGF expression in other cell types which negate the changes in VEGF expression in HRECs alone.

To confirm whether the CFB mediated change in VEGFR2 protein expression confers functional changes in VEGF signalling, the effect of exogenous CFB on HRECs following inhibition of the VEGF signalling cascade using the small molecule tyrosine kinase inhibitor for VEGFR2, Linifanib, was explored using the *in vitro* Matrigel® network formation assay. Blocking of VEGFR2 with Linifanib, attenuated the promoting effect of rhCFB on HREC Matrigel® network formation. This suggests that the pro-angiogenic effect of CFB is likely to be dependent on the activation of VEGF signalling and that CFB mediates its pro-angiogenic effect through VEGFR2 signalling.

5 Conclusion and Future Work

The complement system, a central constituent of innate immunity, has primarily been considered as a rapid and efficient immune surveillance system, however, genetic studies, clinical observations, and insights from improved disease models have renewed the views of human complement system in disease^{277,278}. It is important to appreciate that biological systems are not rigid entities but are highly dynamic and interactive networks that influence physiological responses. This study aimed to take a more global appreciation of what would traditionally be viewed as isolated biological processes, and presented findings that indicate a possible cross-talk between the AP component, CFB, and retinal angiogenesis associated with DR.

The first aim of this study was to characterise the expression level of CFB in rodent models of PDR and human PDR patient samples. Although initial characterisation pointed towards an increase in local CFB levels with retinopathy, caution must be observed when drawing conclusions from this data. Although there was an upregulation of CFB in the aqueous humor of patients with retinopathy, this observation was only confirmed in one patient sample per group. To obtain a more reliable protein profile, CFB expression should be confirmed in more patient samples and in human vitreous samples. While the STZ-induced diabetic mice are routinely used as a model for mechanistic studies of other diabetic complications, they only develop the early vascular changes associated with retinopathy and do not develop the late-stage proliferative vascular pathology that is routinely seen in PDR.²⁷⁹ Although relevant to diabetes, the STZ-induced diabetic mouse is not the most relevant model to study PDR pathology and future *in vivo* characterisation should be carried out using the OIR model. A more detailed characterisation of CFB expression is needed to help determine whether it also has a role in retinal vascular development. Future studies should compare the retinal vasculature of CFB knockout (CFB^{-/-}) with wild-type (WT) mice at different postnatal stages to explore whether expression correlates with physiological vascular development,

and to determine whether CFB^{-/-} mice have defective retinal vascular development. The effect of CFB ^{-/-} on pathological neovascularisation has already been reported²³¹, but to confirm these observations and follow on from this it would be interesting to observe the effect of OIR on neovascularisation using mice over-expressing CFB: is neovascularisation strengthened or attenuated? Additional characterisation should be carried by immunofluorescent staining of mice retinal cross-sections to confirm which cell types are the main source of CFB.

The second aim of this study was to investigate the role of CFB in retinal vascular endothelial cell behaviour and angiogenesis. *In vitro* cell based assays demonstrated a promoting effect of CFB on HREC behaviour and angiogenic potential, suggesting that CFB has a role in driving retinal neovascularisation by promoting angiogenesis. However, a significant challenge in the study of angiogenesis is selection of the appropriate assay that accurately reflects the complexity of the processes that occur *in vivo*. Using multiple *in vitro* assays in this study helped provide a more comprehensive overview of CFBs function in angiogenesis, however they were only carried out using one cell type. Angiogenesis is mediated by multiple cell types and besides ECs, pericytes are also crucial for angiogenesis. Therefore, future studies should look at the effect of CFB on retinal pericytes, both alone and in co-culture with ECs. In addition, to better capitulate the diabetic pathology, it would also be insightful to study CFB under high glucose conditions. Continuous hyperglycaemia in long-standing DM majorly perturbs vascular homeostasis and leads to endothelial dysfunction, mainly attributable to increased accumulation of oxidative stress and advanced glycation end-products (AGEs)^{6,9}. It would therefore be beneficial to establish *in vitro* models of angiogenesis using high glucose or glycated collagen. Although the aortic ring and fetal metatarsal assays provide a more physiologically relevant platform to study angiogenesis it might not be an accurate representation of the process within the eye. Other *ex vivo* assays should be carried out to supplement the aortic ring data including the more

pertinent choroid assay. The choroid assay would provide information regarding ocular specific microvascular behaviour.

The final aim of this study to elucidate the mechanism through which CFB contributes to vascular pathology in DR. Although the data obtained in this study gives an indication to a possible mechanism through which CFB may exert its pro-angiogenic effect, future work should confirm the results of the VEGF and VEGFR2 gene and protein studies, using both rhCFB treatment and CFB over-expressing cells. Additionally, it would be interesting to see if the promoting effect of CFB is attenuated upon VEGFR2 inhibition in other functionality assays such as viability, proliferation and Transwell migration. The effect of CFB in the absence and presence of Linifanib, on signalling pathways downstream of VEGF/VEGFR2 would also help to supplement this data.

Thus far, these preliminary studies have shown that CFB mediates VEGF gene expression, and VEGFR2 gene and protein expression. These studies have also demonstrated that the pro-angiogenic function of CFB is upstream of, and acts at least partially through the VEGF signalling pathway: the blocking of VEGFR2 causes the promoting effect of CFB to be lost. This now raises the question, '**how** does CFB induce these changes and regulate VEGF signalling? One explanation could be the crosstalk between the complement pathway and VEGF. Increased deposition of MAC²⁵⁴, the end-product of complement activation has been reported in other ocular neovascular disorders. It has also been implicated in the expression of angiogenic growth factors²⁸⁰ including VEGF^{281,282}. It is therefore plausible that increased levels of CFB cause over-activation of the AP, leading to increased formation of MAC. MAC mediated VEGF expression could be a pathogenic mechanism through which CFB promotes angiogenesis. To investigate this further, the relationship between CFB expression and MAC formation should be explored both *in vivo* using CFB^{-/-} mice, and *in vitro* using HRECs. Following this, the effect of MAC inhibition on the VEGF signalling pathway and angiogenesis should be explored.

The effect of CFB on the VEGF signalling system could also be controlled via other mechanisms. Perhaps CFB controls VEGF signalling at the gene expression level by activating transcription factors that are involved in the regulation of VEGF/VEGFR2 gene transcription. Perhaps CFB is involved in regulating VEGF/VEGFR2 protein stability and proteolytic processing, or ligand receptor interactions, or receptor endocytosis and trafficking. It is important not to over interpret this data and until further work is carried out, we can only speculate. A more extensive investigation should be carried out before a complete mechanistic framework can emerge. Microarray and proteomics studies could help identify genes or proteins that are differentially regulated by CFB. Any that are up- or downregulated could then be investigated further to see if they are involved in mediating the relationship between CFB and VEGF/VEGFR2.

In conclusion, this study presents a more precise role of CFB in driving retinal neovascularisation, providing a framework for a more in-depth exploration of CFB-mediated effects on retinal angiogenesis in the future. Given the conflicting nature of the results obtained in this study, a more in-depth exploration of CFB's role in driving retinal neovascularisation associated with PDR is needed, particularly in regards to mechanism of action studies. However, data taken together and examined in the light of other relevant studies and existing literature has led to a tentative proposed mechanism of action (*please refer to **Figure 33** for the proposed mechanism of action*).

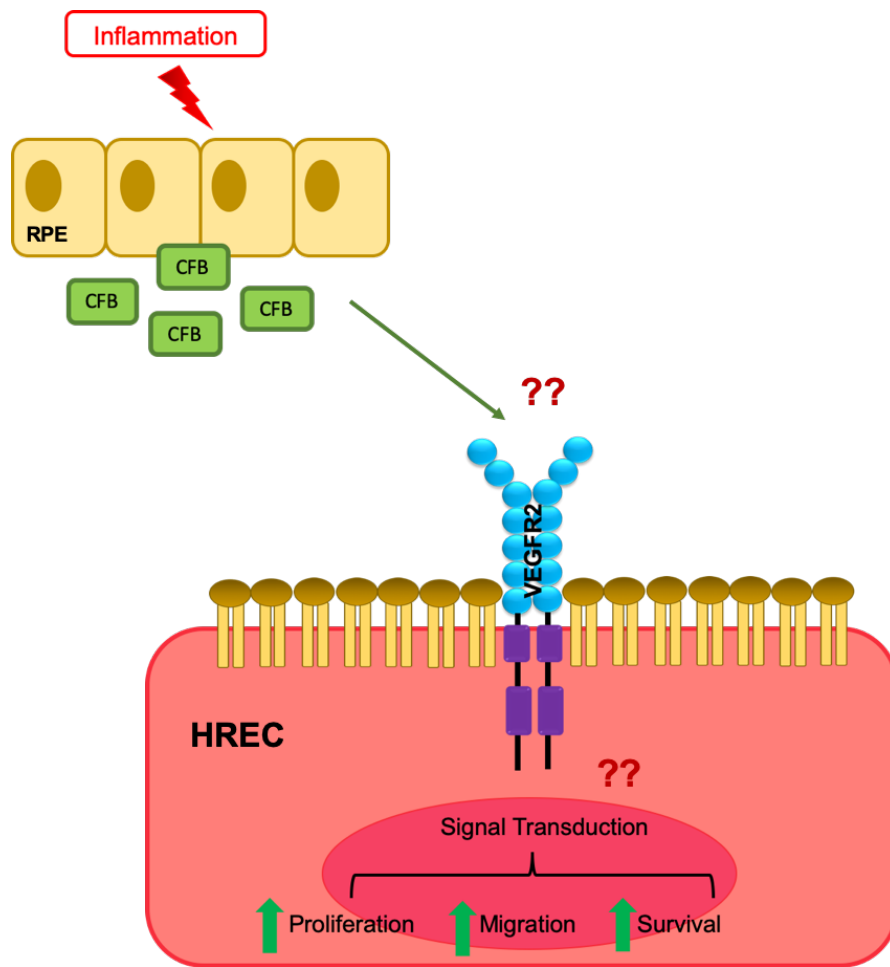


Figure 33: A schematic representation of the proposed mechanism of action of CFB in retinal neovascularisation in DR. The inflammatory microenvironment in DR induces RPE cells to secrete CFB, which acts in a paracrine manner on retinal ECs, inducing the VEGF signalling cascade, resulting in enhanced EC survival, proliferation, migration, and network-formation

6 References

- 1 Das, A. Diabetic retinopathy: a global epidemic. *Middle East African journal of ophthalmology* **22**, 133-134, doi:10.4103/0974-9233.154385 (2015).
- 2 Harlan, D. M. & Hirsch, I. B. The upside down world of diabetes care medical economics and what we might do to improve it. *Current Opinion in Endocrinology Diabetes and Obesity* **24**, 112-118, doi:10.1097/med.0000000000000325 (2017).
- 3 Guariguata, L. *et al.* Global estimates of diabetes prevalence for 2013 and projections for 2035. *Diabetes Research and Clinical Practice* **103**, 137-149, doi:10.1016/j.diabres.2013.11.002 (2014).
- 4 Tiwari, A. K. & Rao, J. M. Diabetes mellitus and multiple therapeutic approaches of phytochemicals: Present status and future prospects. *Current Science* **83**, 30-38 (2002).
- 5 Kawahito, S., Kitahata, H. & Oshita, S. Problems associated with glucose toxicity: Role of hyperglycemia-induced oxidative stress. *World Journal of Gastroenterology* **15**, 4137-4142, doi:10.3748/wjg.15.4137 (2009).
- 6 Brownlee, M. The pathobiology of diabetic complications - A unifying mechanism. *Diabetes* **54**, 1615-1625, doi:10.2337/diabetes.54.6.1615 (2005).
- 7 Beckman, J. A. & Creager, M. A. Vascular Complications of Diabetes. *Circulation Research* **118**, 1771-1785, doi:10.1161/circresaha.115.306884 (2016).
- 8 Madonna, R. & De Caterina, R. Cellular and molecular mechanisms of vascular injury in diabetes - Part I: Pathways of vascular disease in diabetes. *Vascular Pharmacology* **54**, 68-74, doi:10.1016/j.vph.2011.03.005 (2011).
- 9 Brownlee, M. Biochemistry and molecular cell biology of diabetic complications. *Nature* **414**, 813-820, doi:10.1038/414813a (2001).
- 10 Thakur, P. & Kumar, A. Targeting oxidative stress through antioxidants in diabetes mellitus. *Journal of Drug Targeting* **26**, 766-776, doi:10.1080/1061186x.2017.1419478 (2018).
- 11 Yau, J. W. Y. *et al.* Global Prevalence and Major Risk Factors of Diabetic Retinopathy. *Diabetes Care* **35**, 556-564, doi:10.2337/dc11-1909 (2012).
- 12 Khazaei, M., Moien-Afshari, F. & Laher, I. Vascular endothelial function in health and diseases. *Pathophysiology* **15**, 49-67, doi:10.1016/j.pathophys.2008.02.002 (2008).
- 13 Stamatelos, S. K., Kim, E., Pathak, A. P. & Popel, A. S. A bioimage informatics based reconstruction of breast tumor microvasculature with computational blood flow predictions. *Microvasc Res* **91**, 8-21, doi:10.1016/j.mvr.2013.12.003 (2014).

- 14 Blinder, P. *et al.* The cortical angiome: an interconnected vascular network with noncolumnar patterns of blood flow. *Nature Neuroscience* **16**, 889-897, doi:10.1038/nn.3426 (2013).
- 15 Nolan, Daniel J. *et al.* Molecular Signatures of Tissue-Specific Microvascular Endothelial Cell Heterogeneity in Organ Maintenance and Regeneration. *Developmental Cell* **26**, 204-219, doi:<https://doi.org/10.1016/j.devcel.2013.06.017> (2013).
- 16 Moore, J. P., Dyson, A., Singer, M. & Fraser, J. Microcirculatory dysfunction and resuscitation: why, when, and how. *British journal of anaesthesia* **115**, 366-375, doi:10.1093/bja/aev163 (2015).
- 17 Aird, W. C. Endothelial Cell Heterogeneity. *Cold Spring Harbor Perspectives in Medicine* **2**, doi:10.1101/cshperspect.a006429 (2012).
- 18 Betz, C., Lenard, A., Belting, H. G. & Affolter, M. Cell behaviors and dynamics during angiogenesis. *Development* **143**, 2249-2260, doi:10.1242/dev.135616 (2016).
- 19 Jain, R. K. Molecular regulation of vessel maturation. *Nature Medicine* **9**, 685-693, doi:10.1038/nm0603-685 (2003).
- 20 Rajendran, P. *et al.* The vascular endothelium and human diseases. *Int J Biol Sci* **9**, 1057-1069, doi:10.7150/ijbs.7502 (2013).
- 21 Onat, D., Brillon, D., Colombo, P. C. & Schmidt, A. M. Human vascular endothelial cells: a model system for studying vascular inflammation in diabetes and atherosclerosis. *Current diabetes reports* **11**, 193-202, doi:10.1007/s11892-011-0182-2 (2011).
- 22 Aird, W. C. Endothelial cell heterogeneity. *Cold Spring Harbor perspectives in medicine* **2**, a006429-a006429, doi:10.1101/cshperspect.a006429 (2012).
- 23 Aird, W. C. Phenotypic heterogeneity of the endothelium II. Representative vascular beds. *Circulation Research* **100**, 174-190, doi:10.1161/01.RES.0000255690.03436.ae (2007).
- 24 Ndisang, J. F. Glomerular Endothelium and its Impact on Glomerular Filtration Barrier in Diabetes: Are the Gaps Still Illusive? *Curr Med Chem* **25**, 1525-1529, doi:10.2174/0929867324666170705124647 (2018).
- 25 Bosetti, F. *et al.* "Small Blood Vessels: Big Health Problems?": Scientific Recommendations of the National Institutes of Health Workshop. *Journal of the American Heart Association* **5**, e004389, doi:10.1161/JAHA.116.004389.
- 26 Stratman, A. N. *et al.* Interactions between mural cells and endothelial cells stabilize the developing zebrafish dorsal aorta. *Development* **144**, 115-127, doi:10.1242/dev.143131 (2017).
- 27 Bou-Gharios, G., Ponticos, M., Rajkumar, V. & Abraham, D. Extra-cellular matrix in vascular networks. *Cell proliferation* **37**, 207-220, doi:10.1111/j.1365-2184.2004.00306.x (2004).
- 28 Potente, M., Gerhardt, H. & Carmeliet, P. Basic and Therapeutic Aspects of Angiogenesis. *Cell* **146**, 873-887, doi:10.1016/j.cell.2011.08.039 (2011).
- 29 Mazurek, R. *et al.* Vascular Cells in Blood Vessel Wall Development and Disease. *Advances in pharmacology (San Diego, Calif.)* **78**, 323-350, doi:10.1016/bs.apha.2016.08.001 (2017).

- 30 Helfrich, I. & Schadendorf, D. Blood vessel maturation, vascular phenotype and angiogenic potential in malignant melanoma: one step forward for overcoming anti-angiogenic drug resistance? *Molecular oncology* **5**, 137-149, doi:10.1016/j.molonc.2011.01.003 (2011).
- 31 Armulik, A., Abramsson, A. & Betsholtz, C. Endothelial/pericyte interactions. *Circulation Research* **97**, 512-523, doi:10.1161/01.RES.0000182903.16652.d7 (2005).
- 32 Majesky, M. W. Adventitia and perivascular cells. *Arteriosclerosis, thrombosis, and vascular biology* **35**, e31-35, doi:10.1161/atvbaha.115.306088 (2015).
- 33 Stenmark, K. R. *et al.* The adventitia: essential regulator of vascular wall structure and function. *Annu Rev Physiol* **75**, 23-47, doi:10.1146/annurev-physiol-030212-183802 (2013).
- 34 Schöneberg, J. *et al.* Engineering biofunctional in vitro vessel models using a multilayer bioprinting technique. *Scientific Reports* **8**, 10430, doi:10.1038/s41598-018-28715-0 (2018).
- 35 Adair, T. & Montani, J. (Morgan & Claypool Life Sciences, San Rafael (CA), 2010).
- 36 Conway, E. M., Collen, D. & Carmeliet, P. Molecular mechanisms of blood vessel growth. *Cardiovasc Res* **49**, 507-521, doi:10.1016/s0008-6363(00)00281-9 (2001).
- 37 Chung, A. S. & Ferrara, N. Developmental and pathological angiogenesis. *Annual review of cell and developmental biology* **27**, 563-584, doi:10.1146/annurev-cellbio-092910-154002 (2011).
- 38 Grant, G. A. & Janigro, D. in *The Cell Cycle in the Central Nervous System* (ed Damir Janigro) 31-41 (Humana Press, 2006).
- 39 Patan, S. Vasculogenesis and angiogenesis as mechanisms of vascular network formation, growth and remodeling. *Journal of Neuro-Oncology* **50**, 1-15, doi:10.1023/a:1006493130855 (2000).
- 40 Lubarsky, B. & Krasnow, M. A. Tube morphogenesis: making and shaping biological tubes. *Cell* **112**, 19-28, doi:10.1016/s0092-8674(02)01283-7 (2003).
- 41 Caduff, J. H., Fischer, L. C. & Burri, P. H. SCANNING ELECTRON-MICROSCOPE STUDY OF THE DEVELOPING MICROVASCULATURE IN THE POSTNATAL RAT LUNG. *Anatomical Record* **216**, 154-164, doi:10.1002/ar.1092160207 (1986).
- 42 Burri, P. H., Hlushchuk, R. & Djonov, V. Intussusceptive angiogenesis: Its emergence, its characteristics, and its significance. *Developmental Dynamics* **231**, 474-488, doi:10.1002/dvdy.20184 (2004).
- 43 Djonov, V., Baum, O. & Burri, P. H. Vascular remodeling by intussusceptive angiogenesis. *Cell and Tissue Research* **314**, 107-117, doi:10.1007/s00441-003-0784-3 (2003).
- 44 Pugh, C. W. & Ratcliffe, P. J. Regulation of angiogenesis by hypoxia: role of the HIF system. *Nature Medicine* **9**, 677-684, doi:10.1038/nm0603-677 (2003).
- 45 Gupta, K. & Zhang, J. Angiogenesis: a curse or cure? *Postgrad Med J* **81**, 236-242, doi:10.1136/pgmj.2004.023309 (2005).

- 46 Baker, M. *et al.* Use of the mouse aortic ring assay to study angiogenesis. *Nature Protocols* **7**, 89-104, doi:10.1038/nprot.2011.435 (2012).
- 47 van Hinsbergh, V. W. M. & Koolwijk, P. Endothelial sprouting and angiogenesis: matrix metalloproteinases in the lead. *Cardiovascular Research* **78**, 203-212, doi:10.1093/cvr/cvm102 (2008).
- 48 Maeshima, Y. in *Apoptosis, Cell Signaling, and Human Diseases: Molecular Mechanisms* Vol. 1 (ed R. Srivastava) (Human Press, 2007).
- 49 Horowitz, A. & Simons, M. Branching Morphogenesis. *Circulation Research* **104**, E21-E21, doi:10.1161/circresaha.108.191494 (2009).
- 50 Song, J. W., Bazou, D. & Munn, L. L. Anastomosis of endothelial sprouts forms new vessels in a tissue analogue of angiogenesis. *Integrative Biology* **4**, 857-862, doi:10.1039/c2ib20061a (2012).
- 51 Ribatti, D., Nico, B. & Crivellato, E. The role of pericytes in angiogenesis. *International Journal of Developmental Biology* **55**, 261-268, doi:10.1387/ijdb.103167dr (2011).
- 52 Logsdon, E. A., Finley, S. D., Popel, A. S. & Mac Gabhann, F. A systems biology view of blood vessel growth and remodelling. *Journal of cellular and molecular medicine* **18**, 1491-1508, doi:10.1111/jcmm.12164 (2014).
- 53 Carmeliet, P. Angiogenesis in health and disease. *Nature Medicine* **9**, 653-660, doi:10.1038/nm0603-653 (2003).
- 54 Epstein Stephen, E., Kornowski, R., Fuchs, S. & Dvorak Harold, F. Angiogenesis Therapy. *Circulation* **104**, 115-119, doi:10.1161/01.CIR.104.1.115 (2001).
- 55 Senger, D. R. *et al.* Tumor cells secrete a vascular permeability factor that promotes accumulation of ascites fluid. *Science* **219**, 983, doi:10.1126/science.6823562 (1983).
- 56 Leung, D. W., Cachianes, G., Kuang, W. J., Goeddel, D. V. & Ferrara, N. Vascular endothelial growth factor is a secreted angiogenic mitogen. *Science* **246**, 1306, doi:10.1126/science.2479986 (1989).
- 57 Bhisitkul, R. B. Vascular endothelial growth factor biology: clinical implications for ocular treatments. *The British journal of ophthalmology* **90**, 1542-1547, doi:10.1136/bjo.2006.098426 (2006).
- 58 Woolard, J., Bevan, H. S., Harper, S. J. & Bates, D. O. Molecular diversity of VEGF-A as a regulator of its biological activity. *Microcirculation (New York, N.Y. : 1994)* **16**, 572-592, doi:10.1080/10739680902997333 (2009).
- 59 Peach, C. J. *et al.* Molecular Pharmacology of VEGF-A Isoforms: Binding and Signalling at VEGFR2. *International journal of molecular sciences* **19**, 1264, doi:10.3390/ijms19041264 (2018).
- 60 Ferrara, N., Gerber, H. P. & LeCouter, J. The biology of VEGF and its receptors. *Nature Medicine* **9**, 669-676, doi:10.1038/nm0603-669 (2003).
- 61 Zachary, I. & Gliki, G. Signaling transduction mechanisms mediating biological actions of the vascular endothelial growth factor family. *Cardiovascular Research* **49**, 568-581, doi:10.1016/S0008-6363(00)00268-6 (2001).

- 62 Shibuya, M., Ito, N. & Claesson-Welsh, L. Structure and function of vascular endothelial growth factor receptor-1 and -2. *Vascular Growth Factors and Angiogenesis* **237**, 59-83 (1999).
- 63 Ferrara, N. & Gerber, H. P. The role of vascular endothelial growth factor in angiogenesis. *Acta Haematologica* **106**, 148-156, doi:10.1159/000046610 (2001).
- 64 Ferrara, N., Gerber, H. P. & LeCouter, J. The biology of VEGF and its receptors. *Nat Med* **9**, 669-676, doi:10.1038/nm0603-669 (2003).
- 65 Matsumoto, T. & Claesson-Welsh, L. VEGF Receptor Signal Transduction. *Science*'s *STKE* **2001**, re21, doi:10.1126/stke.2001.112.re21 (2001).
- 66 Koch, S., Tugues, S., Li, X., Gualandi, L. & Claesson-Welsh, L. Signal transduction by vascular endothelial growth factor receptors. *The Biochemical journal* **437**, 169-183, doi:10.1042/bj20110301 (2011).
- 67 Karlstetter, M. *et al.* Retinal microglia: Just bystander or target for therapy? *Progress in Retinal and Eye Research* **45**, 30-57, doi:10.1016/j.preteyeres.2014.11.004 (2015).
- 68 Santiago, A. R., Boia, R., Aires, I. D., Ambrósio, A. F. & Fernandes, R. Sweet Stress: Coping With Vascular Dysfunction in Diabetic Retinopathy. *Frontiers in Physiology* **9**, doi:10.3389/fphys.2018.00820 (2018).
- 69 Progress in Molecular Biology and Translational Science: Animal Models of Human Disease, Vol 100. *Animal Models of Human Disease* **100**, 1-526 (2011).
- 70 Curcio, C. A., Sloan, K. R., Kalina, R. E. & Hendrickson, A. E. HUMAN PHOTORECEPTOR TOPOGRAPHY. *Journal of Comparative Neurology* **292**, 497-523, doi:10.1002/cne.902920402 (1990).
- 71 Bates, N. M. *et al.* Relationship between the morphology of the foveal avascular zone, retinal structure, and macular circulation in patients with diabetes mellitus. *Scientific Reports* **8**, 5355, doi:10.1038/s41598-018-23604-y (2018).
- 72 Bringmann, A. *et al.* The primate fovea: Structure, function and development. *Progress in Retinal and Eye Research* **66**, 49-84, doi:10.1016/j.preteyeres.2018.03.006 (2018).
- 73 Weale, R. A. WHY DOES HUMAN RETINA POSSESS A FOVEA. *Nature* **212**, 255-&, doi:10.1038/212255a0 (1966).
- 74 Sunderland, M. in *Neuroscience* (eds D. Purves *et al.*) (Sinauer Associates, 2001).
- 75 Euler, T., Haverkamp, S., Schubert, T. & Baden, T. Retinal bipolar cells: elementary building blocks of vision. *Nature Reviews Neuroscience* **15**, 507-519, doi:10.1038/nrn3783 (2014).
- 76 Chapot, C. A., Euler, T. & Schubert, T. How do horizontal cells 'talk' to cone photoreceptors? Different levels of complexity at the cone-horizontal cell synapse. *Journal of Physiology-London* **595**, 5495-5506, doi:10.1113/jp274177 (2017).
- 77 Sorrentino, F. S., Alikabes, M., Salsini, G., Bonifazzi, C. & Perri, P. The importance of glial cells in the homeostasis of the retinal microenvironment and their pivotal role in the course of diabetic

- retinopathy. *Life Sciences* **162**, 54-59, doi:10.1016/j.lfs.2016.08.001 (2016).
- 78 Reichenbach, A. & Bringmann, A. New functions of Muller cells. *Glia* **61**, 651-678, doi:10.1002/glia.22477 (2013).
- 79 Fu, S. *et al.* Muller Glia Are a Major Cellular Source of Survival Signals for Retinal Neurons in Diabetes. *Diabetes* **64**, 3554-3563, doi:10.2337/db15-0180 (2015).
- 80 Newman, E. A. Glial cell regulation of neuronal activity and blood flow in the retina by release of gliotransmitters. *Philosophical transactions of the Royal Society of London. Series B, Biological sciences* **370**, doi:10.1098/rstb.2014.0195 (2015).
- 81 Rubsam, A., Parikh, S. & Fort, P. E. Role of Inflammation in Diabetic Retinopathy. *International Journal of Molecular Sciences* **19**, doi:10.3390/ijms19040942 (2018).
- 82 Stone, J. *et al.* DEVELOPMENT OF RETINAL VASCULATURE IS MEDIATED BY HYPOXIA-INDUCED VASCULAR ENDOTHELIAL GROWTH-FACTOR (VEGF) EXPRESSION BY NEUROGLIA. *Journal of Neuroscience* **15**, 4738-4747 (1995).
- 83 Stone, J. & Dreher, Z. RELATIONSHIP BETWEEN ASTROCYTES, GANGLION-CELLS AND VASCULATURE OF THE RETINA. *Journal of Comparative Neurology* **255**, 35-49, doi:10.1002/cne.902550104 (1987).
- 84 Fernandez-Sanchez, L., Lax, P., Campello, L., Pinilla, I. & Cuenca, N. Astrocytes and Muller Cell Alterations During Retinal Degeneration in a Transgenic Rat Model of Retinitis Pigmentosa. *Frontiers in Cellular Neuroscience* **9**, doi:10.3389/fncel.2015.00484 (2015).
- 85 Vecino, E., Rodriguez, F. D., Ruzafa, N., Pereiro, X. & Sharma, S. C. Glia-neuron interactions in the mammalian retina. *Progress in Retinal and Eye Research* **51**, 1-40, doi:10.1016/j.preteyeres.2015.06.003 (2016).
- 86 Pekny, M., Wilhelmsson, U. & Pekna, M. The dual role of astrocyte activation and reactive gliosis. *Neuroscience Letters* **565**, 30-38, doi:10.1016/j.neulet.2013.12.071 (2014).
- 87 Ransohoff, R. M. & Cardona, A. E. The myeloid cells of the central nervous system parenchyma. *Nature* **468**, 253-262, doi:10.1038/nature09615 (2010).
- 88 Kim, S. U. & de Vellis, J. Microglia in health and disease. *Journal of Neuroscience Research* **81**, 302-313, doi:10.1002/jnr.20562 (2005).
- 89 Ramirez, A. I. *et al.* The Role of Microglia in Retinal Neurodegeneration: Alzheimer's Disease, Parkinson, and Glaucoma. *Frontiers in Aging Neuroscience* **9**, doi:10.3389/fnagi.2017.00214 (2017).
- 90 Okunuki, Y. *et al.* Microglia inhibit photoreceptor cell death and regulate immune cell infiltration in response to retinal detachment. *Proc. Natl. Acad. Sci. U. S. A.* **115**, E6264-E6273, doi:10.1073/pnas.1719601115 (2018).
- 91 Saint-Geniez, M. & D'Amore, P. A. Development and pathology of the hyaloid, choroidal and retinal vasculature. *International Journal of Developmental Biology* **48**, 1045-1058, doi:10.1387/ijdb.041895ms (2004).

- 92 Tan, P., Yu, P., Balaratnasingam, C. & Yu, D. Y. MICROVASCULATURE STRUCTURE AND ORGANISATION IN THE HUMAN RETINA. *Clinical and Experimental Ophthalmology* **38**, 71-71 (2010).
- 93 Kolb, H. in *The Organization of the Retina and Visual System* (eds Helga Kolb, Ralph Nelson, Eduardo Fernandez, & Bryan Jones).
- 94 Archer, D., Gardiner, T. & Stitt, A. in *Retinal Vascular Disease* (eds AM Jousseaume, TW Gardner, B Kirchof, & SJ Ryan) (Springer, Verlag Berlin Heidelberg, 2007).
- 95 Kiel, J. in *The Ocular Circulation* (Morgan & Claypool Life Sciences, San Rafael, CA, 2010).
- 96 Taylor, A. in *Immune Response and The Eye* (eds JY. Niederkorn & HJ. Kaplan) (Karger, 2007).
- 97 Wenkel, H. & Streilein, J. W. Evidence that retinal pigment epithelium functions as an immune-privileged tissue. *Investigative Ophthalmology & Visual Science* **41**, 3467-3473 (2000).
- 98 Campbell, M. & Humphries, P. in *Biology and Regulation of Blood-Tissue Barriers. Advances in Experimental Biology Advances in Experimental Biology* (ed CY. Cheng) (Springer, New York, 2013).
- 99 Biology and Regulation of Blood-Tissue Barriers. *Biology and Regulation of Blood-Tissue Barriers* **763**, 1-361, doi:10.1007/978-1-4614-4711-5 (2013).
- 100 Harhaj, N. S. & Antonetti, D. A. Regulation of tight junctions and loss of barrier function in pathophysiology. *International Journal of Biochemistry & Cell Biology* **36**, 1206-1237, doi:10.1016/j.biocel.2003.08.007 (2004).
- 101 Xu, H. & Chen, M. Diabetic retinopathy and dysregulated innate immunity. *Vision Research* **139**, 39-46, doi:10.1016/j.visres.2017.04.013 (2017).
- 102 Chen, M. & Heping, X. in *Therapies For Retinal Degeneration: Targeting Common Processes* (eds Enrique. De la Rosa & G Thomas Cotter) (RSC Publishing, 2018).
- 103 Forrester, J. V. & Xu, H. P. Good news-bad news: the Yin and Yang of immune privilege in the eye. *Front. Immunol.* **3**, doi:10.3389/fimmu.2012.00338 (2012).
- 104 Griffith, T. S., Brunner, T., Fletcher, S. M., Green, D. R. & Ferguson, T. A. FAS LIGAND-INDUCED APOPTOSIS AS A MECHANISM OF IMMUNE PRIVILEGE. *Science* **270**, 1189-1192, doi:10.1126/science.270.5239.1189 (1995).
- 105 Streilein, J. W. Immunoregulatory mechanisms of the eye. *Progress in Retinal and Eye Research* **18**, 357-370, doi:10.1016/s1350-9462(98)00022-6 (1999).
- 106 Zhou, R. & Caspi, R. R. Ocular immune privilege. *F1000 Biology Reports* (2010).
- 107 Kharroubi, A. T. & Darwish, H. M. Diabetes mellitus: The epidemic of the century. *World journal of diabetes* **6**, 850-867, doi:10.4239/wjd.v6.i6.850 (2015).
- 108 Zimmet, P. Z. & Alberti, K. G. Epidemiology of Diabetes-Status of a Pandemic and Issues Around Metabolic Surgery. *Diabetes Care* **39**, 878-883, doi:10.2337/dc16-0273 (2016).

- 109 Zhou, B. *et al.* Worldwide trends in diabetes since 1980: a pooled analysis of 751 population-based studies with 4#4 million participants. *The Lancet* **387**, 1513-1530, doi:10.1016/S0140-6736(16)00618-8 (2016).
- 110 Laakso, M. & Kuusisto, J. Insulin resistance and hyperglycaemia in cardiovascular disease development. *Nature reviews. Endocrinology* **10**, 293-302, doi:10.1038/nrendo.2014.29 (2014).
- 111 Sena, C. M., Pereira, A. M. & Sea, R. Endothelial dysfunction - a major mediator of diabetic vascular disease. *Biochimica et biophysica acta* **1832**, 2216-2231, doi:10.1016/j.bbadis.2013.08.006 (2013).
- 112 Dei Cas, A. *et al.* Impact of diabetes on epidemiology, treatment, and outcomes of patients with heart failure. *JACC. Heart failure* **3**, 136-145, doi:10.1016/j.jchf.2014.08.004 (2015).
- 113 Yau, J. W. Y. *et al.* Global Prevalence and Major Risk Factors of Diabetic Retinopathy. *Diabetes Care* **35**, 556-564, doi:10.2337/dc11-1909 (2012).
- 114 Orchard, T. J. *et al.* PREVALENCE OF COMPLICATIONS IN IDDM BY SEX AND DURATION - PITTSBURGH EPIDEMIOLOGY OF DIABETES COMPLICATIONS STUDY-II. *Diabetes* **39**, 1116-1124, doi:10.2337/diabetes.39.9.1116 (1990).
- 115 Perez-Perdomo, R., Perez-Cardona, C. M. & Suarez-Perez, E. L. Trends in diabetes mellitus mortality in Puerto Rico: 1980-1997. *P R Health Sci J* **20**, 19-24 (2001).
- 116 Kempen, J. H. *et al.* The prevalence of diabetic retinopathy among adults in the United States. *Arch Ophthalmol* **122**, 552-563, doi:10.1001/archophth.122.4.552 (2004).
- 117 Zheng, Y., He, M. & Congdon, N. The worldwide epidemic of diabetic retinopathy. *Indian J Ophthalmol* **60**, 428-431, doi:10.4103/0301-4738.100542 (2012).
- 118 Hernandez, C., Dal Monte, M., Simo, R. & Casini, G. Neuroprotection as a Therapeutic Target for Diabetic Retinopathy. *Journal of Diabetes Research*, doi:10.1155/2016/9508541 (2016).
- 119 Wang, N. L. Neurodegeneration in Diabetic Retinopathy: Current Concepts and Therapeutic Implications. *Chinese Medical Journal* **129**, 3001-3003, doi:10.4103/0366-6999.195478 (2016).
- 120 Cunha-Vaz, J., Bernades, R. & Lobo, C. in *Visual Dysfunction in Diabetes: The Science of Patient Impairment and Care Ophthalmology Research* (eds J. Tombran-Tink, C.J. Barnstable, & T.W. Gardner) 53-68 (Springer).
- 121 van Dijk, H. W. *et al.* Selective Loss of Inner Retinal Layer Thickness in Type 1 Diabetic Patients with Minimal Diabetic Retinopathy. *Investigative Ophthalmology & Visual Science* **50**, 3404-3409, doi:10.1167/iovs.08-3143 (2009).
- 122 de Faria, J. M. L., Russ, H. & Costa, V. P. Retinal nerve fibre layer loss in patients with type 1 diabetes mellitus without retinopathy. *British Journal of Ophthalmology* **86**, 725-728 (2002).
- 123 van Dijk, H. W. *et al.* Decreased Retinal Ganglion Cell Layer Thickness in Patients with Type 1 Diabetes. *Investigative Ophthalmology & Visual Science* **51**, 3660-3665, doi:10.1167/iovs.09-5041 (2010).

- 124 van Dijk, H. W. *et al.* Association of visual function and ganglion cell layer thickness in patients with diabetes mellitus type 1 and no or minimal diabetic retinopathy. *Vision Research* **51**, 224-228, doi:10.1016/j.visres.2010.08.024 (2011).
- 125 Antonetti, D. A. *et al.* Diabetic retinopathy - Seeing beyond glucose-induced microvascular disease. *Diabetes* **55**, 2401-2411, doi:10.2337/db05-1635 (2006).
- 126 Sundstrom, J. M. *et al.* Proteomic Analysis of Early Diabetic Retinopathy Reveals Mediators of Neurodegenerative Brain Diseases. *Investigative Ophthalmology & Visual Science* **59**, 2264-2274, doi:10.1167/iovs.17-23678 (2018).
- 127 Kern, T. S. & Barber, A. J. Retinal ganglion cells in diabetes. *Journal of Physiology-London* **586**, 4401-4408, doi:10.1113/jphysiol.2008.156695 (2008).
- 128 Brown, G. C. & Vilalta, A. How microglia kill neurons. *Brain Research* **1628**, 288-297, doi:10.1016/j.brainres.2015.08.031 (2015).
- 129 Lieth, E., Gardner, T. W., Barber, A. J., Antonetti, D. A. & Penn State Retina Res, G. Retinal neurodegeneration: early pathology in diabetes. *Clinical and Experimental Ophthalmology* **28**, 3-8, doi:10.1046/j.1442-9071.2000.00222.x (2000).
- 130 Sims, D. E. RECENT ADVANCES IN PERICYTE BIOLOGY - IMPLICATIONS FOR HEALTH AND DISEASE. *Canadian Journal of Cardiology* **7**, 431-443 (1991).
- 131 Eshaq, R. S., Aldalati, A. M. Z., Alexander, J. S. & Harris, N. R. Diabetic retinopathy: Breaking the barrier. *Pathophysiology : the official journal of the International Society for Pathophysiology*, doi:10.1016/j.pathophys.2017.07.001 (2017).
- 132 Santos, G. S. P., Prazeres, P., Mintz, A. & Birbrair, A. Role of pericytes in the retina. *Eye* **32**, 483-486, doi:10.1038/eye.2017.220 (2018).
- 133 Pfister, F., Lin, J. H. & Hammes, H. P. Pericyte Loss in the Diabetic Retina. *Experimental Approaches to Diabetic Retinopathy* **20**, 61-78 (2010).
- 134 Hirschi, K. K. & Damore, P. A. Pericytes in the microvasculature. *Cardiovascular Research* **32**, 687-698, doi:10.1016/s0008-6363(96)00063-6 (1996).
- 135 Watkins, P. J. ABC of diabetes - Retinopathy. *British Medical Journal* **326**, 924-926, doi:10.1136/bmj.326.7395.924 (2003).
- 136 Wong, T. Y., Cheung, C. M. G., Larsen, M., Sharma, S. & Simo, R. Diabetic retinopathy. *Nature Reviews Disease Primers* **2**, doi:10.1038/nrdp.2016.12 (2016).
- 137 Cai, J. & Boulton, M. The pathogenesis of diabetic retinopathy: old concepts and new questions. *Eye* **16**, 242-260, doi:10.1038/sj/eye/6700133 (2002).
- 138 Roy, S., Maiello, M. & Lorenzi, M. INCREASED EXPRESSION OF BASEMENT-MEMBRANE COLLAGEN IN HUMAN DIABETIC-RETINOPATHY. *Journal of Clinical Investigation* **93**, 438-442, doi:10.1172/jci116979 (1994).

- 139 Roy, S., Ha, J., Trudeau, K. & Beglova, E. Vascular Basement
Membrane Thickening in Diabetic Retinopathy. *Current Eye Research*
35, 1045-1056, doi:10.3109/02713683.2010.514659 (2010).
- 140 Mesquita, J. *et al.* Vascular endothelial growth factors and placenta
growth factor in retinal vasculopathies: Current research and future
perspectives. *Cytokine & Growth Factor Reviews* **39**, 102-115,
doi:10.1016/j.cytogfr.2017.11.005 (2018).
- 141 Gariano, R. F. & Gardner, T. W. Retinal angiogenesis in development
and disease. *Nature* **438**, 960-966, doi:10.1038/nature04482 (2005).
- 142 Dreyfuss, J. L., Giordano, R. J. & Regatieri, C. V. Ocular Angiogenesis.
Journal of Ophthalmology, doi:10.1155/2015/892043 (2015).
- 143 Lee, R., Wong, T. Y. & Sabanayagam, C. Epidemiology of diabetic
retinopathy, diabetic macular edema and related vision loss. *Eye and
Vision* **2**, doi:10.1186/s40662-015-0026-2 (2015).
- 144 Zhu, C. H. *et al.* Effects of intensive control of blood glucose and blood
pressure on microvascular complications in patients with type II diabetes
mellitus. *International Journal of Ophthalmology* **6**, 141-145,
doi:10.3980/j.issn.2222-3959.2013.02.06 (2013).
- 145 Shamoon, H. *et al.* THE EFFECT OF INTENSIVE TREATMENT OF
DIABETES ON THE DEVELOPMENT AND PROGRESSION OF LONG-
TERM COMPLICATIONS IN INSULIN-DEPENDENT DIABETES-
MELLITUS. *New England Journal of Medicine* **329**, 977-986 (1993).
- 146 Grp, U. K. P. D. Effect of intensive blood glucose control with metformin
on complications in overweight patients with type 2 diabetes (UKPDS 34)
(vol 352, pg 854, 1998). *Lancet* **352**, 1558-1558 (1998).
- 147 Aiello, L. P. & Grp, D. E. R. Diabetic Retinopathy and Other Ocular
Findings in the Diabetes Control and Complications Trial/Epidemiology of
Diabetes Interventions and Complications Study. *Diabetes Care* **37**, 17-
23, doi:10.2337/dc13-2251 (2014).
- 148 Gillow, J. T., Gibson, J. M. & Dodson, P. M. Hypertension and diabetic
retinopathy - what's the story? *British Journal of Ophthalmology* **83**,
1083-1087, doi:10.1136/bjo.83.9.1083 (1999).
- 149 PHOTO-COAGULATION TREATMENT OF PROLIFERATIVE
DIABETIC-RETINOPATHY - CLINICAL-APPLICATION OF DIABETIC-
RETINOPATHY STUDY (DRS) FINDINGS, DRS REPORT NUMBER-8.
Ophthalmology **88**, 583-600 (1981).
- 150 Patz, A. *et al.* PHOTOCOAGULATION FOR DIABETIC MACULAR
EDEMA - EARLY TREATMENT DIABETIC-RETINOPATHY STUDY
REPORT 1. EARLY TREATMENT DIABETIC RETINOPATHY STUDY
RESEARCH GROUP. *Archives of Ophthalmology* **103**, 1796-1806,
doi:10.1001/archoph.1985.01050120030015 (1985).
- 151 Bressler, N. M., Beck, R. W. & Ferris, F. L. Panretinal Photocoagulation
for Proliferative Diabetic Retinopathy. *New England Journal of Medicine*
365, 1520-1526, doi:10.1056/NEJMct0908432 (2011).
- 152 Fong, D. S., Girach, A. & Boney, A. Visual side effects of successful
scatter laser photocoagulation surgery for proliferative diabetic
retinopathy. *Retina-the Journal of Retinal and Vitreous Diseases* **27**, 816-
824, doi:10.1097/IAE.0b013e318042d32c (2007).

- 153 Liang, J. C. & Huamonte, F. U. REDUCTION OF IMMEDIATE COMPLICATIONS AFTER PANRETINAL PHOTOCOAGULATION. *Retina-the Journal of Retinal and Vitreous Diseases* **4**, 166-170, doi:10.1097/00006982-198400430-00007 (1984).
- 154 Smiddy, W. E. & Flynn, H. W. Vitrectomy in the management of diabetic retinopathy. *Survey of Ophthalmology* **43**, 491-507, doi:10.1016/s0039-6257(99)00036-3 (1999).
- 155 Cheung, N., Wong, I. Y. & Wong, T. Y. Ocular Anti-VEGF Therapy for Diabetic Retinopathy: Overview of Clinical Efficacy and Evolving Applications. *Diabetes Care* **37**, 900-905, doi:10.2337/dc13-1990 (2014).
- 156 Kim, L. A. & D'Amore, P. A. A Brief History of Anti-VEGF for the Treatment of Ocular Angiogenesis. *American Journal of Pathology* **181**, 376-379, doi:10.1016/j.ajpath.2012.06.006 (2012).
- 157 Ferrara, N., Hillan, K. J. & Novotny, W. Bevacizumab (Avastin), a humanized anti-VEGF monoclonal antibody for cancer therapy. *Biochemical and Biophysical Research Communications* **333**, 328-335, doi:10.1016/j.bbrc.2005.05.132 (2005).
- 158 Parikh, R. *et al.* Trends of Anti-Vascular Endothelial Growth Factor Use in Ophthalmology Among Privately Insured and Medicare Advantage Patients. *Ophthalmology* **124**, 352-358, doi:10.1016/j.ophtha.2016.10.036 (2017).
- 159 Cabral, T. *et al.* Bevacizumab Injection in Patients with Neovascular Age-Related Macular Degeneration Increases Angiogenic Biomarkers. *Ophthalmol Retina* **2**, 31-37, doi:10.1016/j.oret.2017.04.004 (2018).
- 160 McCloskey, M. *et al.* Anti-VEGF antibody leads to later atypical intravitreal neovascularization and activation of angiogenic pathways in a rat model of retinopathy of prematurity. *Invest Ophthalmol Vis Sci* **54**, 2020-2026, doi:10.1167/iovs.13-11625 (2013).
- 161 Beazley-Long, N. *et al.* VEGF-A(165)b Is an Endogenous Neuroprotective Splice Isoform of Vascular Endothelial Growth Factor A in Vivo and in Vitro. *Am J Pathol* **183**, 918-929, doi:10.1016/j.ajpath.2013.05.031 (2013).
- 162 Hoeben, A. *et al.* Vascular endothelial growth factor and angiogenesis. *Pharmacological Reviews* **56**, 549-580, doi:10.1124/pr.56.4.3 (2004).
- 163 Avery, R. L. *et al.* Systemic Pharmacokinetics and Pharmacodynamics of Intravitreal Aflibercept, Bevacizumab, and Ranibizumab. *Retina* **37**, 1847-1858, doi:10.1097/IAE.0000000000001493 (2017).
- 164 Falavarjani, K. G. & Nguyen, Q. D. Adverse events and complications associated with intravitreal injection of anti-VEGF agents: a review of literature. *Eye (Lond)* **27**, 787-794, doi:10.1038/eye.2013.107 (2013).
- 165 Shima, C. *et al.* Complications in patients after intravitreal injection of bevacizumab. *Acta Ophthalmol* **86**, 372-376, doi:10.1111/j.1600-0420.2007.01067.x (2008).
- 166 Barnum, S. R. Complement: A primer for the coming therapeutic revolution. *Pharmacology & Therapeutics* **172**, 63-72, doi:10.1016/j.pharmthera.2016.11.014 (2017).

- 167 Merle, N. S., Church, S. E., Fremeaux-Bacchi, V. & Roumenina, L. T. Complement System Part I – Molecular Mechanisms of Activation and Regulation. *Front. Immunol.* **6**, doi:10.3389/fimmu.2015.00262 (2015).
- 168 Dunkelberger, J. R. & Song, W.-C. Complement and its role in innate and adaptive immune responses. *Cell Research* **20**, 34-50, doi:10.1038/cr.2009.139 (2010).
- 169 Walport, M. J. Advances in immunology: Complement (First of two parts). *New England Journal of Medicine* **344**, 1058-1066 (2001).
- 170 Klos, A. *et al.* The role of the anaphylatoxins in health and disease. *Molecular immunology* **46**, 2753-2766, doi:10.1016/j.molimm.2009.04.027 (2009).
- 171 Flyvbjerg, A. Diabetic angiopathy, the complement system and the tumor necrosis factor superfamily. *Nature Reviews Endocrinology* **6**, 94-101, doi:10.1038/nrendo.2009.266 (2010).
- 172 Turner, M. W. The role of mannose-binding lectin in health and disease. *Molecular Immunology* **40**, 423-429, doi:[https://doi.org/10.1016/S0161-5890\(03\)00155-X](https://doi.org/10.1016/S0161-5890(03)00155-X) (2003).
- 173 Gál, P., Barna, L., Kocsis, A. & Závodszy, P. Serine proteases of the classical and lectin pathways: Similarities and differences. *Immunobiology* **212**, 267-277, doi:<https://doi.org/10.1016/j.imbio.2006.11.002> (2007).
- 174 Ricklin, D., Reis, E. S. & Lambris, J. D. Complement in disease: a defence system turning offensive. *Nature Reviews Nephrology* **12**, 383-401, doi:10.1038/nrneph.2016.70 (2016).
- 175 Morgan, B. P. The membrane attack complex as an inflammatory trigger. *Immunobiology* **221**, 747-751, doi:<https://doi.org/10.1016/j.imbio.2015.04.006> (2016).
- 176 Esser, A. F. The membrane attack complex of complement. Assembly, structure and cytotoxic activity. *Toxicology* **87**, 229-247, doi:[https://doi.org/10.1016/0300-483X\(94\)90253-4](https://doi.org/10.1016/0300-483X(94)90253-4) (1994).
- 177 Ricklin, D., Hajishengallis, G., Yang, K. & Lambris, J. D. Complement: a key system for immune surveillance and homeostasis. *Nature Immunology* **11**, 785-797, doi:10.1038/ni.1923 (2010).
- 178 Actor, J. K. in *Introductory Immunology* (ed Jeffrey K. Actor) 16-27 (Academic Press, 2014).
- 179 Liszewski, M. K., Farries, T. C., Lublin, D. M., Rooney, I. A. & Atkinson, J. P. Control of the complement system. *Advances in immunology* **61**, 201-283, doi:10.1016/s0065-2776(08)60868-8 (1996).
- 180 Sim, R. B., Day, A. J., Moffatt, B. E. & Fontaine, M. in *Methods in Enzymology* Vol. 223 13-35 (Academic Press, 1993).
- 181 Changeux, J. P., Devillers-Thiéry, A., Galzi, J. L. & Bertrand, D. New mutants to explore nicotinic receptor functions. *Trends Pharmacol Sci* **13**, 299-301, doi:10.1016/0165-6147(92)90094-m (1992).
- 182 Ricklin, D. & Lambris, J. D. Complement in Immune and Inflammatory Disorders: Pathophysiological Mechanisms. *Journal of Immunology* **190**, 3831-3838, doi:10.4049/jimmunol.1203487 (2013).

- 183 Holers, V. M. The complement system as a therapeutic target in autoimmunity. *Clinical immunology (Orlando, Fla.)* **107**, 140-151, doi:10.1016/s1521-6616(03)00034-2 (2003).
- 184 Mohlin, C., Sandholm, K., Kvanta, A., Ekdahl, K. N. & Johansson, K. A model to study complement involvement in experimental retinal degeneration. *Uppsala Journal of Medical Sciences* **123**, 28-42, doi:10.1080/03009734.2018.1431744 (2018).
- 185 Wong, W. L. *et al.* Global prevalence of age-related macular degeneration and disease burden projection for 2020 and 2040: a systematic review and meta-analysis. *Lancet Global Health* **2**, E106-E116, doi:10.1016/s2214-109x(13)70145-1 (2014).
- 186 Maugeri, A., Barchitta, M., Mazzone, M. G., Giuliano, F. & Agodi, A. Complement System and Age-Related Macular Degeneration: Implications of Gene-Environment Interaction for Preventive and Personalized Medicine. *BioMed research international* **2018**, 7532507-7532507, doi:10.1155/2018/7532507 (2018).
- 187 Hageman, G. S. *et al.* An Integrated Hypothesis That Considers Drusen as Biomarkers of Immune-Mediated Processes at the RPE-Bruch's Membrane Interface in Aging and Age-Related Macular Degeneration. *Progress in Retinal and Eye Research* **20**, 705-732, doi:[https://doi.org/10.1016/S1350-9462\(01\)00010-6](https://doi.org/10.1016/S1350-9462(01)00010-6) (2001).
- 188 Baudouin, C. *et al.* Immunohistological study of subretinal membranes in age-related macular degeneration. *Japanese journal of ophthalmology* **36**, 443-451 (1992).
- 189 van der Schaft, T. L., Mooy, C. M., de Bruijn, W. C. & de Jong, P. T. Early stages of age-related macular degeneration: an immunofluorescence and electron microscopy study. *The British journal of ophthalmology* **77**, 657-661, doi:10.1136/bjo.77.10.657 (1993).
- 190 Sivaprasad, S. *et al.* Estimation of Systemic Complement C3 Activity in Age-Related Macular Degeneration. *Archives of Ophthalmology* **125**, 515-519, doi:10.1001/archophth.125.4.515 (2007).
- 191 Scholl, H. P. *et al.* Systemic complement activation in age-related macular degeneration. *PloS one* **3**, e2593, doi:10.1371/journal.pone.0002593 (2008).
- 192 Reynolds, R. *et al.* Plasma complement components and activation fragments: associations with age-related macular degeneration genotypes and phenotypes. *Invest Ophthalmol Vis Sci* **50**, 5818-5827, doi:10.1167/iovs.09-3928 (2009).
- 193 Machalińska, A. *et al.* Elevated Plasma Levels of C3a Complement Compound in the Exudative Form of Age-Related Macular Degeneration. *Ophthalmic Research* **42**, 54-59, doi:10.1159/000219686 (2009).
- 194 Edwards, A. O. *et al.* Complement Factor H Polymorphism and Age-Related Macular Degeneration. *Science* **308**, 421, doi:10.1126/science.1110189 (2005).
- 195 Hageman, G. S. *et al.* A common haplotype in the complement regulatory gene factor H (CFH) predisposes individuals to age-related macular degeneration. *Proc. Natl. Acad. Sci. U. S. A.* **102**, 7227, doi:10.1073/pnas.0501536102 (2005).

- 196 Haines, J. L. *et al.* Complement Factor H Variant Increases the Risk of Age-Related Macular Degeneration. *Science* **308**, 419, doi:10.1126/science.1110359 (2005).
- 197 Klein, R. J. *et al.* Complement Factor H Polymorphism in Age-Related Macular Degeneration. *Science* **308**, 385, doi:10.1126/science.1109557 (2005).
- 198 Gold, B. *et al.* Variation in factor B (BF) and complement component 2 (C2) genes is associated with age-related macular degeneration. *Nature genetics* **38**, 458-462, doi:10.1038/ng1750 (2006).
- 199 Spencer, K. L. *et al.* Protective effect of complement factor B and complement component 2 variants in age-related macular degeneration. *Hum Mol Genet* **16**, 1986-1992, doi:10.1093/hmg/ddm146 (2007).
- 200 Montes, T., Tortajada, A., Morgan, B. P., Rodríguez de Córdoba, S. & Harris, C. L. Functional basis of protection against age-related macular degeneration conferred by a common polymorphism in complement factor B. *Proc Natl Acad Sci U S A* **106**, 4366-4371, doi:10.1073/pnas.0812584106 (2009).
- 201 Chen, M., Forrester, J. V. & Xu, H. Synthesis of complement factor H by retinal pigment epithelial cells is down-regulated by oxidized photoreceptor outer segments. *Experimental Eye Research* **84**, 635-645, doi:<https://doi.org/10.1016/j.exer.2006.11.015> (2007).
- 202 Chen, M., Muckersie, E., Robertson, M., Forrester, J. V. & Xu, H. Up-regulation of complement factor B in retinal pigment epithelial cells is accompanied by complement activation in the aged retina. *Exp Eye Res* **87**, 543-550, doi:10.1016/j.exer.2008.09.005 (2008).
- 203 Williams, J. A. E. *et al.* Regulation of C3 Activation by the Alternative Complement Pathway in the Mouse Retina. *PloS one* **11**, e0161898 (2016). <<http://europepmc.org/abstract/MED/27564415>
<https://doi.org/10.1371/journal.pone.0161898>
<https://europepmc.org/articles/PMC5001704>
<https://europepmc.org/articles/PMC5001704?pdf=render>>.
- 204 Bora, N. S. *et al.* Complement activation via alternative pathway is critical in the development of laser-induced choroidal neovascularization: role of factor B and factor H. *Journal of immunology (Baltimore, Md. : 1950)* **177**, 1872-1878, doi:10.4049/jimmunol.177.3.1872 (2006).
- 205 Kleinman, M. E. *et al.* Sequence- and target-independent angiogenesis suppression by siRNA via TLR3. *Nature* **452**, 591-597, doi:10.1038/nature06765 (2008).
- 206 Rohrer, B. *et al.* The alternative pathway is required, but not alone sufficient, for retinal pathology in mouse laser-induced choroidal neovascularization. *Mol Immunol* **48**, e1-8, doi:10.1016/j.molimm.2010.12.016 (2011).
- 207 Schnabolk, G. *et al.* Local Production of the Alternative Pathway Component Factor B Is Sufficient to Promote Laser-Induced Choroidal Neovascularization. *Investigative Ophthalmology & Visual Science* **56**, 1850-1863, doi:10.1167/iovs.14-15910 (2015).

- 208 Wang, W. & Lo, A. C. Y. Diabetic Retinopathy: Pathophysiology and Treatments. *International journal of molecular sciences* **19**, 1816, doi:10.3390/ijms19061816 (2018).
- 209 Das, A. & Byrd, J. in *Pathobiology of Human Disease* (eds Linda M. McManus & Richard N. Mitchell) 2137-2161 (Academic Press, 2014).
- 210 Al-Shabrawey, M. *et al.* Targeting Neovascularization in Ischemic Retinopathy: Recent Advances. *Expert Rev Ophthalmol* **8**, 267-286, doi:10.1586/eop.13.17 (2013).
- 211 Frank, R. N. Diabetic Retinopathy. *New England Journal of Medicine* **350**, 48-58, doi:10.1056/NEJMra021678 (2004).
- 212 Shahulhameed, S. *et al.* A Systematic Investigation on Complement Pathway Activation in Diabetic Retinopathy. *Front. Immunol.* **11**, doi:10.3389/fimmu.2020.00154 (2020).
- 213 Chen, M. & Xu, H. Parainflammation, chronic inflammation, and age-related macular degeneration. *Journal of Leukocyte Biology* **98**, 713-725, doi:10.1189/jlb.3RI0615-239R (2015).
- 214 Xu, H. P. & Chen, M. Targeting the complement system for the management of retinal inflammatory and degenerative diseases. *European Journal of Pharmacology* **787**, 94-104, doi:10.1016/j.ejphar.2016.03.001 (2016).
- 215 Silverman, S. M. & Wong, W. T. in *Retinal Degenerative Diseases*. (eds Catherine Bowes Rickman *et al.*) 33-37 (Springer International Publishing).
- 216 Wang, J. *et al.* Association of CFH and CFB gene polymorphisms with retinopathy in type 2 diabetic patients. *Mediators Inflamm* **2013**, 748435-748435, doi:10.1155/2013/748435 (2013).
- 217 Ghosh, P., Sahoo, R., Vaidya, A., Chorev, M. & Halperin, J. A. Role of Complement and Complement Regulatory Proteins in the Complications of Diabetes. *Endocrine Reviews* **36**, 272-288, doi:10.1210/er.2014-1099 (2015).
- 218 Qin, X. *et al.* Glycation inactivation of the complement regulatory protein CD59: a possible role in the pathogenesis of the vascular complications of human diabetes. *Diabetes* **53**, 2653-2661, doi:10.2337/diabetes.53.10.2653 (2004).
- 219 Zhang, A., Gerhardinger, C. & Lorenzi, M. Early complement activation and decreased levels of glycosylphosphatidylinositol-anchored complement inhibitors in human and experimental diabetic retinopathy. *Diabetes* **51**, 3499-3504 (2002).
- 220 Chen, G. Z. *et al.* Proteomic analysis identifies protein targets responsible for decapeptide sensitivity in tumor cells. *Journal of Proteome Research* **7**, 2733-2742, doi:10.1021/pr7008753 (2008).
- 221 Kim, S. J. *et al.* Differential expression of vitreous proteins in proliferative diabetic retinopathy. *Current Eye Research* **31**, 231-240, doi:10.1080/02713680600557030 (2006).
- 222 Koyama, R., Nakanishi, T., Ikeda, T. & Shimizu, A. Catalogue of soluble proteins in human vitreous humor by one-dimensional sodium dodecyl sulfate-polyacrylamide gel electrophoresis and electrospray ionization mass spectrometry including seven angiogenesis-regulating factors.

- Journal of Chromatography B-Analytical Technologies in the Biomedical and Life Sciences* **792**, 5-21, doi:10.1016/s1570-0232(03)00133-8 (2003).
- 223 Nakanishi, T., Koyama, R., Ikeda, T. & Shimizu, A. Catalogue of soluble proteins in the human vitreous humor: comparison between diabetic retinopathy and macular hole. *Journal of Chromatography B-Analytical Technologies in the Biomedical and Life Sciences* **776**, 89-100, doi:10.1016/s1570-0232(02)00078-8 (2002).
- 224 Yamane, K. *et al.* Proteome analysis of human vitreous proteins. *Molecular & Cellular Proteomics* **2**, 1177-1187, doi:10.1074/mcp.M300038-MCP200 (2003).
- 225 Wang, H., Feng, L., Hu, J. W., Xie, C. L. & Wang, F. Differentiating vitreous proteomes in proliferative diabetic retinopathy using high-performance liquid chromatography coupled to tandem mass spectrometry. *Exp Eye Res* **108**, 110-119, doi:10.1016/j.exer.2012.11.023 (2013).
- 226 Garcia-Ramirez, M. *et al.* Proteomic analysis of human vitreous fluid by fluorescence-based difference gel electrophoresis (DIGE): a new strategy for identifying potential candidates in the pathogenesis of proliferative diabetic retinopathy. *Diabetologia* **50**, 1294-1303, doi:10.1007/s00125-007-0627-y (2007).
- 227 Simó-Servat, O., Hernández, C. & Simó, R. Usefulness of the vitreous fluid analysis in the translational research of diabetic retinopathy. *Mediators Inflamm* **2012**, 872978-872978, doi:10.1155/2012/872978 (2012).
- 228 Gerl, V. B. *et al.* Extensive deposits of complement C3d and C5b-9 in the choriocapillaris of eyes of patients with diabetic retinopathy. *Investigative Ophthalmology & Visual Science* **43**, 1104-1108 (2002).
- 229 Scott, A. & Fruttiger, M. Oxygen-induced retinopathy: a model for vascular pathology in the retina. *Eye* **24**, 416-421, doi:10.1038/eye.2009.306 (2010).
- 230 Stahl, A. *et al.* The Mouse Retina as an Angiogenesis Model. *Investigative Ophthalmology & Visual Science* **51**, 2813-2826, doi:10.1167/iovs.10-5176 (2010).
- 231 Sweigard, J. H. *et al.* The alternative complement pathway regulates pathological angiogenesis in the retina. *Faseb Journal* **28**, 3171-3182, doi:10.1096/fj.14-251041 (2014).
- 232 Das, A., Stroud, S., Mehta, A. & Rangasamy, S. New treatments for diabetic retinopathy. *Diabetes Obesity & Metabolism* **17**, 219-230, doi:10.1111/dom.12384 (2015).
- 233 Lock, J. H. & Fong, K. C. An update on retinal laser therapy. *Clin Exp Optom* **94**, 43-51, doi:10.1111/j.1444-0938.2010.00529.x (2011).
- 234 Ciulla, T. A., Amador, A. G. & Zinman, B. Diabetic retinopathy and diabetic macular edema: pathophysiology, screening, and novel therapies. *Diabetes Care* **26**, 2653-2664 (2003).
- 235 Chew, E. Y. *et al.* The long-term effects of laser photocoagulation treatment in patients with diabetic retinopathy - The early treatment

- diabetic retinopathy follow-up study. *Ophthalmology* **110**, 1683-1689, doi:10.1016/s0161-6420(03)00579-7 (2003).
- 236 Wong, T. Y., Cheung, C. M., Larsen, M., Sharma, S. & Simo, R. Diabetic retinopathy. *Nat Rev Dis Primers* **2**, 16012, doi:10.1038/nrdp.2016.12 (2016).
- 237 Kurihara, T., Westenskow, P. D., Bravo, S., Aguilar, E. & Friedlander, M. Targeted deletion of Vegfa in adult mice induces vision loss. *J Clin Invest* **122**, 4213-4217, doi:10.1172/JCI65157 (2012).
- 238 Park, H. Y., Kim, J. H. & Park, C. K. Neuronal cell death in the inner retina and the influence of vascular endothelial growth factor inhibition in a diabetic rat model. *Am J Pathol* **184**, 1752-1762, doi:10.1016/j.ajpath.2014.02.016 (2014).
- 239 Mathebula, S. D. Biochemical changes in diabetic retinopathy triggered by hyperglycaemia: A review. *African Vision and Eye Health Journal* **77**, doi:10.4102/aveh.v77i1.439 (2018).
- 240 de Cordoba, S. R., Tortajada, A., Harris, C. L. & Morgan, B. P. Complement dysregulation and disease: from genes and proteins to diagnostics and drugs. *Immunobiology* **217**, 1034-1046, doi:10.1016/j.imbio.2012.07.021 (2012).
- 241 Graham, M. L., Janecek, J. L., Kittredge, J. A., Hering, B. J. & Schuurman, H.-J. The streptozotocin-induced diabetic nude mouse model: differences between animals from different sources. *Comparative medicine* **61**, 356-360 (2011).
- 242 Connor, K. M. *et al.* Quantification of oxygen-induced retinopathy in the mouse: a model of vessel loss, vessel regrowth and pathological angiogenesis. *Nat Protoc* **4**, 1565-1573, doi:10.1038/nprot.2009.187 (2009).
- 243 Song, W. *et al.* The fetal mouse metatarsal bone explant as a model of angiogenesis. *Nature Protocols* **10**, 1459-1473, doi:10.1038/nprot.2015.097 (2015).
- 244 Smith, L. E. H. *et al.* OXYGEN-INDUCED RETINOPATHY IN THE MOUSE. *Investigative Ophthalmology & Visual Science* **35**, 101-111 (1994).
- 245 Safi, S. Z., Qvist, R., Kumar, S., Batumalaie, K. & Bin Ismail, I. S. Molecular Mechanisms of Diabetic Retinopathy, General Preventive Strategies, and Novel Therapeutic Targets. *Biomed Research International*, doi:10.1155/2014/801269 (2014).
- 246 Carmeliet, P. Angiogenesis in life, disease and medicine. *Nature* **438**, 932-936, doi:10.1038/nature04478 (2005).
- 247 Arroyo, A. G. & Iruela-Arispe, M. L. Extracellular matrix, inflammation, and the angiogenic response. *Cardiovascular research* **86**, 226-235, doi:10.1093/cvr/cvq049 (2010).
- 248 Al-Soudi, A., Kaaij, M. H. & Tas, S. W. Endothelial cells: From innocent bystanders to active participants in immune responses. *Autoimmunity reviews* **16**, 951-962, doi:10.1016/j.autrev.2017.07.008 (2017).
- 249 Jeon, H. *et al.* Activation of the complement system in an osteosarcoma cell line promotes angiogenesis through enhanced production of growth factors. *Scientific Reports* **8**, doi:10.1038/s41598-018-23851-z (2018).

- 250 Nozaki, M. *et al.* Drusen complement components C3a and C5a promote choroidal neovascularization. *Proc Natl Acad Sci U S A* **103**, 2328-2333, doi:10.1073/pnas.0408835103 (2006).
- 251 Bora, P. S. *et al.* Role of Complement and Complement Membrane Attack Complex in Laser-Induced Choroidal Neovascularization. *The Journal of Immunology* **174**, 491-497, doi:10.4049/jimmunol.174.1.491 (2005).
- 252 Wang, X. *et al.* Complement factor B knockdown by short hairpin RNA inhibits laser-induced choroidal neovascularization in rats. *International Journal of Ophthalmology* **13**, 382-389 (2020).
- 253 Pauly, D. *et al.* Cell-Type-Specific Complement Expression in the Healthy and Diseased Retina. *Cell Rep* **29**, 2835-2848.e2834, doi:10.1016/j.celrep.2019.10.084 (2019).
- 254 Bora, P. S. *et al.* Role of complement and complement membrane attack complex in laser-induced choroidal neovascularization. *Journal of Immunology* **174**, 491-497, doi:10.4049/jimmunol.174.1.491 (2005).
- 255 Montes, T., Tortajada, A., Morgan, B. P., de Cordoba, S. R. & Harris, C. L. Functional basis of protection against age-related macular degeneration conferred by a common polymorphism in complement factor B. *Proc. Natl. Acad. Sci. U. S. A.* **106**, 4366-4371, doi:10.1073/pnas.0812584106 (2009).
- 256 Luo, C., Chen, M. & Xu, H. P. Complement gene expression and regulation in mouse retina and retinal pigment epithelium/choroid. *Molecular Vision* **17**, 1588-1597 (2011).
- 257 Cunha-Vaz, J. G. The blood–retinal barriers system. Basic concepts and clinical evaluation. *Experimental Eye Research* **78**, 715-721, doi:[https://doi.org/10.1016/S0014-4835\(03\)00213-6](https://doi.org/10.1016/S0014-4835(03)00213-6) (2004).
- 258 Chrzanowska, M., Modrzejewska, A. & Modrzejewska, M. New insight into the role of the complement in the most common types of retinopathy-current literature review. *International Journal of Ophthalmology* **11**, 1856-1864, doi:10.18240/ijo.2018.11.19 (2018).
- 259 Walia, S., Clermont, A. C., Gao, B.-B., Aiello, L. P. & Feener, E. P. Vitreous proteomics and diabetic retinopathy. *Semin Ophthalmol* **25**, 289-294, doi:10.3109/08820538.2010.518912 (2010).
- 260 Nawaz, I. M. *et al.* Human vitreous in proliferative diabetic retinopathy: Characterization and translational implications. *Progress in Retinal and Eye Research* **72**, 100756, doi:<https://doi.org/10.1016/j.preteyeres.2019.03.002> (2019).
- 261 Balaiya, S., Zhou, Z. & Chalam, K. V. Characterization of Vitreous and Aqueous Proteome in Humans With Proliferative Diabetic Retinopathy and Its Clinical Correlation. *Proteomics Insights* **8**, 1178641816686078-1178641816686078, doi:10.1177/1178641816686078 (2017).
- 262 Sun, C. *et al.* Angiogenic and inflammatory biomarker levels in aqueous humor and vitreous of neovascular glaucoma and proliferative diabetic retinopathy. *International Ophthalmology* **40**, 467-475, doi:10.1007/s10792-019-01207-4 (2020).

- 263 Noma, H. *et al.* Aqueous humour levels of cytokines are correlated to vitreous levels and severity of macular oedema in branch retinal vein occlusion. *Eye* **22**, 42-48, doi:10.1038/sj.eye.6702498 (2008).
- 264 Feng, J. & Jiang, Y. Differences in Aqueous Concentrations of Various Cytokines in Macular Edema Due to Non-proliferative and Proliferative Diabetic Retinopathy. *Investigative Ophthalmology & Visual Science* **54**, 2425-2425 (2013).
- 265 Funatsu, H. *et al.* Aqueous humor levels of cytokines are related to vitreous levels and progression of diabetic retinopathy in diabetic patients. *Graefe's archive for clinical and experimental ophthalmology = Albrecht von Graefes Archiv fur klinische und experimentelle Ophthalmologie* **243**, 3-8, doi:10.1007/s00417-004-0950-7 (2005).
- 266 Grus, F. H., Joachim, S. C. & Pfeiffer, N. Proteomics in ocular fluids. *PROTEOMICS – Clinical Applications* **1**, 876-888, doi:10.1002/prca.200700105 (2007).
- 267 Liu, Y. J., Lian, Z. Y., Liu, G., Zhou, H. Y. & Yang, H. J. RNA sequencing reveals retinal transcriptome changes in STZ-induced diabetic rats. *Mol Med Rep* **13**, 2101-2109, doi:10.3892/mmr.2016.4793 (2016).
- 268 Olivares, A. M. *et al.* Animal Models of Diabetic Retinopathy. *Current Diabetes Reports* **17**, doi:10.1007/s11892-017-0913-0 (2017).
- 269 Kim, C. B., D'Amore, P. A. & Connor, K. M. Revisiting the mouse model of oxygen-induced retinopathy. *Eye and Brain* **8**, 67-79, doi:10.2147/eb.s94447 (2016).
- 270 Wang, X. *et al.* LRG1 promotes angiogenesis by modulating endothelial TGF-beta signalling. *Nature* **499**, 306-+, doi:10.1038/nature12345 (2013).
- 271 Staton, C. A., Reed, M. W. R. & Brown, N. J. A critical analysis of current in vitro and in vivo angiogenesis assays. *International Journal of Experimental Pathology* **90**, 195-221, doi:10.1111/j.1365-2613.2008.00633.x (2009).
- 272 Langer, H. F. *et al.* Complement-mediated inhibition of neovascularization reveals a point of convergence between innate immunity and angiogenesis. *Blood* **116**, 4395-4403, doi:10.1182/blood-2010-01-261503 (2010).
- 273 Grigsby, J. G. *et al.* Autocrine and Paracrine Secretion of Vascular Endothelial Growth Factor in the Pre-Hypoxic Diabetic Retina. *Curr Diabetes Rev* **13**, 161-174, doi:10.2174/1573399812666161007165944 (2017).
- 274 Simo, R., Carrasco, E., Garcia-Ramirez, M. & Hernandez, C. Angiogenic and antiangiogenic factors in proliferative diabetic retinopathy. *Current diabetes reviews* **2**, 71-98, doi:10.2174/157339906775473671 (2006).
- 275 Pierce, E. A., Avery, R. L., Foley, E. D., Aiello, L. P. & Smith, L. E. Vascular endothelial growth factor/vascular permeability factor expression in a mouse model of retinal neovascularization. *Proc. Natl. Acad. Sci. U. S. A.* **92**, 905-909, doi:10.1073/pnas.92.3.905 (1995).
- 276 Rohrer, B., Coughlin, B., Bandyopadhyay, M. & Holers, V. M. Systemic human CR2-targeted complement alternative pathway inhibitor

- ameliorates mouse laser-induced choroidal neovascularization. *J Ocul Pharmacol Ther* **28**, 402-409, doi:10.1089/jop.2011.0212 (2012).
- 277 Ricklin, D., Reis, E. S. & Lambris, J. D. Complement in disease: a defence system turning offensive. *Nat Rev Nephrol* **12**, 383-401, doi:10.1038/nrneph.2016.70 (2016).
- 278 Mastellos, D. & Lambris, J. D. Complement: more than a 'guard' against invading pathogens? *Trends in Immunology* **23**, 485-491, doi:10.1016/s1471-4906(02)02287-1 (2002).
- 279 Lai, A. K. W. & Lo, A. C. Y. Animal Models of Diabetic Retinopathy: Summary and Comparison. *Journal of Diabetes Research*, doi:10.1155/2013/106594 (2013).
- 280 Benzaquen, L. R., Nicholsonweller, A. & Halperin, J. A. TERMINAL COMPLEMENT PROTEINS C5B-9 RELEASE BASIC FIBROBLAST GROWTH-FACTOR AND PLATELET-DERIVED GROWTH-FACTOR FROM ENDOTHELIAL-CELLS. *Journal of Experimental Medicine* **179**, 985-992, doi:10.1084/jem.179.3.985 (1994).
- 281 Liu, J. *et al.* Relationship between Complement Membrane Attack Complex, Chemokine (C-C Motif) Ligand 2 (CCL2) and Vascular Endothelial Growth Factor in Mouse Model of Laser-induced Choroidal Neovascularization. *Journal of Biological Chemistry* **286**, 20991-21001, doi:10.1074/jbc.M111.226266 (2011).
- 282 Kunchithapautham, K. & Rohrer, B. Sublytic Membrane-Attack-Complex (MAC) Activation Alters Regulated Rather than Constitutive Vascular Endothelial Growth Factor (VEGF) Secretion in Retinal Pigment Epithelium Monolayers. *Journal of Biological Chemistry* **286**, 23717-23724, doi:10.1074/jbc.M110.214593 (2011).

7 Supplementary Figures

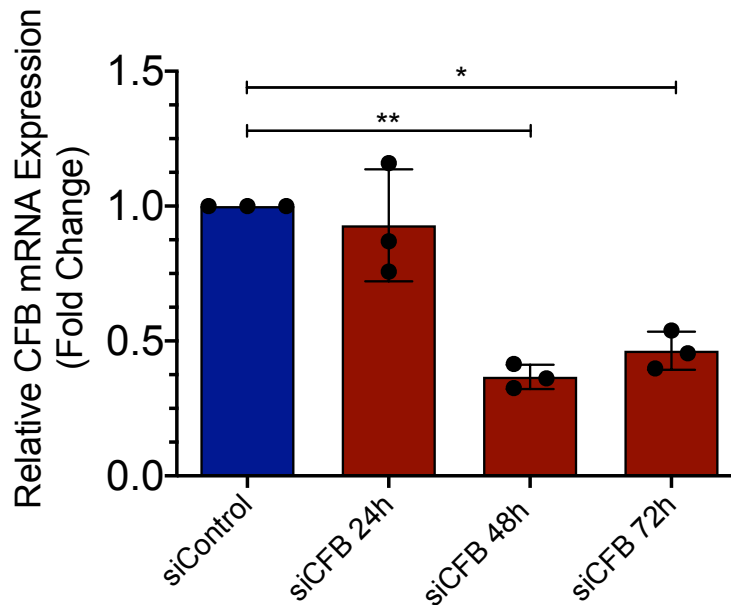


Figure 34: Transient transfection of HRECs using siRNA results in a downregulation of CFB mRNA expression. Primary HRECs were transfected with 66nM siCFB or 66nM siRNA control and changes in CFB mRNA levels were analysed at 24, 48 and 72 hours of transfection. The changes in gene expression were calculated using fold change ($-2(\Delta\Delta cT)$). RT-qPCR analysis of CFB transcript levels is represented by fold change normalised to siControl. Results represent the mean \pm SD. Statistical significance was determined on raw delta-CT values by unpaired two-tailed students' t-test; n=3, *: $p < 0.05$, **: $p < 0.01$.

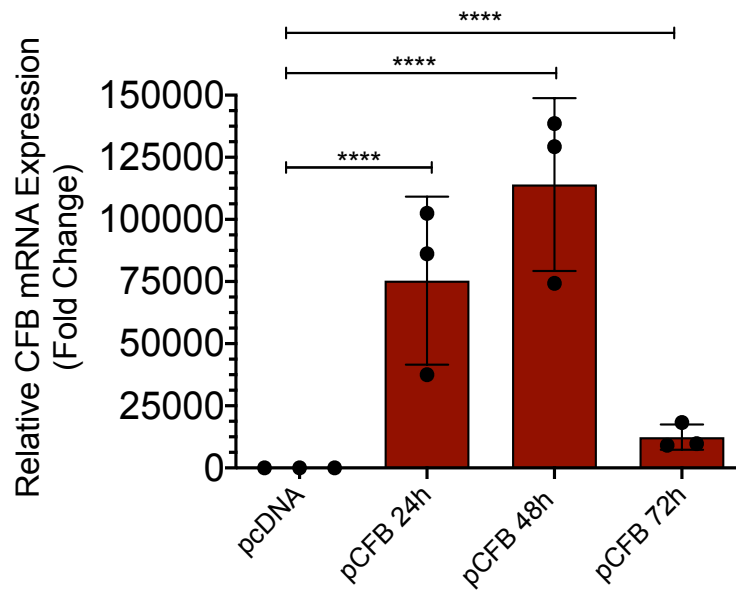


Figure 35: Transient transfection of HRECs results in an up-regulation of CFB mRNA expression. Primary HRECs were transfected with 1 μ g pCFB or 1 μ g pcDNA control and changes in CFB mRNA levels were analysed at 24, 48 and 72 hours of transfection. The changes in gene expression were calculated using fold change ($-2(\Delta\Delta cT)$). RT-qPCR analysis of CFB transcript levels is represented by fold change normalised to pcDNA. Results represent the mean \pm SD. Statistical significance was determined on raw delta-CT values by unpaired two-tailed students' t-test; n=3, ****: p< 0.01.

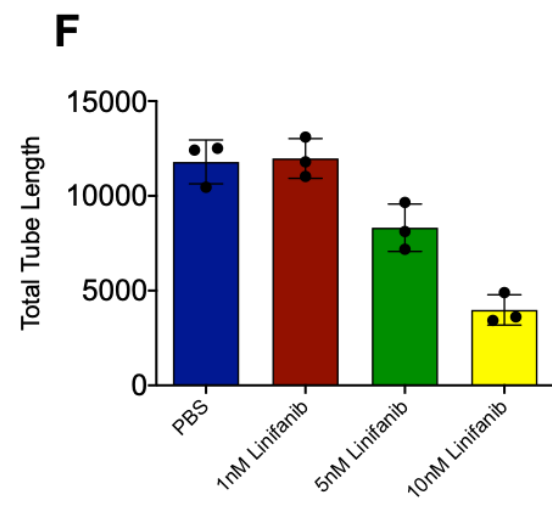
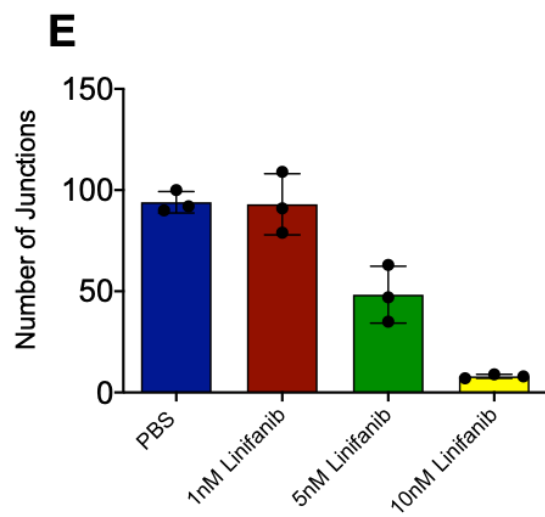
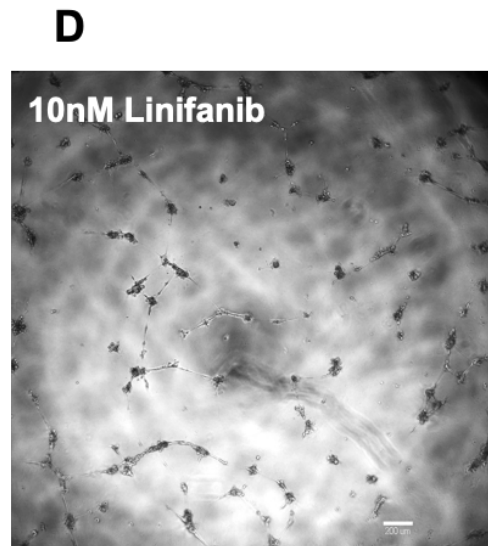
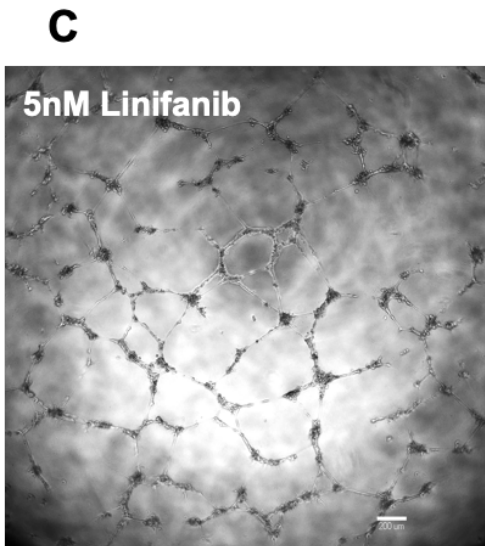
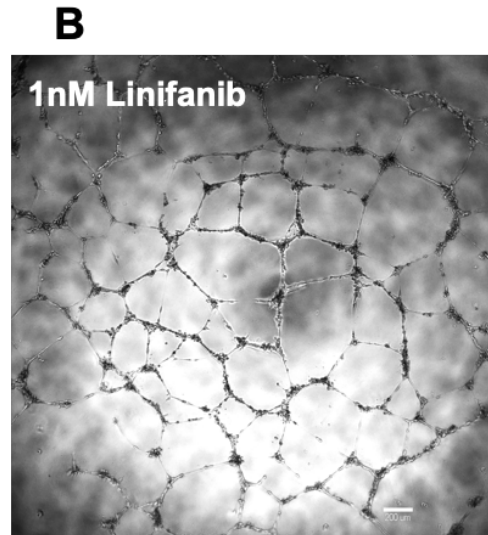
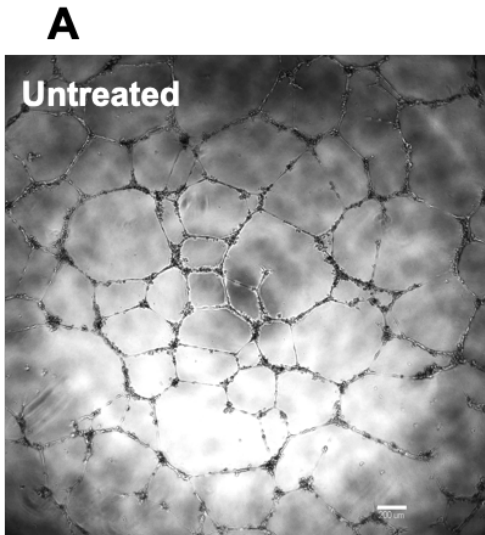


Figure 36: Linifanib treatment reduces HREC network formation in a dose dependent manner. Primary HRECs were treated with 1nM, 5nM and 10nM of the VEGFR2 inhibitor, Linifanib. Functional changes were measured as changes in EC network formation after 16 hours incubation **A-D**, Representative images of Matrigel® network formation. **E-F**, Quantification of HREC Matrigel® network formation reported as the total number of junctions and total tubule length. Results represent the mean \pm SD of one experiment per treatment performed in triplicate (the symbols representing the technical repeats). No statistical significance was determined for this data since only one biological repeat was carried out for optimisation purposes.

8 Appendix

8.1 General Laboratory Equipment and Consumables

Table 3: List of general laboratory equipment used

Equipment	Model	Supplier
Biological Safety Cabinet	1300 Series Class II, Type B2	Thermo Scientific, USA
Cell Counter	BRAND® Counting Chamber BLAUBRAND® Neubauer Improved	Merck, Singapore
Centrifuges	Sorvall™ ST 40R	Thermo Scientific, USA
	Sorvall™ Legend™ Micro 21R	Thermo Scientific, USA
	IKA Mini G	IKA® Works Asia, Malaysia
Fridge/Freezers	-80°C Panasonic MDF-U55V	SciMed Asia, Singapore
	-20°C PHCbi MDF-MU539D	SciMed Asia, Singapore
	+4°C	Thermo Scientific, USA
Gel Electrophoresis	Mini Protean® Tetra System (Acrylamide Gels)	Bio-Rad, USA
	Sub® Cell GT (Agarose Gels)	Bio-Rad, USA
Glucoemter	Accu-Chek Performa	Roche, Switzerland
Heating Block	MS Major Scienc EL-02 Dual Block Heater	BioLab, Singapore
CR Cycler	C1000 Touch™ Thermal Cycler	Bio-Rad, USA
Gilson Pipettes	2 µl, 10 µl, 20 µl, 100 µl, 200 µl, 1000 µl	Bio-Rad, USA
Plate Reader	Synergy H1 Hybrid Multi Mode Reader	BioTek, Singapore
Power Supply	PowerPac™ Basic Power Supply	Bio-Rad, USA
Rocker	Stuart™ SSL4 See-Saw Rocker	Thermo Scientific, USA
Serological Pipette	BRAND® accu-jet® pro pipette controller	Merck, Singapore
Spectrophotometer	NanoDrop™ 2000c	Thermo Scientific, USA
VORTEX	VX200 Vortex Mixer	BioLab, Singapore
Water Bath	Grant T100-ST38 Heated Circulating Bath	Insta Bioanalytik, Singapore
Real Time PCR System	Applied Biosystems StepOnePlus™ Real Time PCR System	Life Technologies, USA

Table 4: List of general laboratory consumables used

Consumable	Supplier
0.2 mL PCR Strip Tubes	Axygen
8µM Trasnwell® 24-Well Plate Insert	Corning, USA
Amicon® Pro Affinity Column	Merck, Singapore
Cell Scraper	SPL Lifesciences
Cryotubes (1mL)	Thermo Scientific, USA
Dissection Kit	Thermo Scientific, USA
Eppendorf Tubes (1.5mL)	Axygen
Film	Carestream
Filter Pipette Tips	Neptune
Microtitre plates (96-well, 24-well, 12-well, 6-well)	Thermo Scientific, USA
BD Precision Glide Needles (18, 23 and 26G)	Sigma Aldrich, USA
Nitrocellulose Membrane	Merck, Singapore
NUNC Petri Dishes	Thermo Scientific, USA
Pipette Tips	Neptune
Polyvinylidene Fluoride (PVDF) Membrane	Merck, Singapore
Scientific Slide-A-Lyzer MINI Dialysis Device	Thermo Scientific, USA
Serological Pipettes (5mL, 10mL, 25 mL, 50mL)	SPL Lifesciences
Sterile Filters (0.22µM)	Merck, Singapore
Syringes	Thermo Scientific, USA
NUNC Tissue Culture Vessels (25 cm ² , 75 cm ²)	Thermo Scientific, USA
Universal Tubes (15mL, 50mL)	Thermo Scientific, USA

Table 5: List of general laboratory chemicals used

Chemical	Supplier
2-mercaptoethanol	Sigma Aldrich, USA
Acrylamide	Invitrogen, Singapore
Agar Powder	1 st Base, Singapore
Agarose	1 st Base, Singapore
Ammonium Persulfate	Invitrogen, Singapore
Bovine Serum Albumin	Sigma Aldrich, USA
Bradford Reagent	Bio-Rad, USA
Bromophenol Blue	Bio-Rad, USA
Cell Freezing Medium	Lonza, USA
Chloramphenicol	Sigma, USA
Citrate Acid	Sigma Aldrich, USA
Comassie Blue	Bio-Rad, USA
Corning® Matrigel® Matrix	Corning, Singapore
DMSO	Sigma, USA
EDTA (ethylenediaminetetraacetic)	Sigma, USA
Endothelial Basal Media (EBM-2™)	Lonza, USA
Endothelial Growth Supplement Mix	Lonza, USA
Ethanol	Chemtech
Foetal Bovine Serum	Gibco, USA
Freestyle Expression Medium (FEM)	Gibco, USA

GelPilot® DNA Loading Dye	Qiagen, Singapore
GelRed® Nucleic Acid Gel Stain	Thermo Scientific, USA
GeneRuler 1 kb DNA Ladder	Invitrogen, Singapore
Glycerol	Promega
Glycine	1 st Base, Singapore
Imidazole	Sigma, USA
InstantBlue™ Protein Stain	Merck, Singapore
Lipofectamine 2000	Invitrogen, Singapore
Lipofectamine 3000	Invitrogen, Singapore
Luria-Bertani (LB) Media	1 st Base, Singapore
MEM Alpha + GlutaMAX™-1	GE Healthcare, UK
Methanol	Merck, Singapore
Milk Powder	Anlene
Mowiol Mounting Medium	Merck, Singapore
MTS	Sigma, USA
Na₂HPO₄ (dibasic)	Sigma, USA
NaH₂PO₄ (monobasic)	Sigma, USA
Ni Sepharose High Performance Nickel-Charged (IMAC) Resin	GE Healthcare, Singapore
NP-40	Sigma Aldrich, USA
Opti-MEM®	Gibco, USA
p3000	Invitrogen, Singapore
Paraformaldehyde	Sigma Aldrich, USA
PBS	1 st Base, Singapore
Penicillin Streptomycin	Nacalai Tesque, Japan
Phenyl-methylsulfonyl fluoride	Thermo Scientific, USA
Phosphatase Inhibitor	Nacalai Tesque, Japan
Phosphate Buffered Saline	1 st Base, Singapore
Protease Inhibitor	Nacalai Tesque, Japan
Quick Coating Solution	Angio-Proteomie, USA
RNAse free dH₂O	Invitrogen, Singapore
RNAzol®RT	Molecular Research Centre, Inc
Sodium Chloride (NaCl)	Sigma Aldrich, USA
Sodium Citrate	Sigma Aldrich, USA
Sodium Dodecyl Sulphate (SDS)	1 st Base, Singapore
Sodium Phosphate (Na₂HPO₄)	Sigma Aldrich, USA
Streptozocin Powder	Sigma Aldrich, USA
Stripping Buffer	Nacalai Tesque, Japan
SuperSignal™ West Pico PLUS Substrate	Thermo Scientific, USA
TEMED	Invitrogen, Singapore
Tris Base	1 st Base, Singapore
Trypan Blue	Gibco, USA
Tween-20	Promega, Singapore
Type I collagen	Invitrogen, Singapore

8.2 Buffers

8.2.1 General Laboratory Buffers

Table 6: List of general buffers and solutions used

Name	Components
Blocking Buffer - IF (1%)	0.5% BSA 1% Tween-20 3% TritonX-100 DDH ₂ O
Blocking Buffer – WB (5%)	2.5 g Milk Powder 50 mL TBST
Cell Lysis Buffer (pH 8)	20mM Tris – Base 420 mM NaCl 0.1 mM EDTA 10% Glycerol 0.5% NP-40 DDH ₂ O
Inhibitor Cocktail (*Freshly added into RIPA buffer just before use)	*1 X Protease Inhibitor *1 X Phosphatase Inhibitor *0.2M Dithiothreitol (DTT) 0.1M Phenyl-methylsulfonyl fluoride (PMSF)
Laemmli Buffer (pH 6.8) (4X)	8% Sodium Dodecyl Sulphate (SDS) 20% 2-mercaptoethanol 40% Glycerol 0.008% Bromophenol Blue 0.250 M Tris Base
PBS (1X)	Dilute 10X PBS to 1X DDH ₂ O
RIPA Buffer (pH 8)	20mM Tris Base 420 mM NaCl 0.1 mM EDTA 10% Glycerol 0.5% NP-40
Running Buffer (1X)	25 mM Tris Base 190 mM Glycine 0.1% SDS
Transfer Buffer (1X)	25 mM Tris Base 190 mM Glycine 20% Methanol
Tris Base Buffered Saline with Tween (TBST) (1X)	12.5 mM Tris Base 137 mM NaCl* 0.01% Tween-20
Trypsin EDTA (3X)	0.005% Trypsin 0.35 mM EDTA
Sodium Citrate Buffer (0.1M)	0.1 M Sodium Citrate 0.1 M Citrate Acid

8.2.2 Recombinant CFB Protein Purification Buffers

Table 7: Sodium phosphate buffer components

Buffer Component	Molar Mass (g/mol)	Molarity	Amount Needed for 50 mL (g)
NaH ₂ PO ₄ (monobasic)	137.99	1	6.9
Na ₂ HPO ₄ (dibasic)	177.99	1	8.9

Table 8: Stock buffers for binding and elution buffers

Buffer	Composition
Stock Buffer 1 (500 mL)	
20 mM sodium phosphate 300 mM NaCl	100 mL 0.1M sodium phosphate buffer 37.5 mL 4M NaCl
Stock Buffer 2 (500 mL)	
20 mM sodium phosphate 300 mM NaCl 500 mM imidazole	100 mL 0.1M sodium phosphate buffer 37.5 mL 4M NaCl 17.02 g imidazole
Elution Buffer (50 mL)	
20 mM sodium phosphate 300 mM NaCl 20 mM imidazole	48 mL Stock Buffer 1 2 mL Stock Buffer 2
Binding Buffer (500 mL)	
20 mM sodium phosphate 300 mM NaCl 100 mM imidazole	40 mL Stock Buffer 1 10 L Stock Buffer 2

8.2.3 Commercially Available Enzymes and Buffers

Table 9: List of enzymes and commercially available buffers/kits used

Enzyme/Kit	Supplier
10 mM dNTPs	New England Biolabs, USA
5X Q5 GC Enhancer	New England Biolabs, USA
5X Q5 Reaction Buffer	New England Biolabs, USA
5X qScript® cDNA Supermix Kit	New England Biolabs, USA
AflIII Restriction Endonuclease	New England Biolabs, USA
FastDigest Buffer	Thermo Scientific, USA
Q5 DNA Polymerase	Qiagen, Singapore
Q5® High-Fidelity DNA Polymerase	New England Biolabs, USA
QIAprep Spin Miniprep Kit	Qiagen, Singapore
QIAquick Gel Extraction Kit	Qiagen, Singapore
QIAquick PCR Purification Kit	Qiagen, Singapore
Quick Ligation™ Kit	New England Biolabs, USA
SYBR® Green Supermix	Bio-Rad, Singapore
XbaI Restriction Endonuclease	New England Biolabs, USA

8.3 Primary and Secondary Antibodies

Table 10: List of primary antibodies. IF - immunofluorescence WB- Western Blot

Antibody	Target	Application/Dilution	Supplier
Ki67	Proliferating Cells	IF 1:500	Abcam, UK
CD31	Endothelial Cells	IF 1:500	Abcam, UK
Isolectin B4 (conjugated)	Endothelial Cells	IF 1:500	Vector Laboratories, Canada
CFB	-	WB 1:1000	Abcam, USA
VEGF	-	WB 1:1000	Abcam, USA
Phospho-VEGFR2	-	WB 1:1000	Cell Signalling Technology, USA
VEGFR2	-	WB 1:1000	Cell Signalling Technology, USA
GAPDH	-	WB 1:50,000	Santa Cruz Biotechnology, USA

Table 11: List of secondary antibodies. IF - immunofluorescence; WB - Western Blot

Antibody	Supplier	Application/Dilution)
Anti-rabbit HRP conjugated	Bethyl Laboratories, USA	WB/ 1:5000
AlexaFluor® 594 anti-rabbit	Invitrogen, Singapore	IF/ 1:200
AlexaFluor® 488 anti-rat	Invitrogen, Singapore	IF/ 1:200

8.4 Culture Media

Table 12: Summary of the composition of HREC EGM-2 media

Component	Volume
FBS	10 mL
Hydrocortisone	0.2 mL
hFGF-β	2 mL
VEGF	0.5 mL
Ascorbic Acid	0.5 mL
R3-IGF-1	0.5 mL
hEGF	0.5 mL
GA-1000	0.5 mL
Heparin	0.5 mL

Table 13: Summary of the composition of *ex vivo* assay media

Name	Component
Aortic Ring Media	
Metatarsal Dissection Media	10% FBS 1% Penicillin/Streptomycin 1X PBS
Metatarsal Growth Media	10% FBS 1% Penicillin Streptomycin MEM Alpha + GlutaMAX™-1

8.5 Molecular Biology Techniques

8.5.1 Ligation

Table 14: Summary of the Quick Ligation reaction components

Component	20 µL Reaction
Quick Ligase Reaction Buffer (2X)	10 µL
Vector DNA (pcDNA) (4.5 kb)	50 ng
Insert DNA (pCFB) (2.5 kb)	83.3 ng
Nuclease-free Water	Up to 20 µL
Quick Ligase	1 µL

8.5.2 Polymerase Chain Reaction

Table 15: Summary of the PCR mastermix components

PCR Mastermix Component	50 µL Reaction	Final Concentration
5X Q5 Reaction Buffer	10 µL	1X
Q5 DNA Polymerase	0.5 µL	0.02 U/ µL
5X Q5 GC Enhancer	10 µL	1X
10 mM dNTPs	1 µL	200 µM
10 µM Forward Primer	2.5 µL	0.5 µM
10 µM Reverse Primer	2.5 µL	0.5 µM
Template DNA	Variable	< 1000 ng ($T_m - 1-2$)°C
Nuclease Free H₂O	Top up to 50 µL	

Table 16: Thermocycling conditions for PCR amplification

Cycling Condition	Temperature	Time
Initial Denaturation	98°C	30 seconds
25-35 cycles	98°C	5-10 seconds
	($T_m - 1-2$)°C	10-30

	72°C	20-30 seconds/kb
Final Extension	72°C	2 minutes
Hold	4°C	Infinite

8.5.3 First Strand cDNA Synthesis

Table 17: Components of qScript® cDNA Supermix reaction

Component	Volume
5X Reaction Mix	4 µl
Template RNA	1 µg
Nuclease Free dH₂O	Up to 20 µl

8.5.4 SYBR® Green Real-Time PCR

Table 18: Mouse primer sequences for RT-qPCR

Gene	Forward Primer Sequence	Reverse Primer Sequence
B- Actin	GGCACACACCTTCTACAATG	GGGGTGTGAAGGTCTCAAAC
CFB	GCTTGCCATGGTTGCTTATG	AAGGCAGGAGAGAAGCTGG

Table 19: Human primer sequences for RT-qPCR

Gene	Forward Primer Sequence	Reverse Primer Sequence
B- Actin	TGAGAGGGAAATCGTGCGTG	TGCTTGCTGATCCACATCTGC
CFB	GGAAGGGAATGTGACCAG	AAGGCAGGAGAGAAGCTGG
VEGF	CTACCTCCACCATGCCAAGT	GCAGTAGCTGCGCTGATAGA
VEGFR2	CCAGCAAAGCAGGGAGTCTGT	TGTCTGTGTCATCGGAGTGATATCC

Table 20: SYBR® Green reaction volume composition

Component	Volume (µl)
Water	7.2
SYBR® Green Supermix	10
Forward Primer	0.9
Reverse Primer	0.9
cDNA	1

Table 21: RT-qPCR Cycling conditions

Cycle Step	Temperature (°C)	Time	Cycles
Step 1	95	10 min	1
Step 2	95	15 s	40
	60	1 min	
Step 3	95	15 s	1
	60	15 s	
	95	15 s	

8.5.5 Sodium Dodecyl Sulphate Polyacrylamide Gel Electrophoresis (SDS-PAGE)

Table 22: Composition of SDS-PAGE gels

Resolving Gel 10% (5 mL)		Stacking Gel (1.5 mL)	
Nuclease Free Water	1.9 mL	Nuclease Free Water	680 µL
30% Acrylamide Mix	1.7 mL	30% Acrylamide Mix	170 µL
Tris-cl (1.5 M pH 8.8)	1.3 mL	Tris-cl (1.5 M pH 8.8)	130 µL
10% Ammonium Persulfate	50 µL	10% Ammonium Persulfate	10 µL
TEMED	2 µL	TEMED	1 µL
SDS 10%	50 µL	SDS 10%	10 µL